Blow-up methods for slow-fast systems

Elena Bossolini

Tesi di Laurea Magistrale
Padova 2014

Principal Supervisor: Prof. Ugo Galvanetto
Co-supervisors: Prof. Benettin Giancarlo, Prof. Morten Brøns, Prof. Kristian Uldall Kristiansen

Università degli Studi di Padova
Dipartimento di Ingegneria Industriale
Facoltà di Ingegneria Aerospaziale
Via Gradenigo, 6/a
35131 Padova, Italy
www.dii.unipd.it

Technical University of Denmark
Department of Applied Mathematics and Computer Science
Matematiktorvet, building 303B,
2800 Kongens Lyngby, Denmark
Phone +45 4525 3351
compute@compute.dtu.dk
www.compute.dtu.dk

Summary (Italian)

Il seguente progetto dimostra come il metodo del blow-up risulti utile nell'analisi di sistemi veloci-lenti. In particolare, due esempi fisici di sistemi veloci-lenti sono presentati.
Il primo esempio riguarda lo studio del comportamento dei fluidi tissotropici con tensione di snervamento. Il modello che descrive da dinamica di questi fluidi non-newtoniani può essere studiato localmente attorno la condizione di equilibrio tramite la teoria geometrica delle perturbazioni singolari. I risultati ottenuti con questa teoria non sono sufficienti per comprendere il comportamento a larghe scale del fluido. Lo studio a larghe scale può essere fatto riscaldando propriamente il problema, ma in questo caso si perdono le informazioni del comportamento a livello locale. Il metodo del blow-up si rivela efficace nell'unire la soluzione a livello locale con la soluzione per larghe scale.
Il secondo esempio riguarda lo studio del problema agli autovalori dell'equazione di Schrödinger al limite classico per un generico potenziale simmetrico. Il problema agli autovalori può essere riportato ad un sistema di equazioni differenziali veloci-lente. Questo sistema ha un punto non-iperbolico nell'origine. Il metodo del blow-up è permette di ottenere iperbolocità nel sistema "esploso" e determinare delle condizioni sull'esistenza della soluzione del problema agli autovalori.

Summary (English)

This project shows the utility of the blow-up method in the analysis of slow-fast systems. In particular the method is applied to two physical problems.
The first problem is the analysis of thixotropic yield stress fluids. The model for this non-newtonian fluids can be written as a slow-fast systems close to the equilibrium point. However when the fluid is far from the equilibrium condition it cannot be considered anymore a slow-fast system and a rescale of the dynamics is needed. With this rescale the local behaviour appears in the higher order terms. The blow-up method helps connecting the solution of the systems on the two scales.
The second problem is the analysis of the Schòdinger eigenvalue problem at the classical limit for a generic symmetric potential. This eigenvalue problem can be rewritten in a slow fast formulation, however a non-hyperbolic point appears in the origin. The use of the blow-up method in the origin allows to obtain some hyperbolicity and thus to find existence conditions on the solution of the eigenvalue problem.

Preface

This thesis was prepared at the department of Compute at the Technical University of Denmark in fulfilment of the requirements for acquiring an M.Sc. in Mathematical Modelling and Computation and a Master Degree in Aerospace Engineering at Università degli Studi di Padova, Italy.

Lyngby, 7-July-2014

Elena Bossolini

Acknowledgements

I would like to thank Professors Kristian Uldall Kristiansen and Morten Brøns for their extraordinary support during the project. I have always felt motivated and comfortable and it has been a great experience to work together. I'm glad that we are going to continue the collaboration for the next years during my Ph.D. at Technical University of Denmark.

I would like to thank Professors Ugo Galvanetto and Giancarlo Benettin for their willingness as being my advisors for the italian degree and for the suggestions that they have given me. Finally, I would like to thank Professor Mads Peter Sørensen for the very useful lecture on quantum mechanics.

I want to thank all my friends and all the people met during the three years of my double Master, both in Italy and in Denmark for the great time spent together.

On the italian side, I would like to thank in particular my long-standing friends from the Aerospace course, all the people of the great people I have met at the dorm Cuamm, my beloved girlfriends from Mantova and Dario who was always ready to support me.

I would like to thank all the people that I have met in Denmark for the good time spent together. In the last two years I have met so many great people that it is impossible for me to remember here you all! I would like to thank especially my housemates of container T and the awesome "big family" group. I'm glad that I have met you all and being the buddy of some of you has been a great experience. Finally I would like to thank all the people of the GH-lige because this last semester with you has been the best danish experience I could ever have! These two last years in Denmark have been a lot of fun for me and that's all to you guys!

For their special effort in helping me in the project I would like to say a special thank you to Antoine, Paolo, Åsa, Amrei, Lef, Yann and Lukas. Thank you for the hours spent together talking, working together in the library and proofreading my project.

The biggest hug and thank you goes to my best friend Marco: even if we are 1500km far, we are always together and I couldn't ask for a better friendship! Thank you for bearing me every time I get nervous or stressed. I wish you all the best for your next experience in Scotland and I hope to exchange back your support.

Finally I would like to thank my family. You have always been there to sustain and motivate me and I love you. I thank you for supporting my decision of studying abroad for such a long time. I really miss you! I wish to my nephews all the best for their future and I hope to be a good example of dedication to what you like.

Three long years, but other three are coming! :-)

Contents

Chapter 1

Introduction

The study of systems of non-linear differential equations is in general rather difficult and an analytical description of the phase-space dynamics is usually impossible. For different classes of non-linear ODEs methods have been developed that can give an insight on the behaviour of the system. One of these classes is related to singular perturbation problems, which can be written in the form

$$\begin{aligned} \dot{x} &= \varepsilon f(x, y, \varepsilon) \\ \dot{y} &= g(x, y, \varepsilon) \end{aligned} \tag{1.1}$$

with $x \in \mathbb{R}^m, y \in \mathbb{R}^n, \varepsilon \in \mathbb{R}, 0 < \varepsilon \ll 1, f : \mathbb{R}^{m+n} \to \mathbb{R}^m, g : \mathbb{R}^{m+n} \to \mathbb{R}^n$ and $f, g \in C^r, r < \infty$. These problems are called singular perturbation in order to distinguish them from the regular perturbation problems. Indeed considering the $\mathcal{O}(\varepsilon)$ terms as perturbations, the approximation of $\varepsilon = 0$ in (1.1) leads to a system which has a different behaviour from the perturbed one. System (1.1) is also called slow-fast, because the set of differential equations is split in two parts which evolve in two different time scales. In equation (1.1) the first m equations evolve slower than the following n. The measure of the separation between the two time scales is given by the parameter $\varepsilon \ll 1$.

The class of singular perturbation problems is rather important and it is common to find physical examples belonging to it. Applications that can be described by a system like (1.1) are from celestial mechanics, control theory, combustion, friction modelling, optics, fluid particle motion, quantum mechanics, adiabatic

Hamiltonian systems, travelling wave problems in reaction diffusion equations and coupled mechanical oscillators to name a few [Kap98].

This project is devoted to the study of slow-fast systems with the use of the blow-up method. In particular two applications will be described in detail and it will be shown the power of the blow-up method to get insight of system (1.1) around degenerate points.

Chapter 2 is devoted to the theoretical description of slow-fast systems of the form (1.1). The mathematical analysis of slow-fast systems is usually performed with the use of geometric singular perturbation theory, also called GSPT. The first efforts on GSPT have been done by Fenichel [Fen71], and his theorem is of key importance to the description of the phase space of slow-fast systems. The theory is called geometric singular perturbation because the geometrical properties of the singular limit $\varepsilon = 0$ of (1.1) are very important for the understanding of the behaviour of the system for $\varepsilon \ll 1$ but different from zero. However the results of the classical GSPT are valid only for non degenerate point of the slow-fast system (1.1). Around non-hyperbolic points it is not possible to use Fenichel's theorem to plot the phase space diagram, other methods become necessary.

During the last decade of the 20th century, Dumortier and Roussaire [DR96] have started using the blow-up method as a new way to get insight of the dynamics of a slow-fast system around non-hyperbolic points. Nowadays the blow-up method is a cutting-edge technique and many papers are being written on this topic, for instance [KS01a], [KS01b], [vGS05], [AFJ11], [Kue07] to name a few. The method blows-up the degenerate point to a higher dimensional structure such as a line, a circle or a sphere in order to obtain more hyperbolicity on the blown-up system than in the original one. The analysis of the dynamics of the blown-up system is then performed. This analysis results to be relevant in order to conclude on the behaviour of the original system around the degenerate point. The blow-up method is presented in chapter 3.

Two physical examples of slow-fast systems which can be solved using the blow-up method are presented in chapters 4 and 5. Chapter 4 considers the behaviour of thixotropic yield stress fluids. These fluids have two important features which distinguish them from the ones modelled by the Navier-Stokes equations:

- they need a stress different from zero to make the fluid start flowing, which is called the yield stress
- they exhibit shear thinning, which means that the shear strain decreases for increasing values of shear stress.

Two common examples of thixotropic yield stress fluids are ketchup and toothpaste.

Ketchup for instance requires to be shaken before being poured out of the bottle. Moreover once it starts flowing it flows very fast, and it is common experience that the poured ketchup is more than what you wanted.

Thixotropic yield stress fluids are very common in the food and cosmetic industry. The understanding of their behavior is a key in improving the manufacturing processes, stability and consumer sensory perception during application or use of a product [ST04]. A recent paper by Renardy [Ren10] presents a model for thixotropic yield stress fluid which can be easily rewritten as a slow-fast system. In chapter 4 it will be shown how this reformulation can make the understanding of the fluid behaviour straightforward. Moreover the aim of the project is to make Renardy's statements in [Ren10] more precise and the blow-up method will be fundamental in this.

Chapter 5 is devoted to the study of the Schrödinger eigenvalue problem at the classical limit. Schrödinger equation is a fundamental equation of quantum mechanics. This equation describes the time evolution of the probability to find a quantum particle in a point of the space. The Schrödinger eigenvalue problem describes the probability to find the quantum particle in the space for each of the states of energy levels allowed. Moreover the equation has to be consistent with Newton's second law at the limit of particles with large mass. This limit is the so-called classical limit, which has been first studied by Dirac in [Dir58]. The question on how the classical limit should be interpreted is still open, and in the present project it is shown how it is possible to obtain a slow-fast formulation under certain assumptions. The blow-up method will result another time to be of fundamental help to make conclusions on the slow-fast system for values of ε different from zero.

Chapter 2

Geometric Singular Perturbation Theory

Consider a system of $m+n$ equations where the first m are evolving on a different time scale than the following n.

$$\begin{aligned} \dot{x} &= \varepsilon f(x, y, \varepsilon) \\ \dot{y} &= g(x, y, \varepsilon) \end{aligned} \tag{2.1}$$

with $x \in \mathbb{R}^m, y \in \mathbb{R}^n, \varepsilon \in \mathbb{R}, 0 < \varepsilon \ll 1, f : \mathbb{R}^{m+n} \to \mathbb{R}^m, g : \mathbb{R}^{m+n} \to \mathbb{R}^n$ and $f, g \in C^r, r < \infty$. The dot is the derivative respect to the time τ. Since ε is small, in times of order of τ the variable x evolves slower than y.

Problems like equation (2.1) are called singular perturbation problems because the unperturbed system obtained setting ε to zero has a different behaviour than the original system. Any problem involving two different time scales can be written in the form (2.1) and the parameter ε can be understood as a measure of the separation of the two time scales.

There are different physical examples that can be written as singular perturbation problems. Applications that give rise to a system like (2.1) are from celestial mechanics, control theory, combustion, friction modelling, optics, fluid particle

motion, quantum mechanics, adiabatic Hamiltonian systems, travelling wave problems in reaction diffusion equations and coupled mechanical oscillators to name a few [Kap98].

Making the rescale of time $t = \varepsilon\tau$ then system (2.1) can be rewritten respect to the new time t as

$$\begin{aligned} x' &= f(x, y, \varepsilon) \\ \varepsilon y' &= g(x, y, \varepsilon) \end{aligned}. \tag{2.2}$$

with $'$ meaning derivative respect to the time t. System (2.2) is called the "slow" system because the time t is slower than the time τ. On the other hand system (2.1) is called the "fast" system.

As long as $\varepsilon \neq 0$ systems (2.1) and (2.2) are equivalent with the time rescale $t = \varepsilon\tau$. However, for $\varepsilon = 0$ the two systems lead to two different limiting cases, which are describing two different dynamics. In particular the fast system (2.1) reduces to the layer problem of equation (2.3) , which is a set of n equations, with $x \in \mathbb{R}^m$ constant parameters.

$$\begin{aligned} \dot{x} &= 0 \\ \dot{y} &= g(x, y, 0) \end{aligned} \tag{2.3}$$

On the other hand, the slow system (2.2) becomes at the limit case $\varepsilon = 0$ the reduced problem (2.4) which is a set of differential-algebraic equations.

$$\begin{aligned} x' &= f(x, y, 0) \\ 0 &= g(x, y, 0) \end{aligned}. \tag{2.4}$$

In this case the number of differential equations decreases from $m+n$ to m. Thus it is possible to note that both the two limiting systems (2.3), (2.4) are lower dimensional respect to the original systems (2.1), (2.2). Moreover the singular perturbation problem described by the two original systems (2.1), (2.2) becomes a regular perturbation problem at the two limiting cases.

The idea behind geometric singular perturbation theory (often called GSPT), is to analyse the dynamical structure of the system from a geometrical point of view such as looking for invariant sets, and invariant manifolds. In particular, the two lower dimensional limiting case are the one analysed, and the aim is to see whether these geometrical structures are preserved for the case of $\varepsilon \neq 0$. The first efforts on the analysis of GSPT were done by Fenichel [Fen71]. In the present chapter Fenichel's theorem is stated as in Khuen's book [Kue07], but other references are in [Fen71], [Jon95], [Kap98]

As it has been introduced previously, geometric singular perturbation theory deals with the analysis of geometrical structures such that invariant sets and invariant manifolds. Thus first of all the definition of invariant set is given.

Definition 2.1 Locally invariant set [Jon95]

A set M is locally invariant under the frow from (2.1) if it has a neighborhood V so that no trajectory can leave M without also leaving V.

Note that the simplest locally invariant set one can think of is a fixed point.

As it is possible to see in both the limit systems (2.3), (2.4), the set $g(x, y, 0) = 0$ looks to be rather important: it is the set of fixed points of the layer problem (2.3), while for the reduced problem it is the algebraic constraint on which dynamics is allowed. Since this set is going to play a key role in the study of singular perturbed problem it is called the critical manifold.

Definition 2.2 Critical manifold

Define critical manifold $C_0 \subset \mathbb{R}^n$ the set of critical points of the layer problem (2.3), i.e.

$$C_0 := \{(x, y) : g(x, y, 0) = 0\}$$

Definition 2.3 Normally hyperbolic subset [Kue07]

A subset $S \subset C_0$ is called normally hyperbolic if the $n \times n$ matrix $(D_y g)(p, 0)$ of first partial derivatives with respect to the fast variables has no eigenvalues with zero real part for all $p \in S$, $p = (x, y)$.

Indeed when considering the $(m + n) \times (m + n)$ Jacobian matrix $Dg(p, 0)$ the first diagonal block $(D_x g)(p, 0)$ is a $m \times m$ matrix with all eigenvalues having trivially a zero real part. In the case that the second diagonal block $(D_y g)(p, 0)$ has all eigenvalues with non-zero real part then the point $(p, 0)$ is called normally hyperbolic.

Definition 2.4 [Kue07]

A normally hyperbolic subset $S \subset C_0$ is called attracting if all eigenvalues of $(D_y g)(p)$ have negative real parts for $p \in S$; similarly S is called repelling if all eigenvalues have positive real parts. If S is normally hyperbolic and neither attracting nor repelling it is of saddle-type.

The next theorem was stated first by Fenichel in [Fen71] and gives an important result for the singularly perturbed systems (2.1), (2.2) for $\varepsilon \neq 0$ when it is possible to identify compact normally hyperbolic submanifolds of C_0 in the corresponding limit problems (2.3), (2.4). The proof of Fenichel's theorem can be found in [Jon95].

Theorem 2.5 Fenichel's theorem, [Kue07]

Suppose $S = S_0$ is a compact normally hyperbolic submanifold (possibly with boundary) of the critical manifold C_0 of the slow system

$$x' = f(x, y, \varepsilon)$$
$$\varepsilon y' = g(x, y, \varepsilon)$$

and suppose that $f, g \in C^r$, $r < \infty$. Then for $\varepsilon > 0$ sufficiently small the following hold

1. *There exists a locally invariant manifold S_ε, diffeomorphic to S_0. Local invariance means that trajectories can enter or leave S_ε only through its boundaries.*
2. *S_ε has a Hausdorff distance $\mathcal{O}(\varepsilon)$ from S_0.*
3. *The flow on S_ε converges to the slow flow as $\varepsilon \to 0$.*
4. *S_ε is C^r-smooth.*
5. *S_ε is normally hyperbolic and has the same stability properties with respect to the fast variables as S_0 (attracting, repelling or saddle-type).*
6. *S_ε is usually not unique. In regions that remain at a fixed distance from ∂S_ε, all manifolds satisfying 1)-5) lie at a Hausdorff distance $\mathcal{O}(e^{-\frac{k}{\varepsilon}})$ from each other for some $k > 0$, $k = \mathcal{O}(1)$.*

Note that all asymptotic notation refers to $\varepsilon \to 0$. The same conclusion as for S_0 hold locally for its stable and unstable manifolds

$$W^s_{loc}(S_0) = \cup_{p \in S_0} W^s_{loc}(p), \quad W^u_{loc}(S_0) = \cup_{p \in S_0} W^u_{loc}(p)$$

where the points $p \in S_0$ are equilibria of the fast system (2.3).

These manifolds also persist for $\varepsilon > 0$ sufficiently small: there exists local stable and unstable manifolds $W^s_{loc}(S_\varepsilon)$ and $W^u_{loc}(S_\varepsilon)$, respectively, for which conclusions 1)-6) hold if we replace S_ε and S_0 by $W^s_{loc}(S_\varepsilon)$ and $W^s_{loc}(S_0)$ (or similarly by $W^u_{loc}(S_\varepsilon)$ and $W^u_{loc}(S_0)$).

The manifold S_ε is called the slow manifold, and it can be noted the theorem says that S_ε is locally invariant. Thus trajectories on the slow manifold can escape from it only through its boundaries. The local and not global invariance of the slow manifold is due to the fact that the theorem considers only compact normally hyperbolic subsets S_0 of the critical manifold C_0.

Moreover S_ε is not unique for the same reasons the centre manifold is not. All the slow manifolds are exponentially close to each other, thus it is not possible to distinguish between them and it will be enough to study the dynamics on one of the slow manifolds to conclude for all the others. Moreover the slow manifold is diffeomorphic to S_0 because f, g are supposed to be smooth enough.

The flow off of the slow manifold is described by the stable and unstable submanifolds $W^s_{loc}(S_\varepsilon), W^u_{loc}(S_\varepsilon)$ of the slow manifold.

Fenichel's theorem 2.5 works only for compact normally hyperbolic submanifold of the critical manifold C_0. Thus if there exists a point of the critical manifold with at least on eigenvalue of its Jacobian matrix $(D_y g)(p, 0)$ with zero real part, it is not possible to use Fenichel's theorem to make conclusion close enough to that point. In points where normal hyperbolicity is lost a different analysis is needed and the blow up method presented in the next chapter is very useful to solve these problems.

Chapter 3

The blow-up method

The blow-up method is a technique that allows to gain insight of the dynamics around a non-hyperbolic point for slow-fast systems. The main idea is to blow-up the degenerate point to a higher dimensional structure such as a line, a circle or a sphere. The dynamics is then studied on this higher dimensional structure, where different non-degenerate singularities will appear. In case that some fixed point of the blown-up system is still non-hyperbolic, the procedure is repeated. Dumoirtier has shown that for vector fields satisfying the Lojasiewicz inequality, it is possible to desingularize the non-hyperbolic point with a finite number of blow-ups [Kue07], [DR96].

Much of the effort on this technique is done by Dumoirtier and Roussaire in [DR96]. Other works are done by Krupa and Szmolyan [KS01a]. The survey by Alvaréz et. al. contains a very good overview of the blow-up technique [AFJ11].

Consider as a generic example a vector field in $\mathbb{R}^3$ such as $\dot{x} = f(x)$, $f : \mathbb{R}^3 \to \mathbb{R}^3$. Suppose that the origin is degenerate, $f(0) = 0$, $J(0) = 0$, with J the Jacobian matrix computed in the degenerate point. Call $B = S^2 \times \mathbb{R}$ and $B_0 = S^2 \times [0, r_0], r_0 > 0$.

The quasi-homogeneous blow-up $\Gamma : B_0 \to \mathbb{R}^3$ is a map that uses different weights for each coordinate of the vector field

$$\Gamma(\bar{x}, \bar{y}, \bar{\varepsilon}, \bar{r}) = (\bar{r}^{a_1}\bar{x}, \bar{r}^{a_2}\bar{y}, \bar{r}^{a_3}\bar{\varepsilon}).$$

with $\bar{r}$ the exceptional divisor, such that when $\bar{r} = 0$ the blown-up coordinates collapse in the fixed point. The aim is find the coefficients $a_i, i = 1, 2, 3$, such that blown-up vector field has common factor of the exceptional divisor $\bar{r}^k$, $k \geq 1$ on each coordinate [AFJ11], [Kue07]. With a time rescaling it is then possible to remove the exceptional divisor and de-trivialize the vector field.

The geometrical interpretation of the quasi-homogeneous blow-up, is that the non-hyperbolic point is blown-up to an ellipsoid, since the coefficients a_i could be different one from the others. In the case that all the coefficients a_i have the same value, then the degenerate point is blown-up to a sphere, and it is the case of an homogeneous blow-up. Figure 3.1 shows the basic idea of the blow-up. Note that for $(\bar{x}, \bar{y}, \bar{z}) \in S^2$ the physical interpretation of these variables is straightforward, since they are the angle combinations for spherical coordinates. Indeed call $\phi \in [0, 2\pi[, \theta \in [0, \pi[$ then

$$\bar{x} = \cos\phi \sin\theta, \quad \bar{y} = \sin\phi \sin\theta, \quad \bar{\varepsilon} = \cos\theta$$

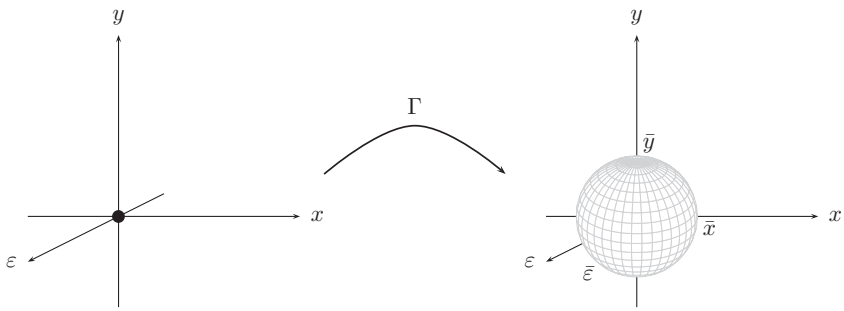

Figure 3.1: Blow-up of the origin to a sphere.

The dynamics of non-linear systems in spherical coordinates $(\bar{x}, \bar{y}, \bar{\varepsilon}, \bar{r})$ is very hard to study. Thus the next step is to find suitable charts where to calculate the blow-up in local coordinates. The main idea is to keep fixed one of the coordinates $(\bar{x}, \bar{y}, \bar{\varepsilon}) \in S^2$, and thus determine a subspace, where the dynamics can be rewritten using coordinates in $\mathbb{R}^3$. Figure 3.2 shows an example of three possible charts $\kappa_i, i = 1, 2, 3$ in which it is possible to study the blow-up dynamics. Note that for chart κ_1 the variable $\bar{x}$ has been kept fixed, while for chart κ_2 and κ_3 have been kept fixed the variables $\bar{y}$ and $\bar{\varepsilon}$ respectively.

In order to find the local coordinates for each chart, the local blow-up map μ_i on the chart κ_i is defined. This map is keeping constant to ± 1 one of the three

coordinates $(\bar{x}, \bar{y}, \bar{\varepsilon})$. Then the local coordinates on the chart κ_i are computed such that $\Gamma = \kappa_i \circ \mu_i$.

The projection of the blown-up sphere into different charts is a stereographic mapping. This map doesn't preserve distances but it is conformal, which means that it preserves angles. This function is commonly used in cartography to plot maps and atlases.

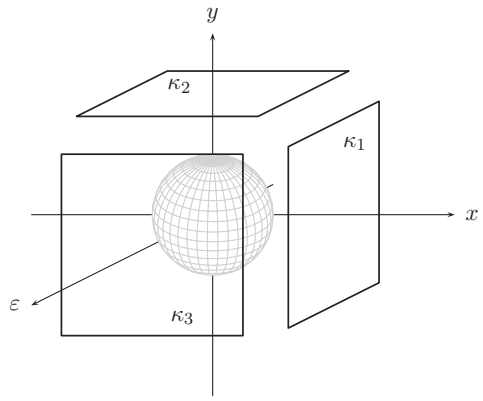

Figure 3.2: Definition of the local charts.

The analysis of the dynamics close to a degenerate point with the blow-up method can be easily split in the following steps:

1. Find a suitable map to desingularize the fold point: the aim in this step is to find the coefficients a_i for the quasi-homogeneous map Γ.

2. Find charts to express the blow-up in local coordinates: this point depends on the physics and on the particular case considered. Indeed not all the charts can be useful to analyse. The aim is to find which charts should be meaningful and determine for the the local map μ_i.

3. Calculate all the local data of the problem. Once the chart κ_i has been defined, the transition map from one chart to the other one κ_{ij} and the dynamics on each chart κ_i should be computed.

4. Investigate the dynamics of the blown-up vector field. This is the most important point, and that's why all the blow-up method is made up. The analysis on the blown-up vector field on each chart should give a complete understanding of the behaviour of the system close to the non-hyperbolic point.

5. Connect the results from the different charts and 'blow-down'. Once the analysis of the blown-up vector field has been performed, and the interaction between the dynamics on each chart has been understood is time to blow-down and remember that all the things computed are valid only very close to the degenerate point, and they are only local results.

Chapter 4

Dynamics of Non-Newtonian fluids

In this chapter the geometric singular perturbation theory and the blow-up method are applied to the analysis of the dynamics of non-Newtonian fluids. This analysis is based on a paper by Renardy [Ren10] and the main goal is to complete Renardy's results and make his statements more precise. It will be shown that the slow-fast formulation and the use of the blow-up method are key tools to have a complete understanding of the dynamics.

Section 4.1 introduces the difference between Newtonian and non-Newtonian fluids. In particular the Bingham fluids are presented. The next section 4.2 extends the concept of Bingham fluid to explain the behaviour of thixotropic yield stress materials. Section 4.3 describes the constitutive equation for visco-elastic fluids and introduces the PEC model. In section 4.4 the equations for the PEC model are re-written as a slow fast system introducing proper variables. It is shown how the results can be interpreted considering the GSPT theory and the next section 4.5 analyse the corresponding layer and reduced problem. In section 4.6 it is shown that the system considered in section 4.4 is not enough to understand the global dynamics and a proper time rescale is performed. For this new system the blow-up method is used in section 4.7 to study the degenerate point in the origin. Two different charts are needed to get a complete overview and the analysis of the solution at the singular case is performed in section 4.9. Finally in section 4.10 the conclusion for the singular perturbed system are shown.

4.1 Introduction

Many industrial processes deal with fluid dynamics. These processes have to take into account the physical properties of the fluid in use in order to have optimal working condition. One of the most important fluid properties for an industrial point of view is fluid viscosity. Fluids can be classified depending on viscosity as Newtonian or non-Newtonian.

4.1.1 Newtonian fluids

A fluid is said to be Newtonian if the stress at each point is linearly proportional to its strain rate at that point. Most of the commonly used fluids like water and air behave as Newtonian fluid.

In this chapter the terms shear stress τ, shear viscosity η, and shear strain κ will be used quite often. In order to understand their meaning, the following example is presented.
Consider the case of an incompressible and isotropic Newtonian fluid on a plane (x, y). Suppose that the fluid is limited by two plates for $y = 0$ and $y = Y$ as it is shown in figure 4.1 on the top. Moreover assume that the upper plate is moving along the x direction with a velocity U. The no-slip condition on the boundary requires that the fluid has zero velocity on the lower plate and the velocity U on the upper plate for $y = Y$. Since the fluid is Newtonian, then the strain rate has to be a linear function along the y axis. The stress - strain rate relation for this fluid is the following

$$\tau = \eta\kappa \tag{4.1}$$

with τ the shear stress in the fluid, η the shear viscosity of the fluid and $\kappa = \frac{du}{dy}$ the shear rate, i.e. the variation of the velocity in the direction of the shear x relative to displacement in the perpendicular direction y. As it is possible to note in figure 4.1 on the top a Newtonian fluid has constant shear viscosity η, which can be interpreted as a constant slope on the variation of the displacement arrows. A second interpretation of the shear stress τ is given in figure 4.1 on the bottom. Indeed considering the continuum mechanics point of view, it is possible to take a squared piece of material which is deformed under the shear stress τ to a different form. Note that τ is the stress acting on the direction of the flow x but on the surface perpendicular to y.

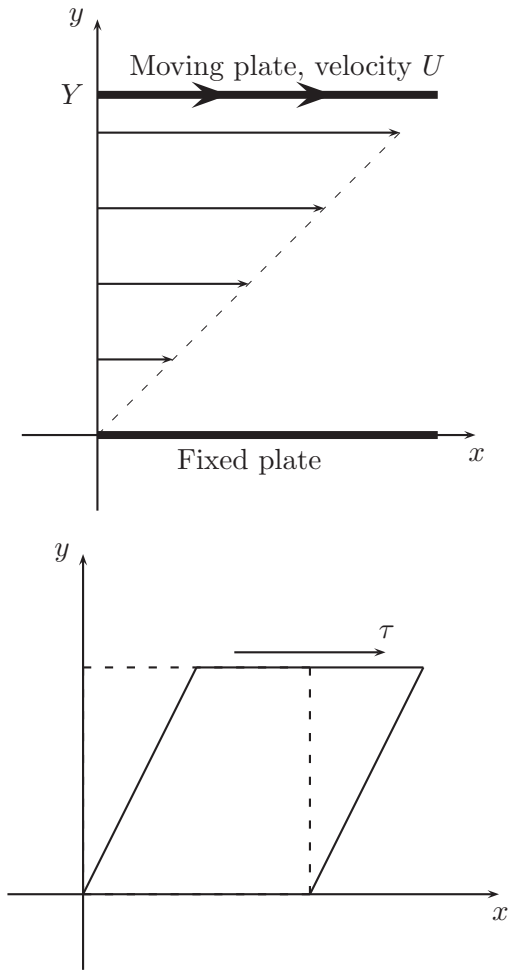

Figure 4.1: Shear flow for a Newtonian fluid.

4.1.2 Non-Newtonian fluids

Not all fluids exhibit a Newtonian behaviour. Slurries for instance, biological fluids such as blood and saliva and many fluids in cosmetic and food industry are non-Newtonian. Depending on the stress - strain relation it is possible to classify these fluids in different classes as it is shown in figure (4.2).

- **Thixotropic fluids** are fluids that exhibits **shear thinning**, which means that their shear viscosity decreases for increasing values of the shear stress

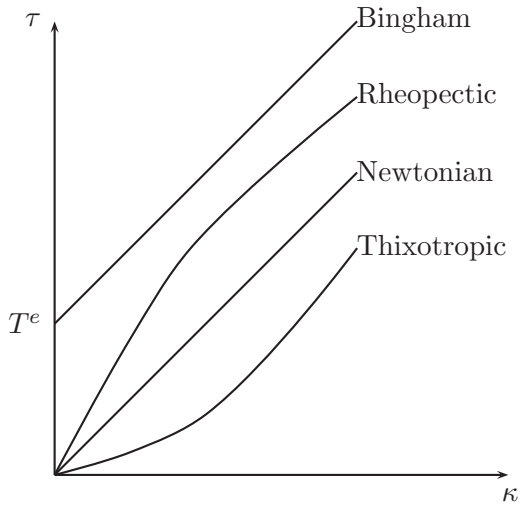

Figure 4.2: Classification of fluids depending on the stress-strain rate relationship.

applied. A common example of this category of fluids is ketchup, indeed when ketchup is flowing a small increase in the shear stress makes large increases in the shear strain. Note that ketchup has also a non zero stress for which it starts flowing (the yield stress), since it is common experience that to make ketchup flow it is needed to shake the bottle at the beginning.

- **Rheopectic fluids** are fluids that exhibits **shear thickening**, which means that their shear viscosity increases for increasing values of the shear stress applied. A common example of this category of fluids is oobleck: a mixture of corn starch and water. If oobleck is stirred slowly than it behaves as a viscous liquid, but if it is stirred fast then it has a solid-like behaviour. Figure 4.3 shows oobleck's behaviour depending on the stress applied. Another example of rheopectic fluid is quicksand, and that's why moving a lot inside of it makes getting out of quicksand harder.

- **Bingham fluids** have a linear stress-strain relationship, but an initial value of stress has to be applied (the **yield stress**) in order to let the fluid flow. These fluids have solid-like behaviour for low values of the applied stress. However, when a certain threshold of stress T^e, called the yield stress is applied, they start flowing as visco-elastic fluids [Bar99]. On a molecular point of view, the yield stress can be understood as the minimum stress required to enable flow or fracture due to the breakdown or alteration of a

materials microstructure [ST04]. The stress - strain relation for a Bingham fluid can be written as

$$\begin{aligned} \tau &= 0 && \tau < T^e \\ \tau &= T^e + \eta\kappa, && \tau \geq T^e \end{aligned}$$

However, recent studies have shown that Bingham fluids are only an idealization of yield stress fluids [BW85], since different experiments show phenomena that are out of the Bingham world. For instance, stress overshoot can appear, and many fluids show time-dependent viscosity. The focus of the next sections is to study a model for non-Bingham fluids with time-dependent viscosity.

Figure 4.3: Demonstration of oobleck's behaviour depending on the stress applied. Figure for `http://junior2m.global2.vic.edu.au`.

4.2 Extending Bingham fluids

In the previous section, it has been claimed that Bingham fluids are only an idealization of yield stress fluids, and in general yield stress fluids present behaviours which are not described by the Bingham model. This section and the next ones will focus on the particular problem of defining the yield stress for thixotropic yield stress fluids with time dependent viscosity.

Thixotropic yield stress fluids are industrially relevant and in particular they are very common in food and cosmetic industry. Common examples are concentrated suspensions, pastes, foodstuffs, emulsions, foams, and composites [NB92]. Toothpaste, ketchup and ice-cream belong as well to this class of materials [Ren10].

The industrial reasons to study the behaviour of these fluids at stress values close to the yield stress are to improve processing manufacturing, stability and consumer sensory perception during application or use of a product [ST04]. Moreover the analysis of yield stress fluids is of importance to understand the shear localization and fracture that can appear in these continuum material for values of stress applied lower than the yield stress. The way to understand shear localization and fracture experimentally is to perform creep experiments. These experiments are very hard to perform close to the yield stress because of the difficulty in defining what the yield stress is for these fluids.

For thixotropic yield stress fluids there have been several attempts in defining the value of the yield stress, but this task has resulted to be more challenging than expected [Che86]. At the state of the art, an exhaustive definition of yield stress for thixotropic yield stress fluids is still missing. There is a school of thought supported by Barnes in [BW85] which believes that yield stress doesn't exists and it is only a myth: for any value of stress lower than T^e it is sufficient to wait enough long time and the material will flow as a visco-elastic fluid sooner or later. There is a second school of thought [CB08], [NB92] which believes instead that yield stress is a non zero value, even though in this case it is very hard to define it, especially with experiments.

What can be deducted from the experiments is summed up in the following:

- Thixotropic yield stress fluids have solid-like behaviour (elastic deformation) for slow values of the stress applied and short times.
- For intermediate values of the stress applied which are still smaller than the yield stress and for long times, the fluid exhibits relaxation behaviour, which is often called aging. This means that waiting long enough times the material will start flowing, even though the shear stress applied is smaller than the yield stress. In the literature this behaviour is referred as the "slow" flow.
- Finally for values of stress bigger than the yield stress, the material flows as a visco-elastic fluid [CB08], [NB92]. In the literature this behaviour is referred as the "fast" flow.

A recent work by Renardy [Ren10] has formulated a model which can analyse these kind of fluids. In this model the yield stress behaviour appears as the limiting case of the non-monotone constitutive theory. The constitutive model has two

contributions to the stress: a visco-elastic contribution with relaxation time going to infinity and a Newtonian contribution. The PEC model is considered to describe the flow dynamics and the particular case of steady shear flow is studied. In the paper Renardy takes seriously the assertion by Barnes that yield stress is a myth, but he is able to show that for his model the yield stress exists and has a value different from zero. Its model has very accurate results compared to some experimental analysis [CB08].

4.3 Constitutive equations for visco-elastic fluids

In this section the constitutive equations for a thixotropic yield stress fluid are presented. For these materials two possible formulations are possible: the first considers the material as constituted of polymer chains with many degrees of freedom. The second formulation instead models the material as a continuum, using the equations of continuum mechanics. The constitutive equations hereby presented follow the second formulation, but sometimes it is referred to the first formulation to justify the assumptions made. It is not the purpose of this thesis to make a complete theoretical description of how to model the constitutive equations for visco-elastic fluids and therefore the main results are only presented. The kinematics equations for continuum solid mechanics are presented in Appendix B.

We consider to model the thixotropic yield stress fluids as done by Renardy in [Ren10]. In this paper it is supposed that two contribution to the stress are acting: a Newtonian contribution for the unyielded flow and a visco-elastic contribution with relaxation time going to infinity to describe the yielded status.

- **Unyielded flow:** It is supposed that the unyielded flow is Newtonian. In the general case the Newtonian stress - strain relation presented in equation (4.1), give a contribution to the stress tensor of the form

$$S = \eta(\nabla v + (\nabla v)^T) \tag{4.2}$$

  with v the velocity vector of the particle at a certain point. This contribution will be the most important one for large times when the fluid is unyielded. Note that this is only an approximation, since a thixotropic yield stress fluid does not behave exactly as a Newtonian fluid when unyielded.

- **Yielded behaviour:** In order to model the behaviour of the material for stress values close to the yield stress, we consider a second contribution to the stress tensor, which is given in terms of a conformation[1] tensor C

$$T = \psi(\mathrm{tr}C)C \tag{4.3}$$

[1]The conformation tensor C is also known in the literature as the configuration tensor, especially in the chemists community. However, since in Lagrangian mechanics the term configuration

The conformation tensor is a measure of the micro-structural state of the material and it can be understood as a descriptor of the local deformation of the material due to the stress application [Agg07]. When considering a fluid composed of polymer chains, C can be seen as a descriptor of the polymer chain shape in the current configuration [FS05]. This tensor is symmetric and positive definite, and if $C = \mathbb{I}$ then the fluid is in equilibrium, i.e. no stress has been applied $T = 0$. As suggested by Hulsen in [Hul14] the conformation tensor C has the same meaning of the remaining elastic Finger strain, i.e. $C = L$, which is presented in Appendix B. The difference is that the conformation tensor describes the deformations at a molecular level while the Finger strain describes the macrostructural deformation. Note that equation (4.3) describe a relation between the microscopic deformations and the macroscopic shear stress applied.

In the present work the conformation tensor is assumed to satisfy an equation of the type

$$C^{\nabla} + \varepsilon(\phi(\mathrm{tr}C)C - \chi(\mathrm{tr}C)\mathbb{I}) = 0 \tag{4.4}$$

with C^{∇} the upper convected derivative[2] defined as

$$C^{\nabla} = \frac{DC}{Dt} - (\nabla v)^T \cdot C - C \cdot (\nabla v)$$

with $\varepsilon \ll 1$ having the meaning of a relaxation rate.

Equation (4.4) describes what is the microscopical evolution of the material deformation and it is able to describe the relaxation behaviour of the material that appears for values of the stress lower than the yield stress and long enough times. This equation has been derived by the dumbbell model for dilute polymer solutions [Ren10]. A theoretical explanation of the Dumbbell model can be found in [Can10], [BE94], [HO97].

The dynamics of the visco-elastic material under the stress T is supposed to satisfy the PEC model which can be written in general as

$$T^{\nabla} + aT - b\mathbb{I} + c\mathrm{tr}((\nabla v)T)T = 0 \tag{4.5}$$

with a, b, c constants. The PEC model, also called Partially Extended Convective strand is a constitutive equation proposed by Larson in 1984 [Lar84]. This equation can describe steady and transient shear flow at the limit case of single visco-elastic species in which the functional form of the breakage rate of the long polymer chains is described by a nonlinear function [ZVCM08]. This equation is the constitutive

is used to describe the state of the system at a certain point and time, in general it is preferred to use the term conformation instead.

[2]The upper convected derivative has the meaning of the rate of change of the tensor properties when written in the local element coordinate system which is rotating and stretching with the fluid. Note that instead $\frac{D}{Dt}$ is the total derivative considering the reference coordinate system, and that's why we are subtracting the other two quantities.

equation for the material, and it describes the variation along time and space of the macroscopic stress in the fluid.

Reformulating the PEC model (4.5) in terms of the conformation tensor C with the use of equation (4.4) is is possible to obtain the constitutive equation for C.

4.4 Non-Newtonian fluids are a slow-fast system

Consider the PEC model for Non-Newtonian fluids in case of constant total shear stress. It is assumed as in [Ren10] that the stress acting on the material has two components: the shear stress[3] T_{12} related to the unyielded behaviour and a Newtonian component $\eta\kappa$.

$$\tau = T_{12} + \eta\kappa \tag{4.6}$$

Moreover suppose the shear flow to be planar and suppose the relaxation time $\varepsilon \ll 1$. The conformation tensor satisfies the equations

$$\begin{aligned} \dot{C}_{11} &= 2\frac{\tau - \psi(s)C_{12}}{\eta}C_{12} + \varepsilon\phi(s)(1 - C_{11}), \\ \dot{C}_{12} &= \frac{\tau - \psi(s)C_{12}}{\eta} - \varepsilon\phi(s)C_{12} \end{aligned} \tag{4.7}$$

with

$$s = C_{11} + 2, \quad \psi(s) = \frac{k_1}{s + \alpha}, \quad \phi(s) = k_2(s + \alpha),$$

$\alpha \geq -2$ and k_1, k_2, η positive constants. The dot means derivative respect to the time t. The direction "1" is the flow direction, while the direction "2" is the one of the velocity gradient. The initial conditions of the fluid at rest for the Cauchy problem (4.7) is then $(C_{11}, C_{12})_0 = (1, 0)$, in order to require no shear flow.

Introduce the new variable $D = C_{11} - C_{12}^2$, thus its derivative is $\dot{D} = \dot{C}_{11} - 2C_{12}\dot{C}_{12}$. The system (4.7), can be rewritten as a slow-fast system as

$$\begin{aligned} \dot{D} &= \varepsilon f(D, C_{12}, \varepsilon), \\ \dot{C}_{12} &= g(D, C_{12}, \varepsilon) \end{aligned} \tag{4.8}$$

[3]The notation of T_{12} is the standard notation for three dimensional stress tensors. The first index on the subscript is the direction along which the stress is acting $1 = x$, and the second index stands for the normal direction to the surface the stress is acting on $2 = y$.

with the slow and fast vector fields given by

$$\begin{aligned} f(D, C_{12}, \varepsilon) &= \phi(s)(1 - D + C_{12}^2), \\ g(D, C_{12}, \varepsilon) &= \frac{\tau - \psi(s) C_{12}}{\eta} - \varepsilon \phi(s) C_{12} \end{aligned} \tag{4.9}$$

Note that in the new variables (D, C_{12}) the quantity s is defined by $s = D + C_{12}^2 + 2$. In these new coordinates D is the slow variable, while C_{12} is the fast one.

By a time rescale $\tilde{t} = \varepsilon t$, it is possible to rewrite the fast system (4.8) as the slow system

$$\begin{aligned} D' &= f(D, C_{12}, \varepsilon), \\ \varepsilon C_{12}' &= g(D, C_{12}, \varepsilon) \end{aligned} \tag{4.10}$$

where the $'$ means derivative respect to the slow time $\tilde{t}$.

4.5 Analysis of the singular limit

As is has been introduced in chapter 2, the singular limit can be studied either for the fast or for the slow system of equation respectively (4.8) and (4.10). These two different analysis are very useful in order to obtain a description of the dynamics for $\varepsilon \neq 0$ but small using the general results of singular perturbation theory.

4.5.1 Fast dynamics

The layer problem is obtained setting $\varepsilon = 0$ on the fast system (4.8)

$$\begin{aligned} \dot{D} &= 0, \\ \dot{C}_{12} &= \frac{\tau - \psi(s) C_{12}}{\eta} \end{aligned} \tag{4.11}$$

The critical manifold S is identified as the set of fixed points for the layer problem $C_0 = \{(D, C_{12}) : g(D, C_{12}, 0) = 0\}$. The set is then determined by the two parabolic branches

$$C_{12} = \frac{k_1 \pm \sqrt{k_1^2 - 4\tau^2(\alpha + D + 2)}}{2\tau} \tag{4.12}$$

which equals at the maximum point $F : (D, C_{12})_{max} = (\frac{k_1}{2\tau}, \frac{k_1^2 - 4\tau^2(\alpha+2)}{4\tau^2})$.

In order to study the stability of the fixed points of the critical manifold, the first derivative is computed

$$\left(\frac{\partial g}{\partial C_{12}}\right)_{C_0} = 2\tau C_{12} - k_1 > 0 \quad \Rightarrow \quad C_{12} > \frac{k_1}{2\tau} = C_{12,max}$$

The points on the right branch of the critical manifold are repelling while the points on the left branch are attracting. Figure 4.4 shows the critical manifold C_0 and its stability properties.

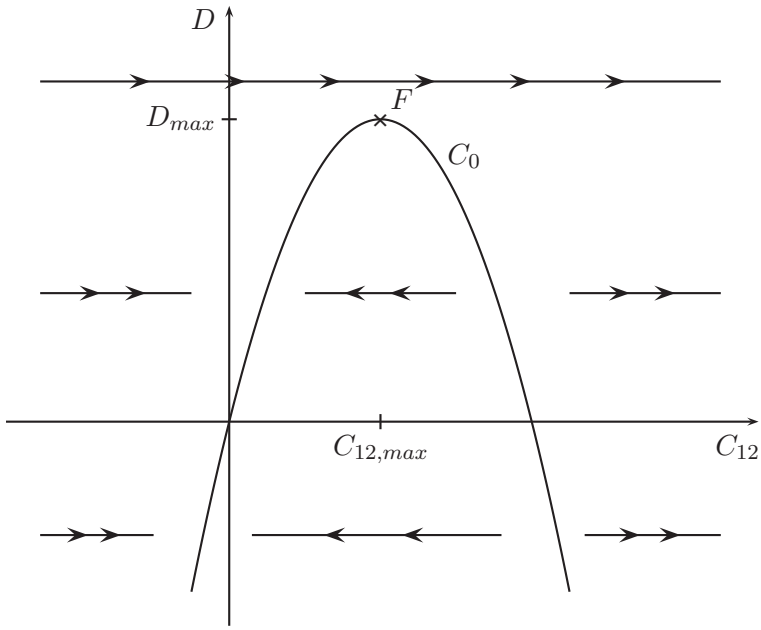

Figure 4.4: Dynamics of the fast system (4.8). It is possible to note that the plane (D, C_{12}) is foliated by a family of curves for D constant. This curves are called fibers and have base points on the critical manifold C_0. The left branch of the critical manifold is attracting, the right one is repelling.

The point of maximum $C_{12} = \frac{k_1}{2\tau}$ is non-hyperbolic and in particular it is a fold. Indeed

$$\left(\frac{\partial g}{\partial C_{12}}\right)_F = 0, \quad \left(\frac{\partial^2 g}{\partial C_{12}^2}\right)_F \neq 0, \quad \left(\frac{\partial g}{\partial D}\right)_F \neq 0$$

with the subscript F meaning that the derivatives have been computed on the fold of the critical manifold $F : (D, C_{12})_{max} = (\frac{k_1}{2\tau}, \frac{k_1^2 - 4\tau^2(\alpha+2)}{4\tau^2})$.

4.5.2 Fixed points

We look for fixed points of the system (4.8). In the case of $\varepsilon = 0$ these points, if they exists, are given by the intersection of the two conditions

$$\begin{array}{l} f(D, C_{12}, 0) = 0, \\ g(D, C_{12}, 0) = 0 \end{array} \quad \Rightarrow \quad \begin{array}{l} D = C_{12}^2 + 1, \\ \tau(D + C_{12}^2 + 2 + \alpha) - k_1 C_{12} = 0 \end{array} \tag{4.13}$$

Substituting the second equation in the first one we get the following condition

$$2\tau C_{12}^2 - k_1 C_{12} + \tau(3 + \alpha) = 0$$

which is satisfied by

$$P_{eq}^{(\pm)} = (D_{eq}^{(\pm)}, C_{12,eq}^{(\pm)}) : \quad \begin{array}{l} D_{eq}^{(\pm)} = \left[\dfrac{k_1 \pm \sqrt{k_1^2 - 8\tau^2(3+\alpha)}}{4\tau} \right]^2 + 1, \\ C_{12,eq}^{(\pm)} = \dfrac{k_1 \pm \sqrt{k_1^2 - 8\tau^2(3+\alpha)}}{4\tau} \end{array} \tag{4.14}$$

The two fixed points $P_{eq}^{(\pm)}$ exists only in the case that the radicand is positive, i.e.

$$\tau \leq \frac{k_1}{2\sqrt{2(3+\alpha)}} = T_{12}^M$$

which is the maximum value of the elastic shear stress T_{12}, as introduced in [Ren10]. This means that up to this value the fluid maintains the elastic properties as if it was a solid and it doesn't have any shear flow solution. From (4.14) it is possible to note that $D_{eq}^{(\pm)} \geq 1$ and $C_{12,eq}^{(\pm)} \geq 0$ and that the two equilibrium points can never coincide with the fold point of the critical manifold F but they always lie both at its left side, i.e. $C_{12,max} > C_{12,eq}^{(\pm)}$. The two fixed points $P_{eq}^{(\pm)}$ are shown in figure 4.5 along with the conditions $f(D, C_{12}, 0) = 0$ and $g(D, C_{12}, 0) = 0$.

The fixed points $P_{eq}^{(\pm)}$ are preserved for $\varepsilon \neq 0$. Indeed the vector fields f, g defined in (4.9) are such that

- the vector field f does not depend upon ε, thus

$$f(D, C_{12}, \varepsilon) = 0 \iff f(D, C_{12}, 0) = 0 \quad \Rightarrow \quad D = C_{12}^2 + 1$$

- the vector field g has the terms on ε appearing as regular perturbation terms. Thus using an implicit function theorem, it is possible to show that these

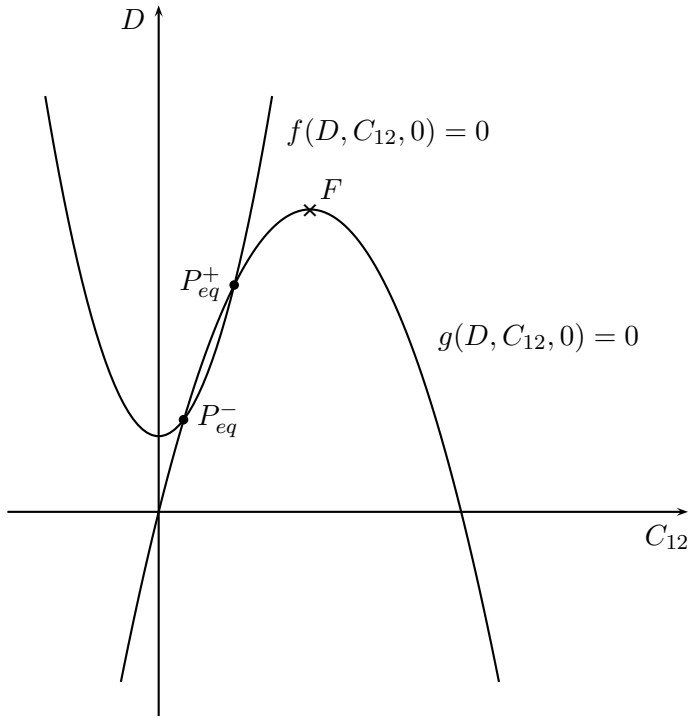

Figure 4.5: Fixed point of the slow-fast system (4.8) for $\varepsilon = 0$.

fixed points are only slightly modified and they preserve the same stability properties. Indeed

$$g(D_{eq}^{(\pm)}, C_{12,eq}^{(\pm)}, 0) = 0, \quad \frac{\partial g}{\partial \varepsilon}(D_{eq}^{(\pm)}, C_{12,eq}^{(\pm)}, 0) \neq 0$$

then by the implicit function theorem there exists a set $E \subset \mathbb{R}$, $0 \in E$ and functions $h, j : \mathbb{R} \to \mathbb{R}$ such that $h(0) = D_{eq}^{(\pm)}$, $j(0) = C_{12,eq}^{(\pm)}$ and such that for $\varepsilon \in E$ we have $g(h(\varepsilon), j(\varepsilon), \varepsilon) = 0$. This last condition means that the vector field g is stationary for $\varepsilon \neq$ in points that are $\mathcal{O}(\varepsilon)$-close to $P_{eq}^{(\pm)}$.

Thus for $\varepsilon \neq 0$ and for a value of the shear stress τ sufficiently small the two equilibrium points $P_{eq}^{(\pm)}$ are preserved.

4.5.3 Slow dynamics

The dynamics for the reduced problem is given by equation (4.10) as

$$\begin{aligned} D' &= f(D, C_{12}, 0), \\ 0 &= g(D, C_{12}, 0) \end{aligned}$$

This is a differential-algebraic equation, which describes the evolution of the slow flow on the constraint described by the critical manifold. The critical manifold has been explicated in equation (4.12) as a function $C_{12}(D)$, which are two parabolic branches. The constrained problem (4.10) can be studied as a one-dimensional ODE

$$D' = f(D, C_{12}(D), 0)$$

Since the critical manifold is a line, the flow direction on it can change only when there are fixed points. Thus it is sufficient to understand the linearized dynamics close to the fixed points $P_{eq}^{(\pm)}$ described by equation (4.14). Remember that the condition of existence of the fixed points $P_{eq}^{(\pm)}$ is $\tau \leq T_{12}^{M}$.

We can compute the first derivative in the fixed point and thus see the value of the eigenvalues to determine the stability properties.

$$\left(\frac{df}{dD}\right)_{D_{eq}^{(\pm)}} = \left[\frac{\partial f}{\partial D} + \frac{\partial f}{\partial C_{12}}\frac{\partial C_{12}}{\partial D}\right]_{D_{eq}^{(\pm)}}$$

The first derivative of function f in the generic point $(D, C_{12}(D), 0)$ on the left parabolic branch is given by

$$\frac{df}{dD} = -\frac{k_1 k_2}{\tau^2}\left(\frac{\tau^2(9 + 6D + 5\alpha) - 2k_1^2 + 2k_1\sqrt{k_1^2 - 4\tau^2(D + \alpha + 2)}}{\sqrt{k_1^2 - 4\tau^2(D + \alpha + 2)}}\right)$$

Computing this quantity in $D_{eq}^{(\pm)}$ we obtain that the leftmost equilibrium is stable, i.e. $\left(\frac{df}{dD}\right)_{D_{eq}^{-}} < 0$, while the rightmost is unstable. The slow dynamics along the critical manifold is depicted in figure 4.6.

For the same argument presented in section 4.5.1 the stability properties of $P_{eq}^{(\pm)}$ are preserved for $\varepsilon \neq 0$ small and $\tau < T_{12}^{M}$.

4.5.4 Conclusion on the dynamics for $\varepsilon \neq 0$

For $\varepsilon \neq 0$ the Fenichel's theorem 2.5 presented in chapter 2 holds when we are far enough from the non-hyperbolic point F. Where Fenichel's theorem holds then

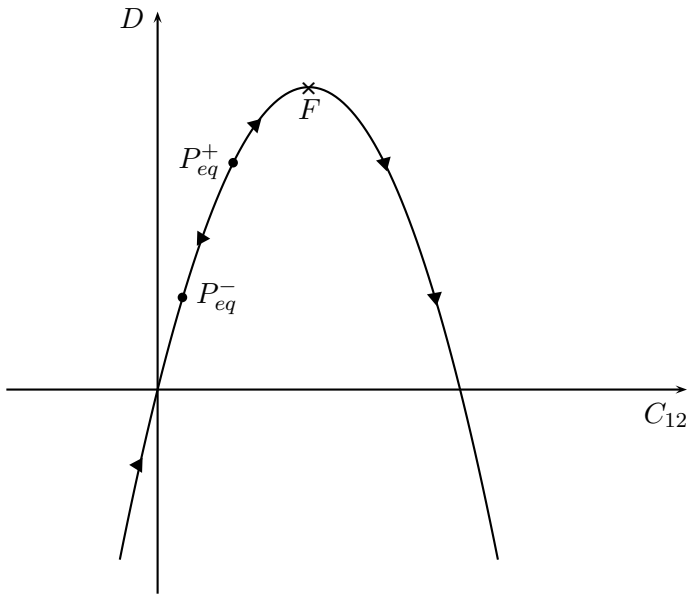

Figure 4.6: Slow flow along the critical manifold C_0. The leftmost equilibria P_{eq}^{-} is stable, while the rightmost P_{eq}^{-} is unstable.

we know that a compact submanifold S_0 of the critical manifold C_0 is perturbed on a compact locally invariant manifold S_ε, $\mathcal{O}(\varepsilon)$-close to S_0 which is called the slow manifold. The flow on the slow manifold converges to the slow flow on S_0 defined by (5.11) for $\varepsilon \to 0$. Moreover the same conclusions holds for the stable and unstable manifolds of S_0.

We are interested in the study of the evolution of the flow for different values of the shear stress τ applied with the initial condition of fluid at rest, i.e. $(D, C_{12})_0 = (1, 0)$. Depending on the value of τ different cases can appear:

$\tau > T_{12}^{M}$: The slow manifold S_ε has no fixed points. Depending on whether $D_0 > D_{max}$ or not two cases can appear. This last condition can be rephrased as a condition on the shear stress τ, thus the following system of condition is obtained

$$\begin{array}{c} \tau > T_{12}^{M} \\ D_0 > D_{max} \end{array} \quad \Rightarrow \quad \begin{array}{l} \tau > \dfrac{k_1}{2\sqrt{2(3+\alpha)}} \\ \tau > \dfrac{k_1}{2} = T^e \end{array}$$

$\tau > T^e$: In this case Fenichel's theorem 2.5 holds because the solution is evolving along the fast fiber $(1, C_{12})$, and by hypothesis $1 > D_{max}$. Thus the

solution is always far enough from the fold point F. Note that the conclusion that the solution evolves along the fast fiber $(1, C_{12})$ is valid only locally, i.e. for $\varepsilon C_{12} \sim \mathcal{O}(\varepsilon)$. For large values of C_{12} the term in ε on the vector field $g(D, C_{12}, \varepsilon)$ of equation (4.9) cannot be neglected when defining of the critical manifold. This case is presented in figure 4.7.

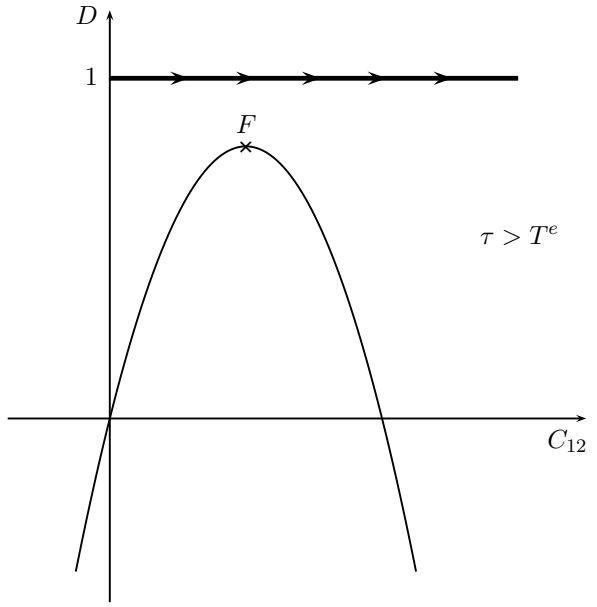

Figure 4.7: Case of $\tau > T^e$. This is the "fast" flow case. Fenichel's theory is enough to study this case for low values of C_{12}.

Note that there is an incongruence with what claimed by Renardy in [Ren10]. Indeed Renardy claims that the maximum value of stress for elastic solid behaviour is $T^e_{12} = \frac{k_1}{2\sqrt{3+\alpha}}$. This value has to be understood as the minimum stress required to make the fluid flow as a "fast" flow. The value found for this project is instead for $D_0 > D_{max}$ and is given by $T^e = \frac{k_1}{2} > T^e_{12}$. In Renardy's paper [Ren10] there is a lack of information on how the stress T^e_{12} has been computed for the PEC model. Moreover there is short supply on the use of the PEC model in this context, thus it is not possible to conclude the reason of this incongruence.

However Renardy's paper agrees on the position of the fold point F : $(D, C_{12})_{max}$. For the slow-fast formulation and the results by Krupa and Szmolyan [KS01a], we conclude that T^e has to be the true maximum elastic shear strain.

$T_{12}^M < \tau \leq T^e$: In this case $1 < D_{max}$, thus for Fenichel's theorem 2.5 the solution evolves along the fast fiber $(1, C_{12})$ until it is $\mathcal{O}(\varepsilon)$-close to the critical manifold C_0. At this point the solution evolves along the slow manifold S_ε towards the fold point F. Once the solution is $\mathcal{O}(\varepsilon)$-close to the point F, the results by Fenichel are not valid anymore. However, the paper by Krupa and Szmolyan [KS01a] shows that the solution will pass ε-close to the fold point and continue evolving $\mathcal{O}(\varepsilon)$-close to the fast fiber (D_{max}, C_{12}) with base point in the fold F. This evolution is valid up to large values of C_{12}. This case is presented in figure 4.8. This case explains the relaxation behaviour of thixotropic yields stress fluids. Indeed this is the "slow flow" case introduced in section 4.2 which was saying that waiting long enough times the material will start flowing, even though the shear stress applied is smaller than the yield stress T^e. From figure 4.8 it is straightforward to understand the reason why the observer has to wait very long times: indeed the solution is evolving along the slow manifold with a velocity of order of ε.

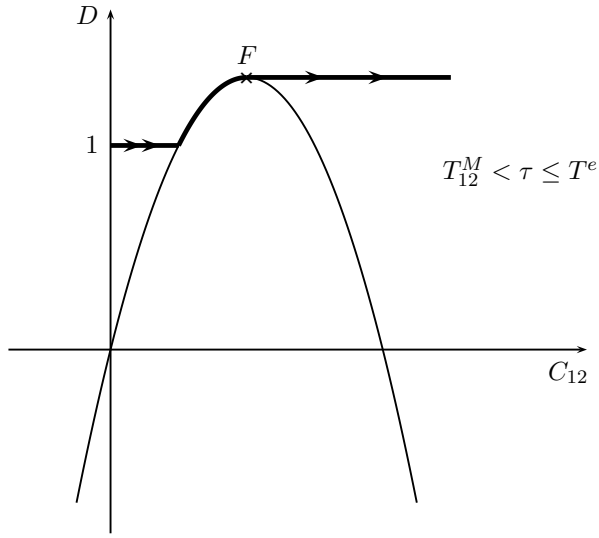

Figure 4.8: Case of $T_{12}^M < \tau < T^e$. The fluid exhibits relation behaviour and the results by Krupa and Szmolyan [KS01a] are necessary to understand the flow dynamics for low values of C_{12}.

$\tau \leq T_{12}^M$: The slow manifold has two fixed points $P_{eq}^{(\pm)}$. Moreover from equation (4.14) it is easy to see that $D_{eq}^+ > 1 = D_0$. Thus from Fenichel's theory the solution will move $\mathcal{O}(\varepsilon)$-close to the fast fiber $(1, C_{12})$ towards the left branch of the critical manifold C_0. When the trajectory is $\mathcal{O}(\varepsilon)$-close to it then it will follow the dynamics on the slow manifold S_ε pointing towards the stable

equilibrium $\mathcal{O}(\varepsilon)$-close to P_{eq}^{-}. This last case is presented in figure 4.9.

The physical meaning of this solution is that the applied shear stress τ is not large enough to make the fluid flow, and the material shows as an elastic solid behaviour.

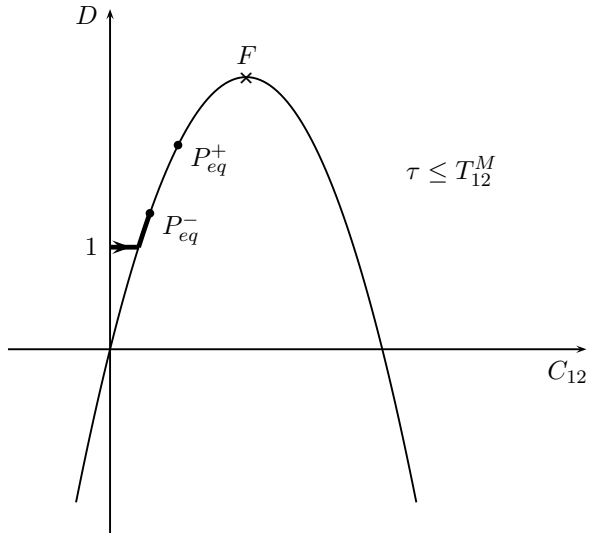

Figure 4.9: Case of $\tau \leq T_{12}^{M}$. This case is the elastic solid behaviour. Fenichel's theory is enough to study this case.

Note that the critical manifold C_0 has been defined for $\varepsilon = 0$. Thus in the two cases depicted in figures 4.7 and 4.8 for large values of C_{12} it is necessary to consider the effect of the perturbation $\mathcal{O}(\varepsilon)$ as well acting on the vector field g defined in (4.9). Indeed for large values of C_{12} it is not possible to say that the solution will keep evolving on the fast fiber $(1, C_{12})$ because the $\mathcal{O}(\varepsilon)$ terms will become relevant for the evolution of the system. Note moreover that the ideal evolution of the solution on the fast fiber $(1, C_{12})$ up to very large values of C_{12} does not make any physical sense because it would mean that the shear deformation would keep increasing up to infinity.

Thus the dynamics of thixotropic yield stress fluids cannot be completely understood only by the use of GSPT on the slow-fast system (4.8), but it is necessary to study the large scale dynamics as well. This analysis is performed in the next section 4.6.

A numerical integration of the fast system (4.8) has been performed. Figure 4.10 shows the two cases of $\tau \leq T_{12}^{M}$ and $\tau > T_{12}^{M}$ in the slow fast coordinates (D, C_{12}).

As it is possible to see these plots are consistent with the figures 4.9 and 4.8. Indeed for $\tau \leq T_{12}^M$ the solution evolves fast on the fiber $(1, C_{12})$ until it approaches the critical manifold and then it evolves slowly to the stable fixed point P_{eq}^-. Thus the fluid is behaving as an elastic solid.

In the second case of $\tau > T_{12}^M$ it is possible to note that the numerics agrees with the results by Krupa and Szmolyan [KS01a]. Indeed, the solution evolves along the fast fiber until it approaches the critical manifold. Then it evolves slowly on the critical manifold until it gets close to the fold point. After this it continues evolving on the fast fiber (D_{max}, C_{12}) but then for higher values of C_{12} we can see that the dynamics evolves on a different trajectory which is not expected by the slow-fast analysis. It is interesting to note that the dynamics is going to end up in a fixed point, which looks to be attracting, and it has the physical meaning of the steady state solution, which is that the shear stress is constant along the fluid.

Figure 4.11 shows the same numerical analysis in the (C_{12}, s) coordinates, with $s = C_{11} + 2$ as done by Renardy in [Ren10]. It is possible to make a comparison between figures 4.11 and 4.12, where the second one shows Renardy's results. The two analysis are completely consistent. By the way for the case of $\tau > T_{12}^M$ Renardy has stopped the numerical simulation before obtaining the large scale dynamics behaviour.

As a remark we would like to note that bullet point 4 in Renardy's paper [Ren10] at page 523 is not well written. Indeed it is possible to restate that bullet point in this project's language as saying that P_{eq}^- is repelling, while P_{eq}^+ is attracting. But as it has been shown in section 4.5.3, it is exactly the opposite.

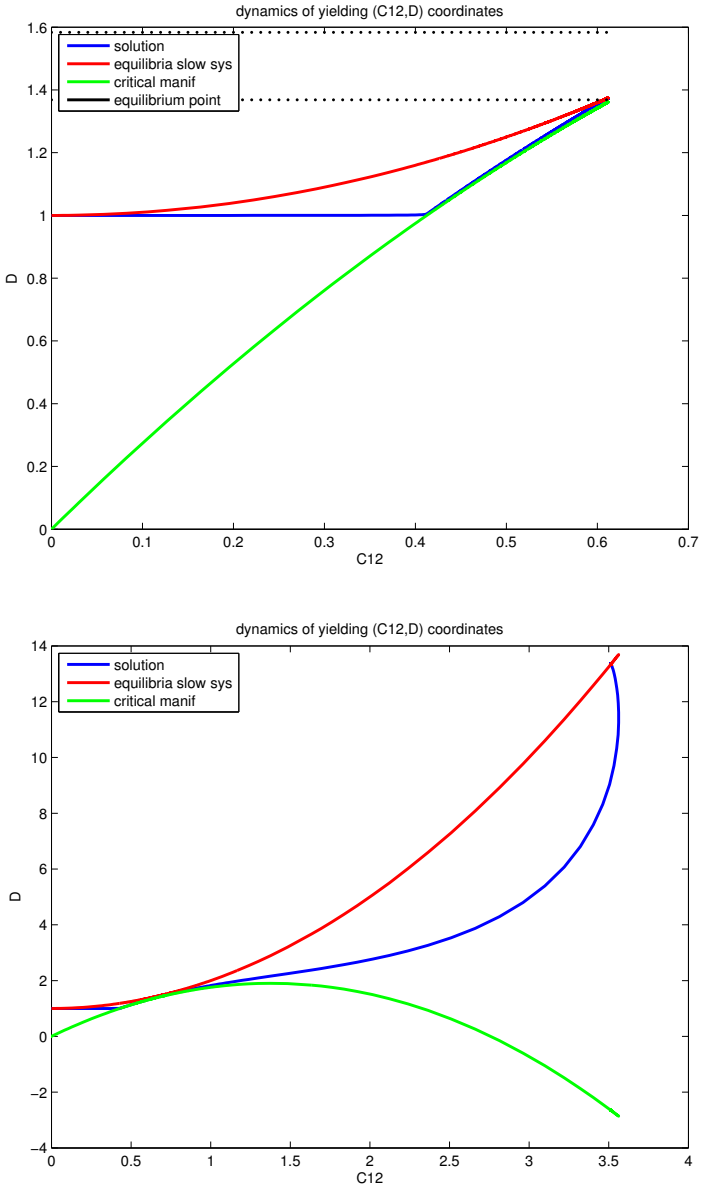

Figure 4.10: The numerical integration of equation (4.8) for $\tau \leq T_{12}^M$ is shown by the blue line. The red line is the condition $f(D, C_{12}, 0) = 0$ while the green line is the condition $g(D, C_{12}, 0) = 0$.

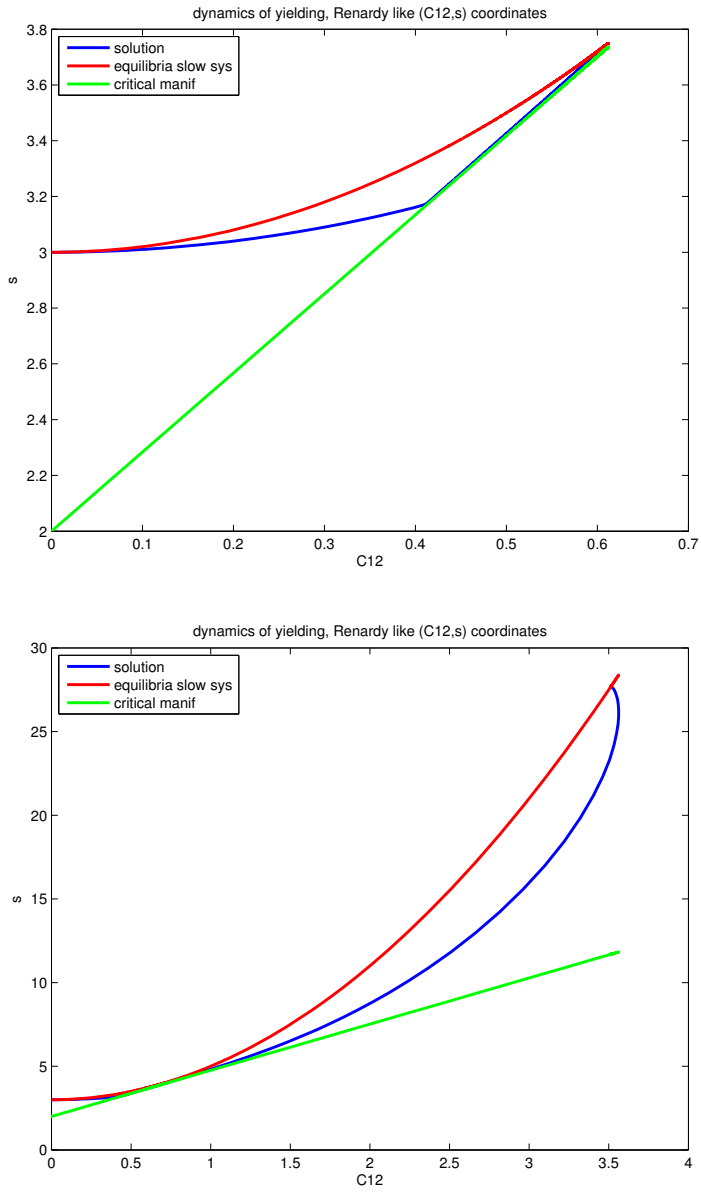

Figure 4.11: The numerical integration of equation (4.8) for $\tau > T_{12}^M$ is shown by the blue line. The red line is the condition $f(D, C_{12}, 0) = 0$ while the green line is the condition $g(D, C_{12}, 0) = 0$.

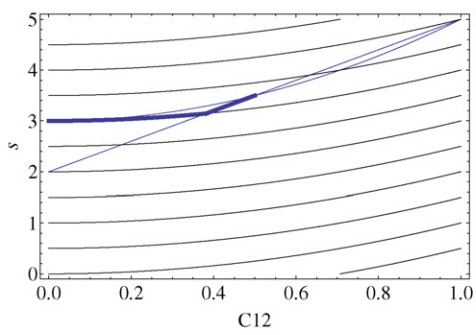

(a) $\tau < T^M$

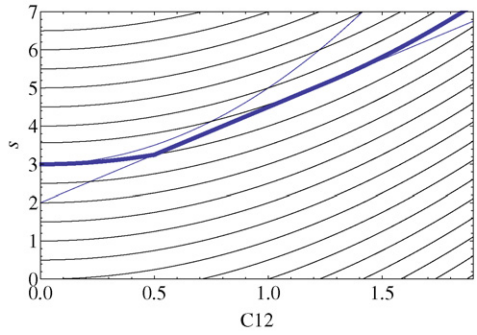

(b) $\tau > T^M$

Figure 4.12: Renardy's results of the dynamics of yielding for the PEC model. Figures from [Ren10].

4.6 Large scale dynamics

A good way to approach the large scale dynamics is to make a proper change of coordinates and a time rescale of equation (4.8). The following change of coordinates[4] is performed

$$t = \varepsilon^{-\frac{1}{3}}\tilde{t}, \quad C_{12} = \varepsilon^{-\frac{1}{3}}x, \quad D = \varepsilon^{-\frac{2}{3}}y$$

We have

$$\begin{aligned}
\frac{dx}{d\tilde{t}} &= \frac{\tau}{\eta} - k_2 x(y + x^2 + (\alpha+2)\varepsilon^{\frac{2}{3}}) - \frac{k_1 x \varepsilon^{\frac{1}{3}}}{\eta(y + x^2 + (\alpha+2)\varepsilon^{\frac{2}{3}})} \\
\frac{dy}{d\tilde{t}} &= k_2(y + x^2 + (\alpha+2)\varepsilon^{\frac{2}{3}})(-y + x^2 + \varepsilon^{\frac{2}{3}}) \\
\frac{d\varepsilon}{d\tilde{t}} &= 0
\end{aligned} \tag{4.15}$$

[4]The new set of variable is called $x, y, \tilde{t}$ in order not to get redundant with the subscripts when doing the blow-up. Note that from now on the first equation is the one related to the evolution of C_{12} while the second one is related to D, while in the previous section it was the opposite. Even though this change of notation could be considered as confusing, it will result very helpful in the understanding of the dynamics. Moreover, the plots on the precedent sections were already following this notation, in order to be consistent with Renardy's results [Ren10].

Make the following change of coordinates: $\delta = \varepsilon^{\frac{1}{3}}$, equation (4.15) becomes

$$\begin{aligned}
\frac{dx}{d\tilde{t}} &= \frac{\tau}{\eta} - k_2 x(y + x^2 + (\alpha+2)\delta^2) - \frac{k_1 x \delta}{\eta(y + x^2 + (\alpha+2)\delta^2)} \\
\frac{dy}{d\tilde{t}} &= k_2(y + x^2 + (\alpha+2)\delta^2)(-y + x^2 + \delta^2) \\
\frac{d\delta}{d\tilde{t}} &= 0
\end{aligned} \tag{4.16}$$

For $\delta = 0$ the system (4.15) has a fixed point in

$$P^* : \qquad x = \left(\frac{\tau}{2\eta k_2}\right)^{\frac{1}{3}}, \quad y = x^2 = \left(\frac{\tau}{2\eta k_2}\right)^{\frac{2}{3}} \tag{4.17}$$

The Jacobian matrix of (4.16) for the (x, y) coordinates in the fixed point P^* is

$$J = \begin{bmatrix} -4k_2\left(\frac{\tau}{2\eta k_2}\right)^{\frac{2}{3}} & -k_2\left(\frac{\tau}{2\eta k_2}\right)^{\frac{1}{3}} \\ \frac{2\tau}{\eta} & -2k_2\left(\frac{\tau}{2\eta k_2}\right)^{\frac{2}{3}} \end{bmatrix}$$

which has the eigenvalues

$$\lambda_{12} = -3k_2\left(\frac{\tau}{2\eta k_2}\right)^{\frac{2}{3}} \pm i\sqrt{3}k_2\left(\frac{\tau}{2\eta k_2}\right)^{\frac{2}{3}}$$

The real part of both eigenvalues λ_{12} is always negative, and thus the fixed point is a stable focus.

Moreover, the Jacobian matrix J is non-singular in the fixed point for $\delta = 0$, indeed

$$\det J = 12k_2^2\left(\frac{\tau}{2\eta k_2}\right)^{\frac{4}{3}} \neq 0$$

Thus, for $\delta \neq 0$ small, the implicit function theorem holds and the fixed point and its stability properties are maintained.

By doing this coordinate rescale all the information about the small scale dynamics of equation (4.8) are on the higher order terms. As we can see, system (4.15) is a regular perturbation problem and it is not anymore a slow-fast system. A very efficient way of connecting the two distinct behaviours of the small and large scale dynamics of equations (4.8) and (4.15) respectively, is to use the blow up method in the origin. Indeed, the blow-up method is a powerful tool every time we need to connect dynamics on two different scales, thus we expect to get a good comprehension of the system using it.

The next goal is to show that using a proper map Γ for the blow-up, the solution starting with initial condition at rest, will end up for large times (going to infinity for ε going to zero) to the steady state shear flow described by the stable fixed point P^* of coordinates (4.17).

4.7 Blow-up of the origin

In order to perform a blow-up of the origin, it is needed to determine the quasi-homogeneous blow-up map Γ for the system (4.16), see chapter 3.

Call $B = S^2 \times \mathbb{R}$ and $B_0 = S^2 \times [0, r_0], r_0 > 0$. The quasi-homogeneous blow-up $\Gamma : B_0 \to \mathbb{R}^3$ is defined such that

$$\Gamma : S^2 \times \mathbb{R} \to \mathbb{R}^3, \quad \Gamma(\bar{x}, \bar{y}, \bar{\delta}, \bar{r}) = (\bar{r}^{a_1}\bar{x}, \bar{r}^{a_2}\bar{y}, \bar{r}^{a_3}\bar{\delta})$$

with $a_i, i = 1, 2, 3$ positive integers. For equation (4.16) the following conditions are obtained:

$$\bar{r}^{k+a_1}\left(\frac{\tau}{\eta} - k_2\bar{x}(\bar{y} + \bar{x}^2 + (\alpha+2)\bar{\delta}^2) - \frac{k_1\bar{x}\bar{\delta}}{\eta(\bar{y} + \bar{x}^2 + (\alpha+2)\bar{\delta}^2)}\right) =$$
$$= \frac{\tau}{\eta} - k_2\bar{r}^{a_1}\bar{x}(\bar{r}^{a_2}\bar{y} + \bar{r}^{2a_1}\bar{x}^2 + (\alpha+2)\bar{r}^{2a_3}\bar{\delta}^2) - \frac{k_1\bar{r}^{a_1}\bar{x}\bar{r}^{a_3}\bar{\delta}}{\eta(\bar{r}^{a_2}\bar{y} + \bar{r}^{2a_1}\bar{x}^2 + (\alpha+2)\bar{r}^{2a_3}\bar{\delta}^2)}$$

$$\bar{r}^{k+a_2}\left(k_2(\bar{y} + (\bar{x}^2 + (\alpha+2)\bar{\delta}^2)(-\bar{y} + \bar{x}^2 + \bar{\delta}^2)\right) =$$
$$k_2(\bar{r}^{a_2}\bar{y} + \bar{r}^{2a_1}\bar{x}^2 + (\alpha+2)\bar{r}^{2a_3}\bar{\delta}^2)(-\bar{r}^{a_2}\bar{y} + \bar{r}^{2a_1}\bar{x}^2 + \bar{r}^{2a_3}\bar{\delta}^2)$$

Thus the following conditions are obtained

$$a_1 = a_3 = \frac{a_2}{2}$$
$$k = a_2$$

Choose $a_1 = 1$ then it follows that $a_2 = 2, a_3 = 1$ and $k = 2$. The blow-up map for system (4.16) is then

$$\Gamma(\bar{x}, \bar{y}, \bar{\delta}, \bar{r}) = (\bar{r}\bar{x}, \bar{r}^2\bar{y}, \bar{r}\bar{\delta}).$$

Note that the degenerate point has been blown-up to an ellipsoid since the powers on the three directions are different.

4.8 Definition of the local charts

The trajectory we want to study is the one of initial point $(x, y) = (0, 1)$ evolving on the fast fiber $(x, 1)$ for long times of system (4.8). As it is possible to see in figure 4.13 two charts are necessary for this analysis

- chart κ_1 such that $\bar{\delta} > 0$ which will reproduce the dynamics of system (4.8)
- chart κ_2 such that $\bar{x} > 0$ which can glue the local dynamics of (4.8) with the large scale dynamics of (4.16).

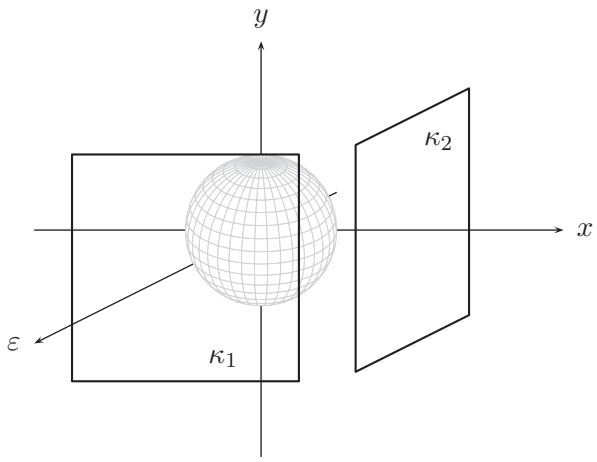

Figure 4.13: Local charts of interest for the study of the blown-up dynamics of the non-Newtonian fluid problem.

Call $B^+_{\bar{\delta}} := B \cap \{\bar{\delta} > 0\}, B^+_{\bar{x}} := B \cap \{\bar{x} > 0\}$ submanifolds of B. On these submanifolds the two charts are well defined.

Instead of the quasi-homogeneous blow-up Γ, on the two charts $\kappa_i, i = 1, 2$ two directional blow-up maps μ_i are defined, such that on each chart $\Gamma = \mu_i \circ \kappa_i$. The computation is shown in detail for the case of chart κ_1. Chart κ_2 can be computed in a similar way, thus only the results will be stated.

Chart κ_1
Consider the directional map $\mu_1 : \mathbb{R}^3 \to \mathbb{R}^3$, such that $\delta_1 = 1$:

$$\mu_1 := \begin{aligned} x &= r_1 x_1 \\ y &= r_1^2 y_1 \\ \delta &= r_1 \end{aligned} \tag{4.18}$$

Require the chart $\kappa_1 : B^+_{\bar\delta} \to \mathbb{R}^3$ such that $\Gamma = \mu_1 \circ \kappa_1$, where $\kappa_1(\bar x, \bar y, \bar\delta, \bar r) = (\bar x \bar\delta^{-b_1}, \bar y \bar\delta^{-b_2}, \bar r \bar\delta^{-b_3}) = (x_1, y_1, r_1)$. Note that the division of each coordinate by the quantity $\bar\delta$ is because this directional blow-up is actually a stereographic mapping.

$$\begin{array}{lll} x : \bar r \bar x & = r_1 x_1 = \bar r \bar x \bar\delta^{-b_1-b_3} & -b_1 - b_3 = 0 \qquad\quad b_1 = 1 \\ y : \bar r^2 \bar y & = r_1^1 y_1 = \bar r^2 \bar y \bar\delta^{-2b_3-b_2} \quad \Rightarrow & -2b_3 - b_2 = 0 \quad \Rightarrow \quad b_2 = 2 \\ \delta : \bar r \bar\delta & = r_1 = \bar r \bar\delta^{-b_3} & -b_3 = 1 \qquad\quad b_3 = -1 \end{array}$$

Thus we have found that the chart κ_1 is given by

$$\kappa_1 : B^+_{\bar\delta} \to \mathbb{R}^3 \quad \text{s.t.} \quad \begin{array}{l} x_1 = \bar x \bar\delta^{-1} \\ y_1 = \bar y \bar\delta^{-2} \\ r_1 = \bar r \bar\delta \end{array}$$

Chart κ_2
Chart $\kappa_2 : B^+_{\bar x} \to \mathbb{R}^3$ is defined such that the directional blow-up $\mu_2 : \mathbb{R}^3 \to \mathbb{R}^3$ is done keeping $x_2 = 1$. In order to have $\Gamma = \mu_2 \circ \kappa_2$ it is obtained

$$\mu_2 := \begin{array}{l} x = r_2 \\ y = r_2^2 y_2 \\ \varepsilon = r_2 \delta_2 \end{array} \qquad\qquad \kappa_2 : \begin{array}{l} r_2 = \bar r \bar x \\ y_2 = \bar y \bar x^{-2} \\ \delta_2 = \bar\delta \bar x^{-1} \end{array} \tag{4.19}$$

The aim is to study a trajectory and follow its evolution along the two different charts. Thus, the transition functions κ_{12}, κ_{21} between the charts need to be computed. Note that these transition functions are defined only in the subspace where both the considered charts are well defined. For instance the transition function κ_{21} from chart κ_1 to chart κ_2 is defined for $x_1 > 0$.

- κ_{12}: from κ_1 to κ_2, for $x_1 > 0$

$$r_2 = r_1 x_1^{-1}, \quad y_2 = y_1 x_1^{-2}, \quad \delta_2 = x_1$$

- κ_{21}: from κ_2 to κ_1, for $\delta_2 > 0$

$$x_1 = \delta_2^{-1}, \quad y_1 = y_2 \delta_2^{-2}, \quad r_1 = r_2 \delta_2$$

4.8.1 Dynamics on chart κ_1

Consider chart κ_1 such that the map μ_1 on this chart is given by

$$\mu_1 : \mathbb{R}^3 \to \mathbb{R}^3 : \qquad x = r_1 x_1, \quad y = r_1^2 y_1, \quad \delta = r_1$$

changing time $t_1 = r_1 \tilde{t}$ we obtain the following system

$$\begin{aligned} \dot{x}_1 &= \frac{\tau}{\eta} - \frac{k_1 x_1}{\eta(s_1+\alpha)} - k_2 r_1^3 x_1 (s_1+\alpha) \\ \dot{y}_1 &= r_1^3 k_2 (s_1+\alpha)(-y_1 + x_1^2 + 1) \qquad , \quad s_1 = y_1 + x_1^2 + 2 \\ \dot{r}_1 &= 0 \end{aligned} \tag{4.20}$$

with the dot meaning derivative respect to t_1. It is possible to notice that calling $x_1 = C_{12}, y_1 = D, r_1^3 = \varepsilon$ then we obtain exactly the slow-fast system of equation (4.8), which describes the small scales dynamics. The system has been already analysed in section 4.5.4. For $\tau > T_{12}^M$ then the solution for the system initially in rest condition either evolves as in figure 4.14, which is exactly the behaviour described in the figures 4.7, 4.8 in section 4.5.4.

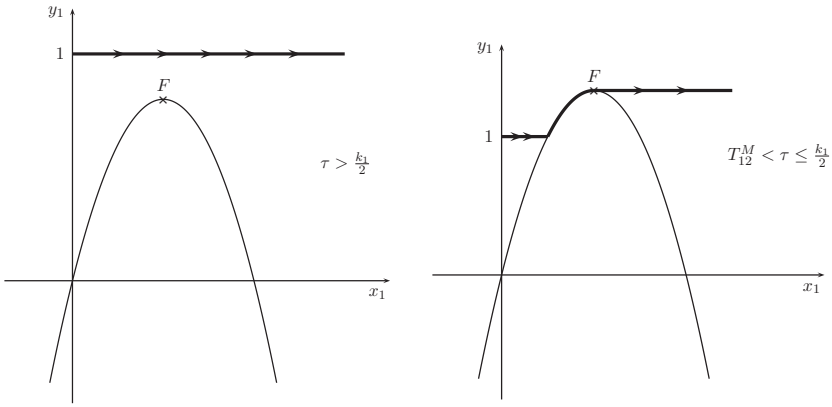

Figure 4.14: Description of the dynamics in chart κ_1 for $\tau > T_{12}^M$.

4.8.2 Dynamics on chart κ_2

Consider chart κ_2 such that the map μ_2 on this chart is given by

$$\mu_2 : \mathbb{R}^3 \to \mathbb{R}^3 : \qquad x = r_2, \quad y = r_2^2 y_2, \quad \delta = r_2 \delta_2$$

changing time $t_2 = r_2\tilde{t}$ we obtain the following system

$$\begin{aligned}
\dot{r}_2 &= r_2 F_2(r_2, y_2, \delta_2) \\
\dot{y}_2 &= -2y_2 F_2(r_2, y_2, \delta_2) + r_2^3 k_2 (1 + y_2 + (\alpha+2)\delta_2^2)(1 - y_2 + \delta_2^2) \\
\dot{\delta}_2 &= -\delta_2 F_2(r_2, y_2, \delta_2)
\end{aligned} \tag{4.21}$$

with $F_2(r_2, y_2, \delta_2) = \frac{\tau}{\eta} - \frac{k_1 r_2 \delta_2}{\eta(y_2+1+(\alpha+2)\delta_2^2)} - k_2 r_2^3(1 + y_2 + (\alpha+2)\delta_2^2)$ and the dot meaning derivative respect to t_2.

System (4.21) has two fixed points. The first one is in the origin, while the second one is for $(r_2, y_2, \delta_2) = \left(\left(\frac{\tau}{2\eta k_2}\right)^{\frac{1}{3}}, 1, 0\right)$. Observe that the second fixed point is exactly the fixed point P^* of coordinates (4.17) rewritten in the coordinates (r_2, y_2, δ_2) found for $\delta = 0$ for the large scale system. The stability properties of P^* have already been studied in section 4.6. On the other hand the fixed point in the origin is a new feature that appears in chart κ_2.

We now check the stability properties of the fixed point in the origin by computing the Jacobian matrix

$$J(0,0,0) = \begin{bmatrix} \frac{\tau}{\eta} & 0 & 0 \\ 0 & -2\frac{\tau}{\eta} & 0 \\ 0 & 0 & -\frac{\tau}{\eta} \end{bmatrix}$$

Thus the origin is an hyperbolic saddle, which has the y_2 and δ_2 directions stable, while r_2 is unstable. Note that the two directions r_2 and δ_2 have opposite linear stability properties, which is as expected since the quantity $\varepsilon = \delta^3 = r_2^3\delta_2^3$ has to remain constant. The local stability properties of the fixed point in the origin are shown in figure 4.15.

The stable manifold is locally tangent to the y_2 axis in the origin and lies in the (y_2, δ_2)-plane . Moreover, from equation (4.21) it is possible to see that the two subspaces defined by the planes $\{r_2 = 0\}$ and $\{\delta_2 = 0\}$ are invariant. Since $\{\delta_2 = 0\}$ is invariant and the unstable manifold is contained in this plane, we conclude that the unstable manifold always to lie in the plane $\{\delta_2 = 0\}$.

4.9 Analysis of the dynamics for $\delta = 0$

For $\delta = 0$ there are two trajectories which are of interest to study close to the fixed point in the origin of chart κ_2. Those two trajectories are depicted with a bold

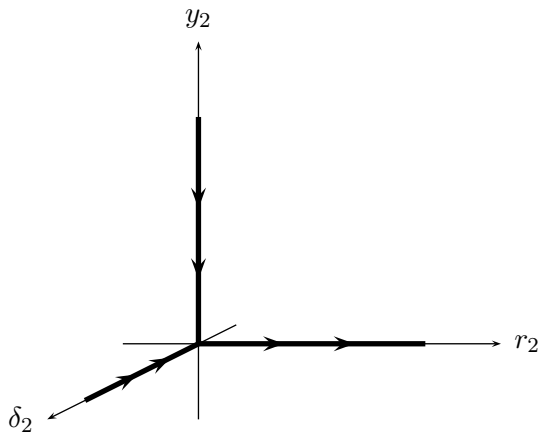

Figure 4.15: Local stability of the fixed point in the origin.

line in figure 4.16. Those two trajectories can be considered as building blocks and are useful to determine the dynamics for $\delta \neq 0$.

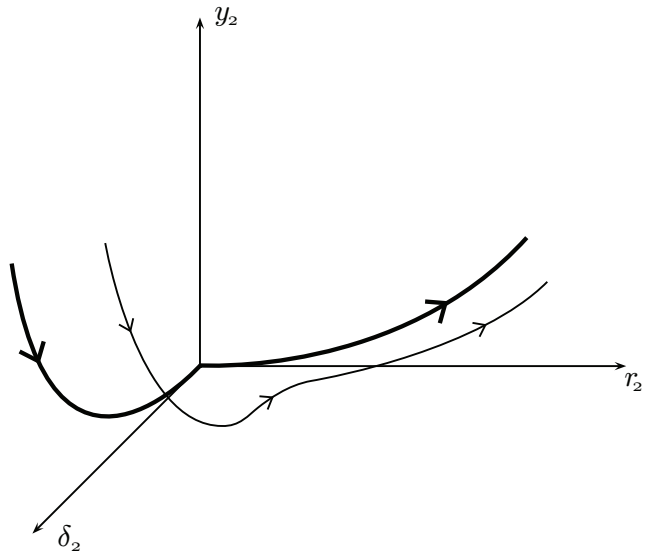

Figure 4.16: Building trajectories for $\delta = 0$ in bold line and example of a trajectory solution for $\delta \neq 0$.

- The first trajectory which is of interest to study is the transformation on chart κ_2 of the trajectory evolving on the fast fiber $(x_1, 1, 0)$ of chart κ_1, see

figure 4.14. The change of coordinates from chart κ_1 to chart κ_2 defined for $x_1 > 0$ is given by

$$\kappa_{12}(x_1, y_1, r_1): \quad r_2 = r_1 x_1, \quad y_2 = \frac{y_1}{x_1^2}, \quad \delta_2 = \frac{1}{x_1}$$

For $\delta = r_1 = 0$ and large values of x_1, the trajectory considered will end up to the origin of chart κ_2 tangent to the stable manifold and it is lying in the invariant plane $\{r_2 = 0\}$.

$$\lim_{x_1 \to \infty} \kappa_{12}(x_1, 1, 0): \quad r_2 = 0, \quad y_2 = 0^+, \quad \delta_2 = 0^+$$

Moreover the trajectory approaches the origin on the plane $\{r_2 = 0\}$ tangent to the δ_2-axis. This trajectory is shown in figure 4.16 on the invariant plane $\{r_2 = 0\}$ with a bold line.

- There is a second trajectory which is moving along the direction of the unstable manifold r_2 and is lying on the invariant plane $\{\delta_2 = 0\}$. In this invariant plane, by the use of the stable manifold theorem it is possible to write the motion on y_2 as a graph of the unstable manifold, i.e.

$$y_2 = U_2(r_2) \tag{4.22}$$

with U_2 at least of the second order in r_2, i.e. $U_2(r_2) = a_2 r_2^2 + a_3 r_2^3 + \dots$.
Substituting (4.22) in equation (4.21), we obtain the coefficients:

$$a_2 = 0, \quad a_3 = \frac{k_2 \eta}{5\tau}$$

Since $a_3 > 0$, then y_2 is locally increasing for increasing values of r_2. The trajectory is the one displayed in figure 4.16 with a bold line in the invariant plane $\{\delta_2 = 0\}$.

The interest is to understand the local evolution of this escaping trajectory for a given r_2. Consider the point P_2 obtained for $r_2 = \rho$:

$$P_2: \qquad r_2 = \rho, \quad y_2 = \frac{k_2 \eta}{5\tau} \rho^3 + \mathcal{O}(\rho^4), \quad \delta_2 = 0$$

In order to follow the evolution of the trajectory passing through point P_2 it is needed to consider either higher order terms in the expansion (4.22) or it is possible to study the point P_2 in the original chart (x, y, δ). Considering this second option, the point P_2 transformed on the original chart becomes the point P of coordinates

$$P: \qquad x = \rho, \quad y = \frac{k_2 \eta}{5\tau} \rho^5 + \mathcal{O}(\rho^6), \quad \delta = 0$$

which is lying in the positive quadrant $x, y > 0$. The next step is to show that given a $\rho > 0$ but possibly small, the trajectory starting from the point P will always end up in the fixed point P^* of the large scale dynamics.

- First of all we will show that the quadrant $x, y > 0$ is invariant for $\delta = 0$. Consider the box B of figure 4.17 defined as

$$x \in [\mu, M], \quad y \in [\eta, N], \qquad \mu, \eta, M, N > 0$$

with $\mu, \eta \ll 1$ small quantities, while $M, N \gg 1$ large. It is possible to show that for system (4.15) the vector field is always pointing inwards the box B. Indeed

  - on the left side $x = \mu$ and $y \in [\eta, N]$ then $\dot{x} > 0, \dot{y} \neq 0$
  - on the lower side $y = \eta$ and $x \in [\mu, M]$ then $\dot{y} > 0, \dot{x} \neq 0$
  - on the right side $x = M$ and $y \in [\eta, N]$ then $\dot{x} < 0, \dot{y} \neq 0$
  - on the upper side $y = N$ and $x \in [\mu, M]$ then $\dot{y} < 0, \dot{x} \neq 0$

Considering $\mu, \eta \to 0$ and $M, N \to +\infty$ it is possible to conclude that the vector field (4.15) is pointing inwards on all the positive quadrant $x, y > 0$ with the two axes $x = 0, y = 0$ excluded. Note that for the $y = 0$ axis it would have not be possible to conclude in the origin, since there the vector field is tangent to the box, i.e. $\dot{y} = 0$ for $y = 0$.

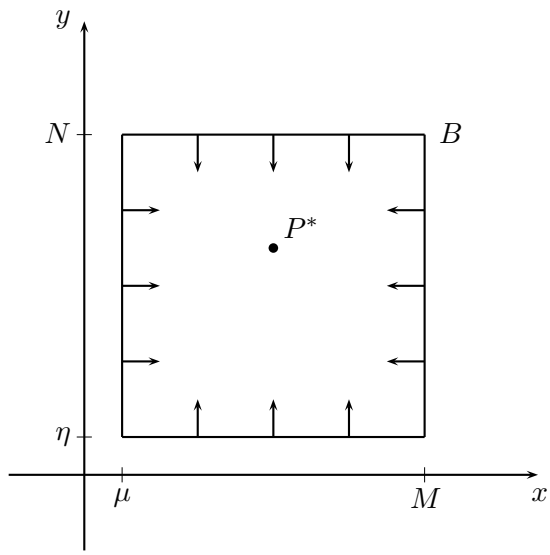

Figure 4.17: Direction of the vector field (4.15) on the positive quadrant. P^* is the fixed point of the large scale dynamics defined by equation (4.17).

The properties of the vector field on the borders of box B are maintained for $\delta \neq 0$ but small.

- The vector field (4.15), has negative divergence in every point of the box B:

$$\frac{\partial \dot{x}}{\partial x} + \frac{\partial \dot{y}}{\partial y} + \frac{\partial \dot{\delta}}{\partial \delta} = -3k_2(y + x^2)$$

  and thus, by Dulac's criterion it is possible to rule out the existence of limit cycles on the subset considered.

- The fixed point P^* of coordinates (4.17) lies inside the region defined by the box B, and it has already been shown with the use of the implicit function theorem that it is persistent for $\delta \neq 0$.

Thus all the trajectories inside the box B have to end up on the fixed point P^* for any value of $\delta \geq 0$ small, and the trajectory starting from point P has to end up there as well.

4.10 Conclusions for $\delta \neq 0$

The interest now is to study the evolution of the fast trajectory of initial conditions

$$Q_0 : \qquad x_1 = 0, \quad y_1 = 1, \quad r_1 = \delta$$

for the case of $\tau > T_{12}^M$ defined in chart κ_1 and follow it along chart κ_2 and the original chart (x, y, δ). Remember that $\delta = \varepsilon^{\frac{1}{3}}$.

- By the use of the results by Krupa and Szmolyan [KS01a] for $\delta \neq 0$ but small, the trajectory of initial condition Q_0 is evolving in chart κ_1 along a fast trajectory which is δ^3-close to the limit trajectory obtained for $\delta = 0$, see equation (4.20). For values of x_1 large, it is necessary to follow the evolution of this trajectory on chart κ_2.

- On chart κ_2 for $\delta \neq 0$ the $\{y_2 = 0\}$ plane is foliated by a family of lines $\delta = r_2\delta_2$. Moreover for $r_2 \neq 0$ we have been able to write y_2 as a graph on r_2 as $y_2 = \frac{k_2\eta}{5\tau} r_2^3 + \mathcal{O}(r_2^4)$. The trajectory is depicted in figure 4.16. Thus it is possible to follow the evolution of the perturbed trajectory on this chart up to some value of $r_2 = \rho$. This point can be written as

$$P_{2,\delta} : \qquad r_2 = \rho, \quad y_2 = \frac{k_2\eta}{5\tau} r_2^3 + \mathcal{O}(r_2^4), \quad \delta_2 = \frac{\varepsilon^{\frac{1}{3}}}{r_2}$$

  Thus it is possible to transform point $P_{2,\delta}$ into the original chart (x, y, δ) and we obtain the point

$$P_\delta : \qquad x = \rho, \quad y = \frac{k_2\eta}{5\tau} \rho^5 + \mathcal{O}(\rho^6), \quad \delta = \varepsilon^{\frac{1}{3}}$$

which is inside the box B_δ defined for $\delta \neq 0$.

- As we have already shown in the previous section, all the trajectories in the positive semiquadrant are going to converge to the stable focus on the initial chart (x, y, δ). Since the properties of the box B are independent of δ, the box B_δ defined for $\delta \neq 0$ has them as well. Thus in this way we can show that for $\delta \neq 0$ but small and $\tau > T_{12}^M$, the trajectory starting in $(D, C_{12}) = 0$ will always end up into the stable fixed point defined by equation (4.17). We can conclude that this point is globally attracting for any physically meaningful initial condition.

We have been able to show with the use of the blow-up method the relation between the large scale and small scale dynamics for a thixotropic yield stress fluid.

Chapter 5

The Schrödinger eigenvalue problem

In this chapter the problem of computing the eigenvalues of the Schrödinger equation at the classical limit is analysed. This problem is rather challenging because it involves the study of a slow fast system of the type introduced in chapter 2. An analytical treatment of this problem is very useful since numerical methods exhibits stiffness issues related to the integration of the appearing differential equation.

In section 5.1 the Schrödinger equation is presented and its physical meaning is explained. The theory of quantum mechanics hereby presented is referred to the books of Picasso [Pic00] and Shankar [Sha80]. Section 5.2 introduces to the particular problem of the classical limit, under which both quantum mechanics and Newton's laws should be capable to explain the dynamics of the system. The next section 5.3 shows how the Schrödinger equation can be rewritten in a slow-fast formulation while in section 5.4 the analytical solution of the problem is presented for the particular case of a quadratic potential. For a generic symmetric potential it is not possible to find an analytical solution of the system of equations. The geometric singular perturbation theory can help in this sense and in section 5.5 the analysis for the limit case of $\varepsilon = 0$ is performed. Unfortunately, the slow fast formulation presents a degenerate point in the origin appears and GSPT is not enough to conclude on the behaviour for $\varepsilon \neq 0$ close to the origin. The blow-up of the singular point is performed in section 5.6 while the local charts and the

analysis of the dynamics on each local chart is described in sections 5.7 and 5.8 respectively. In final section 5.9 the analysis of the dynamics through the different charts is presented, in particular for the case of $\varepsilon \neq 0$.

5.1 The Schrödinger equation

Quantum mechanics is a branch of physics which describes physical phenomena at the atomic scales. Its formulation has started at the beginning of the nineteenth century, when physicists realized that classical mechanics was inaccurate to describe physics at nano scales.
The main result of what is called now the old theory of quantum mechanics is the wave-particle duality. This theory claims that light waves are consisting of entities called photons and to each of these entities is associated a wave function $\varphi(x,T)$, such that $|\varphi|^2$ is the probability of finding the photon in the point x at time T [Pic00], [Sha80].

The dynamics of the wave function $\varphi(x,T)$ is described by Schrödinger equation[1], which is the equivalent of Newton's second law for quantum mechanics. In general it is written as the following linear partial differential equation

$$i\hbar\varphi_T = \hat{H}\varphi \tag{5.1}$$

where φ_T means derivative of φ respect to the time T. $\hbar$ is the reduced Planck's constant such that $\hbar = \frac{h}{2\pi}$ and $\hat{H}$ is the Hamiltonian operator, which describes the total energy of the wave function.
By the Copenhagen interpretation [Sha80], the wave function φ is key to describe quantum systems indeed

- The square of the modulus of the wave function $|\varphi|^2$ represents the probability of a given outcome for a measurement.
- The wave function φ describes completely the evolution along time of the state of the system.

Note that the Copenhagen interpretation requires φ being L^2-integrable

$$\int |\varphi|^2 \, dx = 1$$

and the finiteness of the integral means that φ has to vanish at infinity:

$$\lim_{x\to\pm\infty} \varphi(x) = 0. \tag{5.2}$$

[1]The equation has been formulated by Erwin Schrödinger in 1926.

In the thesis the focus will be on a uni-dimensional system, in the non-relativistic case for a particle moving in an electric field. For this case the Hamiltonian operator can be expressed [Sha80] as

$$\hat{H} = -\frac{\hbar^2}{2m}\frac{\partial^2}{\partial x^2} + V(x,T) \tag{5.3}$$

with m the mass of the particle and V its potential energy in a given point $x \in \mathbb{R}$ at time T. The Schrödinger equation (5.1) becomes

$$i\hbar\varphi_T = -\frac{\hbar^2}{2m}\varphi_{xx} + V(x,T)\varphi \tag{5.4}$$

where the wave function φ is computed in (x,T).

It is possible to observe that for this case there is a strong analogy with classical mechanics. Indeed, in classical mechanics the Hamiltonian function of a point of mass m expressed in the canonical coordinates (q,p) subject to a potential vector field $V(q,T)$ can be described as

$$H(q,p) = \frac{p^2}{2m} + V(q,T).$$

The canonical coordinates in phase space (q,p) in the Hamiltonian formalism are such that they satisfy the Poisson brackets $\{q,p\} = 1$.
For two given functions $f, g \in C^1$, such that $f, g : \mathbb{R}^{2n} \to \mathbb{R}^n$, the Poisson brackets are defined as

$$\{f,g\} = \sum_{i=1}^{n} \frac{\partial f}{\partial q_i}\frac{\partial g}{\partial p_i} - \frac{\partial f}{\partial p_i}\frac{\partial g}{\partial q_i} \tag{5.5}$$

with $q = (q_1, \ldots, q_n), p = (p_1, \ldots, p_n)$ the canonical coordinates. The Poisson brackets have various properties, such that they are linear, anti-symmetric, they satisfy the Leibnitz rule and the Jacobi identity.

If the conjugate momenta p are replaced with the operator $-i\hbar\frac{\partial}{\partial x}$ and $q = x$ then the Hamiltonian operator $\hat{H}$ defined in equation (5.3) is obtained. Note that in this case the definition of Poisson bracket (5.5) is still valid. In this case though it is no more required that $\{q,p\} = 1$, but the canonical coordinates have to satisfy the canonical commutation relation $\{q,p\} = i\hbar$.

It is assumed that the potential $V(x)$ is time independent and symmetric and can be written as $V(x) = ax^2 + \mathcal{O}(x^4), a > 0$. Note that if the higher order terms of the potential are not considered, the Schrödinger equation (5.4) will describe the motion of the quantum harmonic oscillator, while the equivalent formulation in classical mechanics will describe the mechanical harmonic oscillator.
The requirement $a > 0$ is necessary for physical reasons. Consider for example the mechanical harmonic oscillator, then for $a < 0$ the rest position would be unstable

and the particle would tend to escape to infinity for any given initial condition apart the rest point. This behaviour is unphysical and it's not of interest for the purpose of the thesis. The same reasoning applies to the equivalent quantum mechanical system.
As it will be shown in the next sections, the requirement of $V(x)$ being symmetric will make all the computations simpler. The case of an asymmetric potential can be studied in the same manner, but more care has to be taken.
In the next section it will be shown that set of eigenvalues solving the problem (5.4) is a discrete one. This depends on the fact that the potential $V(x)$ is going to infinity for $x \to \pm\infty$. Ideally, the potential $V(x)$ could also go to zero or to a finite value for $x \to \pm\infty$. In this case the solutions of the eigenvalue problem would be a continuum set instead of the discrete one that is going to be found in the next sections [Pic00].

5.2 The classical limit

Schrödinger equation describes well the physics at the atomic scale, while Newton's second law is well working for classical mechanics. The question analysed in this section is how to re-obtain the results of classical mechanics starting from Schrödinger equation when this equation is applied to a sufficiently large system.

Note that it doesn't exists any limit of the Schrödinger equation which leads to re-obtain exactly Newton's second law for two reasons:

- Schrödinger equation (5.4) is a linear partial differential equation, while Newton's second law is a second order ordinary differential equation.
- While Schrödinger equation describes the probability $|\varphi|^2$ of finding a particle at time T in position x, Newton's second law describes exactly the motion of the particle along time.

Thus the question is at which limit the results predicted by Schrödinger equation are going to coincide with the ones predicted by Newton's second law in some sense. The question is non trivial and it has not been completely answered yet. Two different formulations are now presented:

- Planck's formulation [Pla10] supposes to re-obtain Newton's second law from the Schrödinger equation considering the reduced Planck's constant $\hbar \to 0$ when confronted with the characteristics of the system. This statement can also be reformulated as requiring the mass m of the quantum particle to go to infinity, i.e. obtain a point of finite mass m in the classical mechanical

framework. This formulation has been supported by Dirac as well in [Dir58] and it is called the classical limit.

- Bohr's formulation [Boh85] considers the limit of large quantum numbers n in order to re-obtain Newton's second law from the Schrödinger equation. This formulation is called the correspondence principle. Note that when Bohr has applied his formulation to the computation of the transition frequency of the hydrogen atom he has considered large but finite values of the quantum number n, otherwise the transition frequency would collapse to zero [HK89].

The paper by Klein [Kle12] analyses the relation between classical and quantum mechanics by doing in several ways the limit $\hbar \to 0$. It is shown that apart some special case in general this limit does not allow to recover classical mechanics from quantum mechanics.

A work by Hassoun and Kobe [HK89] analyses the Planck's and Bohr's formulations for three different potentials of quantum mechanical systems $V(x) = x^m, m = 0, 1, 2$. Their conclusion is that none of the two formulations alone leads to a complete recovery of Newton's second law. Instead, the classical limit is obtained only in the case that $\hbar \to 0$ and $n \to \infty$, such that the action of the corresponding classical system $J = n\hbar$ remains constant. This requirement supports the equivalence of the Hamiltonian operator $\hat{H}$ with the Hamiltonian function H at the classical limit, since requiring a constant action J is in good accordance with Hamilton's principle of least action.

It is possible to conclude that it doesn't exists a generally accepted theory of the classical limit. Thus for this project, there is freedom in the interpretation on how to get the classical limit. The present work will deal with the classical limit $\hbar \to 0$ supposing the limit of large quantum numbers n and thus the action J is not kept constant. It will be shown that by this decision the system obtained is a slow-fast system with a non-hyperbolic point in the origin. The case of keeping $J = \hbar n$ constant would be in the author's opinion equivalently interesting, but then a different analysis from the one hereby presented should be used. Since in this thesis a generic symmetric potential $V(x) = x^2 + \mathcal{O}(x^4)$ is considered, the results obtained could be considered as an improvement of the analysis done in [HK89], even if J is not kept constant.

5.2.1 Computation of the classical limit

In this section the computation of the classical limit is performed under the hypothesis stated in the previous section.
Introduce a new, slower time t such that $T = t\sqrt{2m}$, then the Schrödinger equation

(5.4) can be reformulated as

$$i\frac{\hbar}{\sqrt{2m}}\varphi_t = -\frac{\hbar^2}{2m}\varphi_{xx} + V(x,t)\varphi$$

and calling $\varepsilon = \frac{\hbar}{\sqrt{2m}}$, the Schrödinger equation at the classical limit can be reformulated as

$$i\varepsilon\varphi_t = -\varepsilon^2\varphi_{xx} + V(x)\varphi \tag{5.6}$$

The aim of this chapter is to study the eigenvalue problem of equation 5.6 for $0 < \varepsilon \ll 1$.

In the next section the Schrödinger equation at the classical limit (5.6) is rewritten as a slow-fast system and then the computation of the analytical solution at the classical limit for different types of potential $V(x)$ is performed.
This analysis is very useful because the numerical integration of a slow-fast system shows stiffness related issues. The WKB method is a numerical algorithm which is generally used to solve the Schrödinger equation at the semiclassical limit. The limit is called semiclassical when the Planck's constant is expanded in power series, and classical mechanics is re-obtained considering only the power 0 term.

Other numerical methods used to solve the one-dimensional Schrödinger equation are presented in [Rap81], [AS96], [MS07] and [San13]. As it is possible to see even without considering the classical limit, a numerical investigation of the problem is not trivial.

5.3 The slow-fast formulation

Guess the following solution

$$\varphi(x,t) = e^{-i\lambda t}\psi(x), \quad \text{s.t.} \quad \lim_{x\to\pm\infty}\psi(x) = 0 \tag{5.7}$$

where the boundary condition on ψ is such that the relative boundary condition of φ (5.2) is satisfied. Substituting the guess in the Schrödinger equation (5.6) the following ODE is obtained

$$\varepsilon^2\psi_{xx} = (V(x) - E)\psi \tag{5.8}$$

with $E = \varepsilon\lambda$ the energy associated with the wave function. This is an eigenvalue problem in the form

$$\frac{d^2}{dx^2}\psi = \frac{(V(x) - E)}{\varepsilon^2}\psi$$

Once a value of $\lambda \in \mathbb{R}$ satisfies this equation then the corresponding ψ is the eigenfunction. These values of (λ, ψ) plugged in the guess (5.7) give a solution for

the Schrödinger equation (5.6).
It is possible to show that the L^2-integrable eigenfunctions ψ form a discrete set with $\lambda \in \mathbb{Z}$. The values of energy E associated to these eigenvalues $\lambda \in \mathbb{Z}$ are the discrete energy levels of the system, see figure 5.1. This is related to the concept of quantization of energy: a particle can assume only specific energy levels. The difference between one energy level and the next one is constant and is related to the quanta of energy i.e. $E_{n+1} - E_n = 2\varepsilon, \forall n \in \mathbb{N}_0$. Each $\lambda = 2n + 1, n \in \mathbb{N}_0$ solution is related to an energy level E_n with n the quantum number. Note that n is related to the number of zeroes of the eigenfunction ψ.

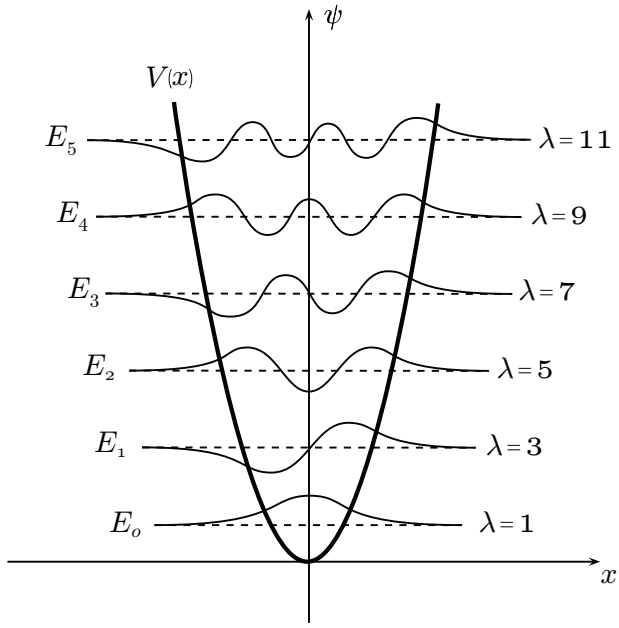

Figure 5.1: Eigenfunctions $\psi(x)$ associated to the respective eigenvalues λ for the quantum harmonic oscillator, $V(x) = x^2$.

Solutions ψ that are limited for $x \to \pm\infty$ but not zero are improper eigenfunctions and it is possible to show that they have a continuous spectrum of eigenvalues $\lambda \in \mathbb{R}$.
Moreover in regions where $E < V(x)$ solutions are not allowed, because in these regions the kinetic energy of the quantum particle would be negative [Pic00].

In order to solve the ODE for ψ (5.6) a change of coordinates can be performed. Introduce the variable $y \in \mathbb{R}$ such that

$$y = \varepsilon \frac{\psi_x}{\psi} \tag{5.9}$$

The change of coordinates is not defined for $\psi = 0$. For the points x in which

$\psi(x) = 0$ it is necessary to require $\psi_x(x) \neq 0$. Otherwise equation (5.8) has the trivial solution $\psi \equiv 0$ which is not an eigenfunction.
With the change of coordinates (5.9) it is possible to explicit the solution of the eigenfunction ψ for a given eigenvalue λ

$$\psi(x) = C_1 e^{\frac{1}{\varepsilon}\int_{x_0}^{x} y(s)\,ds}$$

with C_1 a constant and x_0 some value in the set considered.

Note that the boundary condition $\lim_{x\to\pm\infty}\psi(x) = 0$ becomes a condition on the solution y, in particular

$$\lim_{x\to+\infty}\int_{x_0}^{x} y(s)\,ds = -\infty \quad \text{and} \quad \lim_{x\to-\infty}\int_{x}^{x_0} y(s)\,ds = +\infty \tag{5.10}$$

A second requirement on the solution y is that it has to be defined on all the set $x \in \mathbb{R}$ and not only in subintervals of it.

It is possible to rewrite the Schrödinger equation (5.8) as an autonomous system of two first order equations. Indeed, a differentiation of equation (5.9) leads to:

$$y_x = \varepsilon\frac{\psi_{xx}}{\psi} - \frac{\psi_x^2}{\psi^2} = \frac{V(x) - E - y^2}{\varepsilon}.$$

and the introduction of the variable $t = x$ makes the system autonomous

$$\begin{aligned} x' &= 1 \\ \varepsilon y' &= V(x) - E - y^2 \end{aligned} \tag{5.11}$$

with the $'$ meaning derivative respect to the time t. This is a slow-fast system as the variable y change in a faster time scale than its time $x = t$.
Thus the Schrödinger eigenvalue problem has been transformed to a system of two first order differential equations.

All the results that will be obtained will be independent on the coefficient $a > 0$ of the potential $V(x)$. It is possible to do a coordinate transformation in order to have $a = 1$ without loosing any information.

Make the following rescale of the equations

$$x = \frac{1}{\sqrt{a}}\hat{x}, \quad t = \frac{1}{\sqrt{a}}\hat{t}, \quad \lambda = \frac{1}{\sqrt{a}}\hat{\lambda}, \quad \varepsilon = \sqrt{a}\hat{\varepsilon}.$$

Equation (5.11) becomes

$$\begin{aligned} \frac{d\hat{x}}{d\hat{t}} &= 1 \\ \hat{\varepsilon}\frac{d\hat{y}}{d\hat{t}} &= \hat{x}^2 - \hat{\varepsilon}\hat{\lambda} - \hat{y}^2 + \mathcal{O}(\hat{x}^4) \end{aligned}$$

From now on we will call all the hat-variables without the hat. So we finally obtain the slow-fast system

$$\begin{aligned} x' &= f(x, y, \varepsilon) \\ \varepsilon y' &= g(x, y, \varepsilon) \end{aligned}$$

with

$$\begin{aligned} f(x, y, \varepsilon) &= 1 \\ g(x, y, \varepsilon) &= x^2 - \varepsilon\lambda - y^2 + \mathcal{O}(x^4) \end{aligned} \tag{5.12}$$

Note that if the coefficient a is small, such that $ax \sim \mathcal{O}(x^2)$ this rescaling is not correct and it is necessary to do a rescale considering the next non zero terms of $V(x)$ as well. In this work the working hypothesis will be to have $a > 0$ such that the rescale is well defined.

5.4 Analytic solution for $V(x) = x^2$

As it as already been introduced in section 5.1, the case of $V(x) = x^2$ corresponds to the example of the quantum harmonic oscillator. The classical limit of the quantum harmonic oscillator has a very nice interpretation. In figure 5.2 is shown the value $n = 11$ corresponding to $\lambda = 21$. It is possible to note that the probability density $|\psi^2(x)|$ is non-zero only in a limited region and its borders are corresponding to the turning points of the classical harmonic oscillator, i.e. where it mass has zero velocity. Moreover, for increasing n the probability to find the particle gets higher close to the turning points and very low elsewhere. This is totally agreeing with classical mechanics since the mass of the harmonic oscillator will spend most of its time where it has the lowest velocity, i.e. at the turning points.

We now look for the analytic solution of the Schrödinger eigenvalue problem for the particular case of $V(x) = x^2$. In the previous section it has been shown that using a proper coordinate change, the eigenvalue problem for the Schrödinger equation can be rewritten as a slow system:

$$\begin{aligned} x' &= f(x, y, \varepsilon) \\ \varepsilon y' &= g(x, y, \varepsilon) \end{aligned} \tag{5.13}$$

or as a fast system

$$\begin{aligned} \dot{x} &= \varepsilon f(x, y, \varepsilon) \\ \dot{y} &= g(x, y, \varepsilon) \end{aligned} \tag{5.14}$$

where $'$ stands for derivative respect to the slow time t, while the dot respect to the fast time τ, and $t = \varepsilon\tau$. The functions f and g are shown in equation (5.12).

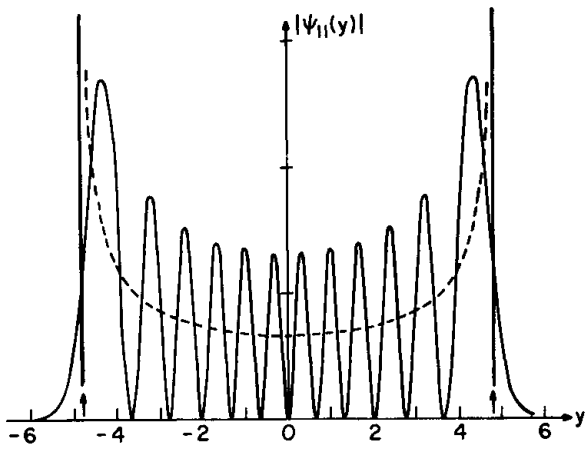

Figure 5.2: Probability density $|\psi^2(x)|$ corresponding to $\lambda = 21$. Figure by [Sha80].

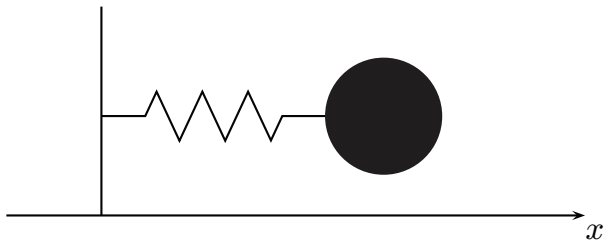

Figure 5.3: Classical harmonic oscillator.

The system of differential equations (5.14) with functions f and g given by (5.12) is a Riccati[2] equation. Indeed the differential equation on y is a first order ODE, which is quadratic in the unknown variable y. On the other hand the equation on x is trivial, and its solution is simply $x(\tau) = \varepsilon\tau + c$ with c an integration constant, considering the fast time τ.

In the case that the potential $V(x)$ is only quadratic $V(x) = x^2$, it is possible to find explicit solutions of problem (5.14) given integer values of $\lambda \in \mathbb{Z}$.
Consider the fast system in the case of $V(x) = x^2$ and $\lambda \in \mathbb{Z}$, $\varepsilon \in \mathbb{R}^+$

$$\begin{aligned} \dot{x} &= \varepsilon \\ \dot{y} &= x^2 - \varepsilon\lambda - y^2 \end{aligned} \tag{5.15}$$

[2]Jacopo Riccati 1676-1754 was an italian mathematician born in Venice. He's mainly famous for his work on the Riccati equation.

guess the following solution of the Riccati equation

$$y(x) = c_0 x + \frac{1}{c_1 x - p_1} + \frac{1}{c_2 x - p_2} + \cdots + \frac{1}{c_n x - p_n} \tag{5.16}$$

with λ, c_0, c_i, p_i constants to be determined, $i = 1 \ldots, n$.

As it has been pointed out in section 5.3, the admissible solutions of the Riccati equation are related to the energy levels of the quantum particle. Solutions of (5.16) are found for odd values of $\lambda = 2n + 1, n \in \mathbb{Z}$. On the other hand, even values of λ are not solutions because as it has been said in section 5.3 they they don't make the jump of the energy level of a quantum $\Delta E = 2\varepsilon$ but only half. Moreover, negative values of λ do not satisfy the boundary condition (5.10), and are related to energy levels not allowed for the quantum particle, see figure 5.1.

In the following, the solution of the Riccati equation (5.15) is described for the case of $\lambda = 1$ and $\lambda = 3$ in detail. For $\lambda > 3$ odd, the procedure is similar.

5.4.1 Case of $\lambda = 1$

The simplest generic solution of (5.15) is given for $y(x) = c_0 x$ for some constant c_0 to determine. Substituting in equation (5.15) it is obtained $c_0 = \pm 1$ for $\lambda = \mp 1$. From now on the focus will be only on the solution for $\lambda = 1$ and $c_0 = -1$, since as it will be shown later, the other solution $\lambda = -1$ and $c_0 = 1$ doesn't satisfy the boundary condition (5.10).

Thus the solution of the Riccati equation (5.15) is given by the trajectory $\gamma^{(\lambda=1)}$

$$\gamma^{(\lambda=1)}(\tau): \quad \begin{aligned} x(\tau) &= \varepsilon\tau \\ y(\tau) &= -\varepsilon\tau \end{aligned}$$

which is shown in figure 5.4 on the left. The trajectory $\gamma^{(\lambda=1)}$ is a solution for the Schrödinger eigenvalue problem because it satisfies the boundary equation (5.10). Indeed for $x \to +\infty$

$$\lim_{x\to+\infty} \int_{x_0}^{x} y(s)\, ds = \lim_{x\to+\infty} \int_{x_0}^{x} -s\, ds = \lim_{x\to+\infty} \left(\frac{x_0^2}{2} - \frac{x^2}{2} \right) = -\infty$$

and the condition for $x \to -\infty$ follows immediately by symmetry reasons.

Plugging this solution in the Schrödinger equation, we obtain that

$$\psi(x) = C_1 e^{\frac{1}{\varepsilon}\int_{x_0}^{x} y(s)\, ds} = C e^{\frac{-x^2}{2\varepsilon}} \tag{5.17}$$

which has the shape of a Gaussian bell and C is a normalization constant s.t. $\int_{-\infty}^{\infty}|\psi(x)|^2\,dx = 1$. The eigenfunction $\psi(x)$ is shown in figure 5.4 on the right.

Thus the Schrödinger eigenvalue problem has for the eigenvalue $\lambda = 1$ the eigenfunction $\psi(x) = Ce^{\frac{-x^2}{2\varepsilon}}$. The complete solution for φ considering the time acting as well can be written as

$$\varphi(x,t) = Ce^{-\frac{x^2}{2\varepsilon}-it}$$

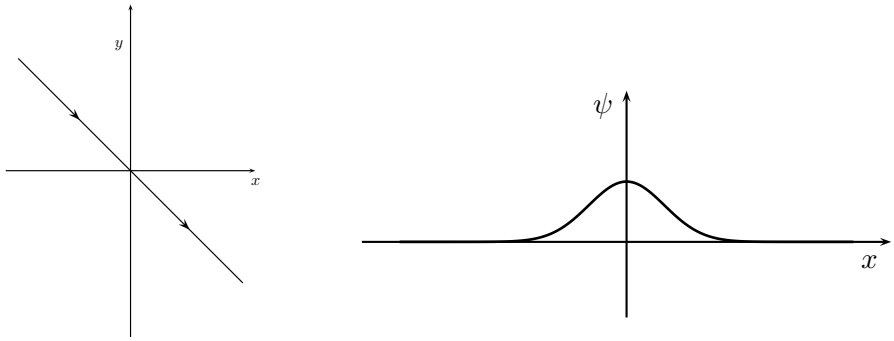

Figure 5.4: Solution $y(x) = -x$ for $\lambda = 1$ and eigenfunction $\psi(x) = \psi_0 e^{\frac{-x^2}{2\varepsilon}}$.

5.4.2 Case of $\lambda = 3$

The next solution of the Riccati equation can be found looking for solutions of the type

$$y = c_0 x + \frac{1}{c_1 x - p_1}$$

with c_0, c_1, p_1 constants to determine. Substituting this guess in equation (5.15) it is obtained $c_0 = \mp 1, c_1 = \frac{1}{\varepsilon}$ and $p_1 = 0$ for $\lambda = \pm 3$. As in the previous case the only interesting solution is for $\lambda = 3$ which is written as a graph over x as

$$y(x) = -x + \frac{\varepsilon}{x} \tag{5.18}$$

This solution is described by the trajectory $\gamma^{(\lambda=3)}$ pictured in figure 5.5 on the left such that

$$\gamma^{(\lambda=3)}(\tau): \quad \begin{aligned} x(\tau) &= \varepsilon\tau \\ y(\tau) &= -\varepsilon\tau + \frac{1}{\tau} \end{aligned}$$

In order to compute the solution of $\psi(x)$, it is necessary to consider the solution $y(x)$ of equation (5.18) in the two separate intervals $x \in]-\infty, 0[$ and $x \in]0, \infty[$ because y is not defined for $x = 0$. Since y is an odd function, it is enough to study the positive interval $x \in]0, \infty[$.

For $x \in]0, \infty[$ the differential equation $\psi_x^+ = \frac{\psi^+ y}{\varepsilon}$ is well posed and it is possible to find an explicit solution for it. The general solution is still given by

$$\psi^+(x) = C_1 e^{\frac{1}{\varepsilon}\int_{x_0}^{x} y(s)\,ds}, \quad x_0, x \in]0, \infty[$$

and C_1 an arbitrary constant. Substituting the expression for $y(x)$, the solution is then

$$\psi^+(x) = Cxe^{-\frac{x^2}{2\varepsilon}}, \quad x \in]0, \infty[$$

with C a normalization constant s.t. $\int_0^\infty |\psi^+(x)|^2\,dx = \frac{1}{2}$. The $\frac{1}{2}$ is by symmetry reasons since it is required that the eigenfunction $\psi(x) = \psi^+(x) \cup \psi^-(x)$ is normalized to one. Note that in this normalization it is excluded only the point $x = 0$, but the integral over a point is zero.

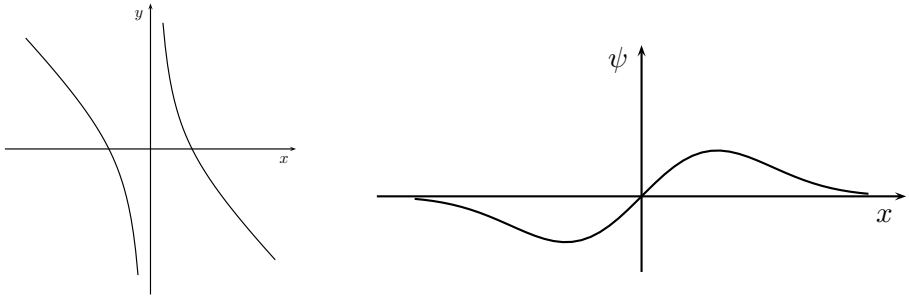

Figure 5.5: Solution $y(x) = -x + \frac{\varepsilon}{x}$ for $\lambda = 3$ and eigenfunction $\psi(x) = Cxe^{-\frac{x^2}{2\varepsilon}}$
.

Moreover since

$$\lim_{x \to 0^+} \psi^+(x) = 0^+$$

the positive ψ^+ solution can be glued by continuity with the negative one ψ^- in $x = 0$ and the eigenfunction $\psi(x)$ for the eigenvalue $\lambda = 3$ given by

$$\psi(x) = Cxe^{-\frac{x^2}{2\varepsilon}}$$

5.4.3 Case of $\lambda < 0$

It has already been claimed in the previous subsections that the solutions obtained for negative values of λ do not satisfy the boundary conditions. Indeed, consider

for instance for the case of $\lambda = -1$, the solution $y(x)$ is then $y(x) = x$. Thus

$$\lim_{x\to+\infty} \int_{x_0}^{x} y(s)\, ds = \lim_{x\to+\infty} \int_{x_0}^{x} s\, ds = +\infty$$

which is not satisfying condition (5.10). Negative values of λ are not eigenvalues of the problem.

All the solutions for $\lambda < -1, \lambda \in \mathbb{Z}$ have the first coefficient $c_0 = 1$. Thus this is sufficient to state that there it doesn't exists any value of $\lambda < 0$ which is an eigenvalue for the Schrödinger eigenvalue problem.

5.5 Analysis of the singular limit

In this section and in the following ones the case of a generic potential $V(x) = x^2 + \mathcal{O}(x^4)$ is treated. In this case it is not possible to find an analytic solution for the Riccati equation on the y coordinate. However, since equations (5.13), (5.14) are a slow-fast system, the Fenichel's theory introduced in chapter 2 holds.

The first step in the analysis of these equations with GSPT is the study of the limit system obtained for $\varepsilon = 0$. At the limit case, the reduced problem of equation (5.19) and the layer problem (5.20) are obtained.

$$\begin{aligned} x' &= 1 \\ 0 &= x^2 - y^2 + \mathcal{O}(x^4) \end{aligned} \tag{5.19}$$

$$\begin{aligned} \dot{x} &= 0 \\ \dot{y} &= x^2 - y^2 + \mathcal{O}(x^4) \end{aligned} \tag{5.20}$$

As it is already known from chapter 2, the time transformation $t = \varepsilon\tau$ between the reduced and the layer problem is not defined at the limit case of $\varepsilon = 0$. Thus for this limit case the two systems have two different dynamics and it is not possible to relate one to the other one. The analysis of the respective dynamics though can give essential information to understand the general behaviour of the system for $\varepsilon \neq 0$ but small.

The critical manifold C_0 is

$$C_0 = \{(x, y) : g(x, y, 0) = 0\} \quad \Rightarrow \quad C_0 = \{(x, y) : x^2 - y^2 + \mathcal{O}(x^4) = 0\} \tag{5.21}$$

The origin is a non-hyperbolic point for the critical manifold, and in particular there is a transcritical bifurcation in it since

$$g(0, 0, 0) = 0, \quad \frac{\partial g}{\partial y}(0, 0, 0) = 0$$

$$\frac{\partial g}{\partial x}(0,0,0) = 0, \quad \frac{\partial^2 g}{\partial x \partial y}(0,0,0) = 0 \quad \text{and} \quad \frac{\partial^2 g}{\partial x^2}(0,0,0) = 2 \neq 0$$

This behaviour is well understood looking at figure 5.6. Note that for a generic potential of the type $V(x) = x^2 + \mathcal{O}(x^4)$, the critical manifold C_0 will be the bisecting line only very close to the degenerate point. While on the other case of $V(x) = x^2$ then the critical manifold is given by $y = \pm x$ everywhere.

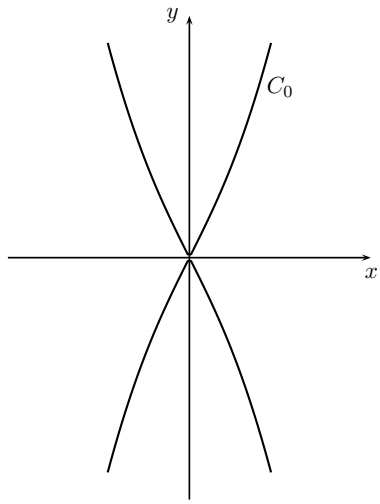

Figure 5.6: Critical manifold for the fast-slow formulation of Schrödinger equation.

5.5.1 Fast Dynamics

The set of the fixed points of the layer problem coincides with the critical manifold C_0 (5.21). The stability analysis of the fixed points of the fast system (5.20) is performed:

$$\left.\frac{\partial g}{\partial y}\right|_{C_0} = \mp 2\sqrt{x^2 + \mathcal{O}(x^4)} \quad \Rightarrow \quad \begin{cases} y > 0 & \text{attracting} \\ y < 0 & \text{repelling} \end{cases}$$

Thus the two critical branches on the upper half plane are attracting, while the two on the lower half plane are repelling.

A symbol is assigned to the four branches of the critical manifold, depending on

their stability properties and their position respect to the y-axis:

$$S_a^+ = \{(x,y) \in C_0 : x > 0, y > 0\}$$
$$S_a^- = \{(x,y) \in C_0 : x < 0, y > 0\}$$
$$S_r^+ = \{(x,y) \in C_0 : x > 0, y < 0\}$$
$$S_r^- = \{(x,y) \in C_0 : x < 0, y < 0\}$$

the a, r subscript means that the fast dynamics is either attracting or repelling. Moreover the $\pm$ superscript determines whether the branch is at the right or at the left of the y-axis. The stability properties of the four branches with their names are depicted in figure 5.7.

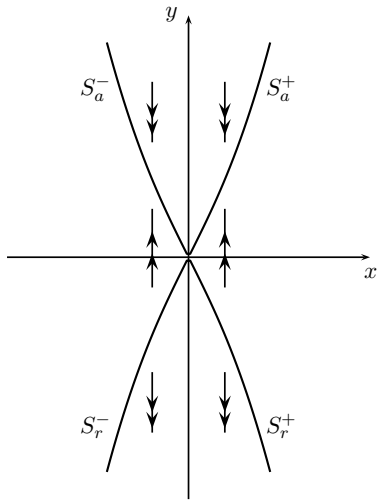

Figure 5.7: Stability properties of the fixed points of the critical manifold. The upper half plane is attracting, while the lower one repelling.

5.5.2 Slow dynamics

The reduced problem (5.19) allows to have dynamics restricted to the critical manifold C_0. On the critical manifold the dynamics is evolving along the x-axis, as it is shown in figure 5.8.

For $\varepsilon \neq 0$ the four normally invariant manifolds are perturbed to slow the manifolds $S_{a,\varepsilon}^{\pm}$ and $S_{r,\varepsilon}^{\pm}$, as assured by Fenichel's theorem 2.5. Close to the origin Fenichel's theorem does not hold and a deeper analysis of the system is needed. The blow-up method presented in chapter 3 is a useful tool to desingularize the degenerate point and understand the dynamics close to it.

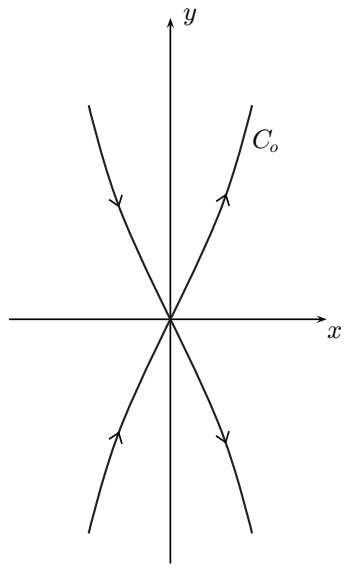

Figure 5.8: Dynamics for the reduced problem.

5.5.3 Conclusion on the dynamics for $\varepsilon \neq 0$

For $\varepsilon \neq 0$ the Fenichel's theorem 2.5 presented in chapter 2 holds when we are far enough from the non-hyperbolic point in the origin. Where Fenichel's theorem holds then we know that a compact submanifold S_0 of the critical manifold C_0 is perturbed on a compact locally invariant manifold S_ε, $\mathcal{O}(\varepsilon)$-close to S_0 which is called the slow manifold. The flow on the slow manifold converges to the slow flow on S_0 defined by (5.11) for $\varepsilon \to 0$. Moreover the same conclusions holds for the stable and unstable manifolds of S_0.

Note that the solution we are interested about is the one lying $\mathcal{O}(\varepsilon)$-close to the critical branch S_a^- for all negative values of x and $\mathcal{O}(\varepsilon)$-close to S_r^+ for positive ones. Thus we are looking for a canard solution. All the solutions that are staying close to these two branches up to a finite value of x are not of interest, because they are related to improper eigenfunctions $\psi(x)$. Indeed their solution would not be defined for all values of x and thus is not in L^2, see section 5.3.

Note that on the other hand the solutions starting close to S_r^- and ending close to S_a^+ are corresponding to negative values of λ and those are not physically reasonable. As it has been already discussed in section 5.3 solutions for $\lambda < 0$ corresponds to regions where $E < V(x)$. In these regions the motion is not allowed, because the kinetic energy of the quantum particle would be negative [Pic00].

5.6 Blow-up of the degenerate point

Consider the fast system of equation (5.14), and introduce the new variable ε evolving under the trivial dynamics $\dot{\varepsilon} = 0$. In this way it is easier to make conclusion on the solution of the system for different values of $\varepsilon \in [0, \varepsilon_0]$, with $\varepsilon_0 \in \mathbb{R}^+$ small enough.

$$\begin{aligned} \dot{x} &= \varepsilon \\ \dot{y} &= x^2 - \varepsilon\lambda - y^2 + \mathcal{O}(x^4) \\ \dot{\varepsilon} &= 0 \end{aligned} \tag{5.22}$$

For this system the origin $(0, 0, 0)$ is degenerate for every value of λ. In order to study the dynamics for $\varepsilon \neq 0$ close to the degenerate point the use of the blow-up method is necessary. The results previously obtained for $V(x) = x^2$ will become useful during the analysis, since the higher other terms on the potential are regular perturbation terms for x small.

The first step in the blow-up method is to determine the quasi-homogeneous blow-up map Γ, see chapter 3. In order to find a suitable map to desingularize the fold point, consider equation (5.22) with only the lowest order term of $V(x)$ acting. Indeed, since this is the dominant term for x close to zero, it should be enough to determine the characteristics of the blow-up, [Kue07]. The system considered to find the map Γ is then

$$\begin{aligned} \dot{x} &= \varepsilon \\ \dot{y} &= x^2 - \varepsilon\lambda - y^2 \\ \dot{\varepsilon} &= 0 \end{aligned} \tag{5.23}$$

Call $B = S^2 \times \mathbb{R}$ and $B_0 = S^2 \times [0, r_0], r_0 > 0$. The quasi-homogeneous blow-up $\Gamma : B_0 \to \mathbb{R}^3$ is defined such that

$$\Gamma(\bar{x}, \bar{y}, \bar{\varepsilon}, \bar{r}) = (\bar{r}^{a_1}\bar{x}, \bar{r}^{a_2}\bar{y}, \bar{r}^{a_3}\bar{\varepsilon})$$

with $a_i, i = 1, 2, 3$ positive integers. For equation (5.23) the conditions are obtained:

$$\begin{aligned} &\bar{r}^{k+a_1}\bar{\varepsilon} = \bar{r}^{a_3}\bar{\varepsilon} \\ &\bar{r}^{k+a_2}(\bar{x}^2 - \bar{\varepsilon}\lambda - \bar{y}^2) = \bar{r}^{2a_1}\bar{x}^2 - \bar{r}^{a_3}\bar{\varepsilon}\lambda - \bar{r}^{2a_2}\bar{y}^2 \end{aligned} \quad \Rightarrow \quad \begin{aligned} &k + a_1 = a_3 \\ &k + a_2 = 2a_1 = a_3 = 2a_2 \end{aligned}$$

Choose $a_1 = 1$ then it follows that $a_2 = 1, a_3 = 2$ and $k = 1$. The blow-up map for system (5.23) is then

$$\Gamma(\bar{x}, \bar{y}, \bar{\varepsilon}, \bar{r}) = (\bar{r}\bar{x}, \bar{r}\bar{y}, \bar{r}^2\bar{\varepsilon}).$$

Note that the degenerate point has been blown-up to an ellipsoid since the powers on the three directions are different.

5.7 Definition of the local charts

The dynamics we aim to study is the solution on the slow manifold $S^-_{a,\varepsilon}$ which continues on the slow manifold $S^+_{r,\varepsilon}$ for a particular choice of the eigenvalue λ. As it is possible to see in figure 5.9 the three charts needed to focus on are:

- chart κ_1 such that $\bar{y} > 0$
- chart κ_3 such that $\bar{y} < 0$
- chart κ_2 which has the purpose of gluing the dynamics on the other two charts and which is obtained keeping $\bar{\varepsilon} > 0$

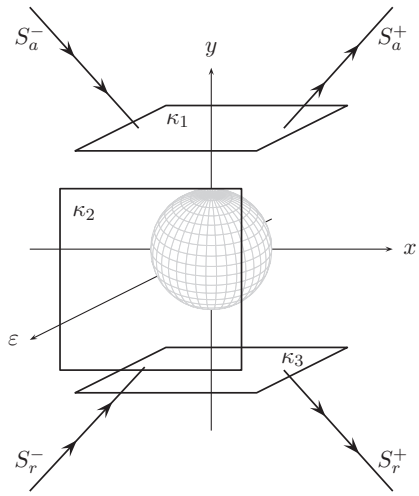

Figure 5.9: Local charts of interest for the study of the blown-up dynamics of the Schrödinger eigenvalue problem.

Call $B^+_{\bar{y}} := B \cap \{\bar{y} > 0\}, B^+_{\bar{\varepsilon}} := B \cap \{\bar{\varepsilon} > 0\}, B^-_{\bar{y}} := B \cap \{\bar{y} < 0\}$, submanifolds of B. On these submanifolds the three charts are well defined.

Instead of the quasi-homogeneous blow-up Γ, on the three charts $\kappa_i, i = 1, 2, 3$ three directional blow-up maps μ_i are defined, such that on each chart $\Gamma = \mu_i \circ \kappa_i$. The computation is shown in detail for the case of chart κ_1. Charts κ_2 and κ_3 can be computed in a similar way, thus only the results will be stated.

Chart κ_1
Consider the directional map $\mu_1 : \mathbb{R}^3 \to \mathbb{R}^3$, such that $y_1 = 1$:

$$\mu_1 := \begin{array}{l} x = r_1 x_1 \\ y = r_1 \\ \varepsilon = r_1^2 \varepsilon_1 \end{array} \tag{5.24}$$

Require the chart $\kappa_1 : B_{\bar{y}}^+ \to \mathbb{R}^3$ such that $\Gamma = \mu_1 \circ \kappa_1$, where $\kappa_1(\bar{x}, \bar{y}, \bar{\varepsilon}, \bar{r}) = (\bar{x}\bar{y}^{-b_1}, \bar{\varepsilon}\bar{y}^{-b_2}, \bar{r}\bar{y}^{-b_3}) = (x_1, \varepsilon_1, r_1)$. Note that the division of each coordinate by the quantity $\bar{y}$ is because this directional blow-up is actually a stereographic mapping.

$$\begin{array}{lcll} x : \bar{r}\bar{x} = r_1 x_1 = \bar{r}\bar{x}\bar{y}^{-b_1-b_3} & & -b_1 - b_3 = 0 & b_1 = 1 \\ y : \bar{r}\bar{y} = r_1 = \bar{r}\bar{y}^{-b_3} & \Rightarrow & -b_3 = 1 & \Rightarrow \quad b_2 = 2 \\ \varepsilon : \bar{r}^2\bar{\varepsilon} = r_1^2\varepsilon_1 = \bar{r}^2\bar{\varepsilon}\bar{y}^{-2b_3-b_2} & & -2b_3 - b_2 = 0 & b_3 = 1 \end{array}$$

Thus we have found that the chart κ_1 is given by

$$\kappa_1 : B_{\bar{y}}^+ \to \mathbb{R}^3 \quad \text{s.t.} \quad \begin{array}{l} x_1 = \bar{x}\bar{y}^{-1} \\ \varepsilon_1 = \bar{\varepsilon}\bar{y}^{-2} \\ r_1 = \bar{r}\bar{y} \end{array}$$

Chart κ_2
Chart $\kappa_2 : B_{\bar{\varepsilon}}^+ \to \mathbb{R}^3$ is defined such that the directional blow-up $\mu_2 : \mathbb{R}^3 \to \mathbb{R}^3$ is done keeping $\varepsilon_2 = 1$. In order to have $\Gamma = \mu_2 \circ \kappa_2$ it is obtained

$$\mu_2 := \begin{array}{l} x = r_2 x_2 \\ y = r_2 y_2 \\ \varepsilon = r_2^2 \end{array} \qquad \kappa_2 : \begin{array}{l} x_2 = \bar{x}\bar{\varepsilon}^{-\frac{1}{2}} \\ y_2 = \bar{y}\bar{\varepsilon}^{-\frac{1}{2}} \\ r_2 = \bar{r}\bar{\varepsilon}^{\frac{1}{2}} \end{array} \tag{5.25}$$

Chart κ_3
Chart $\kappa_3 : B_{\bar{y}}^- \to \mathbb{R}^3$ is defined such that the directional blow-up $\mu_3 : \mathbb{R}^3 \to \mathbb{R}^3$ is done keeping $y_3 = -1$. In order to have $\Gamma = \mu_3 \circ \kappa_3$ it is obtained

$$\mu_3 := \begin{array}{l} x = r_3 x_3 \\ y = -r_3 \\ \varepsilon = r_3^2 \varepsilon_3 \end{array} \qquad \kappa_3 : \begin{array}{l} x_3 = -\bar{x}\bar{y}^{-1} \\ \varepsilon_3 = \bar{\varepsilon}\bar{y}^{-2} \\ r_3 = -\bar{r}\bar{y} \end{array} \tag{5.26}$$

The aim is to study a trajectory and follow its evolution along the three different charts. Thus, the transition functions between the charts $\kappa_i, i = 1, 2, 3$ are here computed. Note that these transition functions are defined only in the subspaces where both the considered charts are well defined. For instance, it is possible to translate points of chart κ_1 to chart κ_2 only for $\varepsilon_1 > 0$ and vice-versa only for $y_2 > 0$.

- κ_{12}: from κ_1 to κ_2, for $\varepsilon_1 > 0$

$$x_2 = x_1 \varepsilon_1^{-\frac{1}{2}}, \quad y_2 = \varepsilon_1^{-\frac{1}{2}}, \quad r_2 = r_1 \varepsilon_1^{\frac{1}{2}}$$

- κ_{21}: from κ_2 to κ_1, for $y_2 > 0$

$$x_1 = x_2 y_2^{-1}, \quad \varepsilon_1 = y_2^{-2}, \quad r_1 = r_2 y_2$$

- κ_{23}: from κ_2 to κ_3, for $y_2 < 0$

$$x_3 = -x_2 y_2^{-1}, \quad \varepsilon_3 = y_2^{-2}, \quad r_3 = -r_2 y_2$$

- κ_{32}: from κ_3 to κ_2, for $\varepsilon_3 > 0$

$$x_2 = -x_3 \varepsilon_3^{-\frac{1}{2}}, \quad y_2 = \varepsilon_3^{-\frac{1}{2}}, \quad r_2 = -r_3 \varepsilon_3^{\frac{1}{2}}$$

Finally

$$\kappa_{13} = \kappa_{12} \circ \kappa_{23}$$

$$\kappa_{31} = \kappa_{32} \circ \kappa_{21}$$

5.8 Dynamics of the blown-up vector field

In this section, the dynamics of system (5.22) is studied on the different charts. For each chart the structure of the local vector field is outlined. The aim is to find the bone structure related to the case of $\varepsilon = 0$ and use it to make conclusions for the case of $\varepsilon \neq 0$ but small.

5.8.1 Dynamics on chart κ_1

Chart κ_1 has coordinates $(x_1, \varepsilon_1, r_1)$ such that $\bar{y} > 0$. The directional blow-up map on this chart is defined as $\mu_1(x_1, \varepsilon_1, r_1) = (r_1 x_1, r_1, r_1^2 \varepsilon_1)$. Thus the dynamics of system (5.22) rewritten in the local coordinates of chart κ_1 is:

$$\begin{aligned}
&\dot{r}_1 x_1 + r_1 \dot{x}_1 = r_1^2 \varepsilon_1 \\
&\dot{r}_1 = r_1^2 x_1^2 - r_1^2 \varepsilon_1 \lambda - r_1^2 + \mathcal{O}(r_1^4 x_1^4) \\
&2 r_1 \dot{r}_1 \varepsilon_1 + r_1^2 \dot{\varepsilon}_1 = 0
\end{aligned}$$

Rescale the time $t_1 = r_1 t$ to remove the exceptional divisor r_1. The dynamics in chart κ_1 is then given by

$$\begin{aligned}
&\dot{x}_1 = \varepsilon_1 - x_1 F_1(x_1, \varepsilon_1, r_1) \\
&\dot{r}_1 = r_1 F_1(x_1, \varepsilon_1, r_1) \qquad , \quad \text{with} \quad F_1(x_1, \varepsilon_1, r_1) = x_1^2 - \varepsilon_1 \lambda - 1 + \mathcal{O}(r_1^2 x_1^4). \quad (5.27) \\
&\dot{\varepsilon}_1 = -2 \varepsilon_1 F_1(x_1, \varepsilon_1, r_1)
\end{aligned}$$

Where the dot means derivative respect to the new time t_1. Note that the time rescale has the physical meaning of studying the system using a slower time t_1. Moreover, since in the original system $r, \varepsilon \geq 0$ for physical reasons, this condition is translated in chart κ_1 requiring $r_1, \varepsilon_1 \geq 0$.

It is possible to note that there are two invariant manifolds $\{r_1 = 0\}$ and $\{\varepsilon_1 = 0\}$. Thus the x_1 axis is an invariant line and the dynamics on it is simply described by

$$\dot{x_1} = -x_1(x_1^2 - 1)$$

The system has the following fixed points

$$p_a^- = (-1, 0, 0), \quad q^{out} = (0, 0, 0), \quad p_a^+ = (1, 0, 0)$$

It is possible to study the stability properties of each of these fixed points. The following three Jacobian matrices are obtained

$$J(p_a^-) = \begin{bmatrix} -2 & 1-\lambda & 0 \\ 0 & 0 & 0 \\ 0 & 0 & 0 \end{bmatrix}, \quad J(q^{out}) = \begin{bmatrix} 1 & 1 & 0 \\ 0 & -1 & 0 \\ 0 & 0 & 2 \end{bmatrix}, \quad J(p_a^+) = \begin{bmatrix} -2 & 1+\lambda & 0 \\ 0 & 0 & 0 \\ 0 & 0 & 0 \end{bmatrix}$$

The two fixed points $p_a^{\pm}$ have a stable direction along the x_1 axis, while they have a 2-D centre eigenspace given by the span of the eigenvectors $\begin{bmatrix} 0 \\ 1 \\ 0 \end{bmatrix}, \begin{bmatrix} 1 \\ 1 \\ \frac{2}{1 \pm \lambda} \end{bmatrix}$. This centre eigenspace is locally tangent to the center manifold of the fixed point $M_a^{\pm}$.

On the other hand, the fixed point q^{out} is an hyperbolic saddle, with a stable direction along the r_1 axis and two unstable directions along the $\begin{bmatrix} 1 \\ 0 \\ 0 \end{bmatrix}$ and $\begin{bmatrix} 1 \\ 0 \\ 1 \end{bmatrix}$ eigenvectors. See figure 5.10 to understand the local dynamics around the three fixed points.

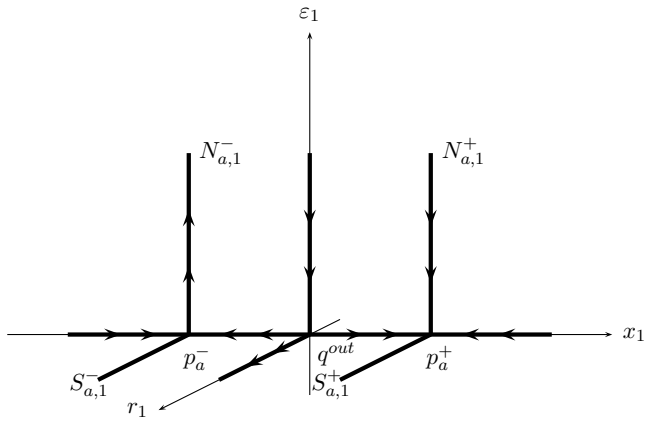

Figure 5.10: Local dynamics around the fixed points $p_a^{\pm}, q^{out}$ in chart κ_1.

In order to establish the dynamics on the centre manifold, it is possible to analyse the dynamics on the two invariant planes $\{r_1 = 0\}$ and $\{\varepsilon_1 = 0\}$ separately once the fixed point is translated in the origin. Introduce the variable $y_1 = x_1 + 1$ such that for $x_1 = -1$ then $y_1 = 0$, system (5.27) becomes

$$\begin{aligned} \dot{y_1} &= -2y_1 + \varepsilon_1(1-\lambda) + \varepsilon_1 y_1 \lambda + 3y_1^2 - y_1^3 + \mathcal{O}(r_1^2 y_1^4) \\ \dot{r_1} &= r_1(y_1 - 1)^2 - r_1\varepsilon_1\lambda - r1 + \mathcal{O}(r_1^2 y_1^4) \\ \dot{\varepsilon_1} &= 4\varepsilon_1 y_1 - 2\varepsilon_1 y_1^2 + 2\varepsilon_1^2\lambda + \mathcal{O}(r_1^2 y_1^4) \end{aligned} \tag{5.28}$$

It is now possible to study system (5.28) on the two invariant planes $\{\varepsilon_1 = 0\}$ and $\{r_1 = 0\}$.

$\{\varepsilon_1 = 0\}$: The system (5.28) becomes

$$\begin{aligned} \dot{y_1} &= -2y_1 + 3y_1^2 - y_1^3 + \mathcal{O}(r_1^2 y_1^4) \\ \dot{r_1} &= -2r_1 y_1 + r_1 y_1^2 + \mathcal{O}(r_1^2 y_1^4) \end{aligned} \tag{5.29}$$

This system has a line of fixed points for $y_1 = 0$, name it $S^-_{a,1}$, this line is locally tangent to the eigenvector $\begin{bmatrix} 0 \\ 1 \\ 0 \end{bmatrix}$. By a time rescale $\tilde{t}_1 = y_1 t_1$ it is possible to desingularize system (5.29) and the following set of equations is obtained

$$\dot{y_1} = -2 + 3y_1 - y_1^2 + \mathcal{O}(r_1^2 y_1^3)$$
$$\dot{r_1} = -2r_1 + r_1 y_1 + \mathcal{O}(r_1^2 y_1^3)$$

with the dot meaning the derivative respect to the new time $\tilde{t}_1$. Thus it is possible to note that on the the line $S^-_{a,1}$ the dynamics is moving towards the fixed point.

It is now shown that $S^-_{a,1}$ is actually the critical branch S^-_a under the coordinate transformation. Indeed the requirement of lying on the invariant plane $\{\varepsilon_1 = 0\}$ for every r_1 means that $\varepsilon = 0$. Moreover, chart κ_1 is a stereographic mapping of the blow-up keeping $\bar{y} > 0$ thus the transformation is defined only for positive values of y. Thus using the coordinate transformation μ_1 it is straightforward to conclude that $S^-_{a,1}$ is actually S^-_a under the coordinate transformation.

$\{r_1 = 0\}$: The system (5.28) becomes

$$\dot{y_1} = -2y_1 + \varepsilon_1(1-\lambda) + \varepsilon_1 y_1 \lambda + 3y_1^2 - y_1^3$$
$$\dot{\varepsilon_1} = 4\varepsilon_1 y_1 - 2\varepsilon_1 y_1^2 + 2\varepsilon_1^2 \lambda$$

It is possible to notice that while the solution on y_1 will reach the zero exponentially fast, the dynamics on ε_1 will evolve slower, since the solution is only algebraic. On this direction, which is called $N^-_{a,1}$ and it is locally tangent to the eigenvector $\begin{bmatrix} 1 \\ 1 \\ \frac{2}{1-\lambda} \end{bmatrix}$, the dynamics is escaping from the fixed point.

Finally it is possible to show that the $N^-_{a,1}$ direction is unique.

Thus the 2D centre manifold on the point p^-_a has boundaries lying on the two invariant planes $\{\varepsilon_1 = 0\}$ and $\{r_1 = 0\}$ given by $S^-_{a,1}$ and $N^-_{a,1}$ respectively.

5.8.2 Dynamics on chart κ_3

Chart κ_3 has coordinates $(x_3, \varepsilon_3, r_3)$ and it is defined for $\bar{y} < 0$. The directional blow-up map on this chart is defined as $\mu_3(x_3, \varepsilon_3, r_3) = (r_3 x_3, -r_3, r_3^2 \varepsilon_3)$. The dynamics of system (5.22) rewritten in chart κ_3 is:

$$\dot{r}_3 x_3 + r_3 \dot{x}_3 = r_3^2 \varepsilon_3$$
$$-\dot{r}_3 = r_3^2 x_3^2 - r_3^2 \varepsilon_3 \lambda - r_3^2 + \mathcal{O}(r_3^4 x_3^4)$$
$$2r_3 \dot{r}_3 \varepsilon_3 + r_3^2 \dot{\varepsilon}_3 = 0$$

Make a time rescale $t_3 = r_3 t$ in order to cancel the exceptional divisor r_3. Thus on chart κ_3 the dynamics is given by

$$\begin{aligned} \dot{x}_3 &= \varepsilon_3 - x_3 F_3(x_3, \varepsilon_3, r_3) \\ \dot{r}_3 &= r_3 F_3(x_3, \varepsilon_3, r_3) \qquad , \quad \text{with} \quad F_3(x_3, \varepsilon_3, r_3) = -x_3^2 + \varepsilon_3 \lambda + 1 + \mathcal{O}(r_3^2 x_3^4). \\ \dot{\varepsilon}_3 &= -2\varepsilon_3 F_3(x_3, \varepsilon_3, r_3) \end{aligned} \tag{5.30}$$

With the dot meaning derivative respect to the slower time t_3.

It is possible to notice that the two manifolds $\{r_3 = 0\}$ and $\{\varepsilon_3 = 0\}$ are invariant. Thus the x_3 axis is an invariant line, and the dynamics on it is given by

$$\dot{x}_3 = -x_3(1 - x_3^2)$$

The analysis of the dynamics of this system is very similar to the one for chart κ_1 and the main results depicted in figure 5.11 are only claimed.

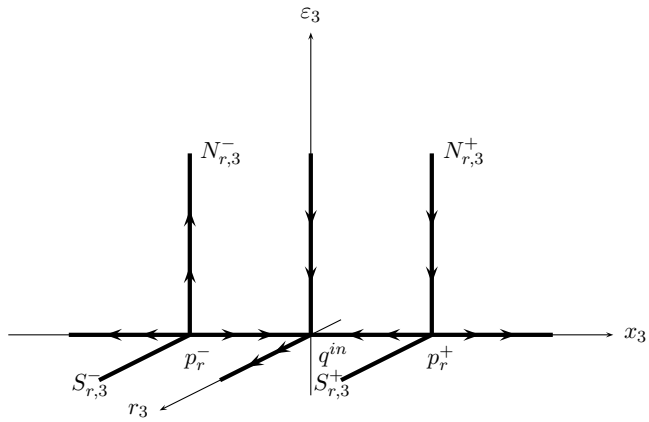

Figure 5.11: Local dynamics around the fixed points $p_r^{\pm}, q^{in}$ in chart κ_3.

On chart κ_3 there are three fixed points: $p_r^{\pm} = (\pm 1, 0, 0), q^{in} = (0, 0, 0)$. The first two fixed points are repelling along the x_3 direction and on the other directions they have a 2D centre manifold. Each centre manifold has boundaries on the two invariant planes $\{\varepsilon_3 = 0\}, \{r_3 = 0\}$ given by the lines $S^{\pm}_{r,3}$ and $N^{\pm}_{r,3}$ respectively. The lines $S^{\pm}_{r,3}$ are locally tangent to the $\begin{bmatrix} 0 \\ 1 \\ 0 \end{bmatrix}$ eigenvector, while the lines $N^{\pm}_{r,3}$ are locally tangent to the $\begin{bmatrix} 1 \\ 1 \\ \frac{2}{-\lambda \pm 1} \end{bmatrix}$ eigenvectors.

The dynamics along $N^{\pm}_{r,3}$ is attracting for p^+_r and repelling for p^-_r, while the dynamics along $S^{\pm}_{r,3}$ is repelling on p^+_r and attracting on p^-_r. The two lines $S^{\pm}_{r,3}$ correspond under the coordinate transformation to the two branches of the critical manifold $S^{\pm}_r$.

The last fixed point q^{in} is an hyperbolic saddle, and it has a stable direction along the x_3 axis and two unstable directions along the $\begin{bmatrix}0\\1\\0\end{bmatrix}$ and $\begin{bmatrix}1\\0\\-1\end{bmatrix}$ vectors.

5.8.3 Dynamics on chart κ_2

Chart κ_2 has coordinates (x_2, y_2, r_2) and it is defined for $\bar{\varepsilon} > 0$. The directional blow-up map on this chart is $\mu_2(x_2, y_2, r_2) = (r_2x_2, r_2y_2, r_2^2)$. System (5.22) in chart κ_2 becomes:

$$\begin{aligned}
&\dot{r}_2x_2 + r_2\dot{x}_2 = r_2^2\\
&\dot{r}_2y_2 + r_2\dot{y}_2 = r_2^2x_2^2 - r_2^2\lambda - r_2^2y_2^2 + \mathcal{O}(r_2^4x_2^4)\\
&2r_2\dot{r}_2 = 0
\end{aligned}$$

Make a time rescale $t_2 = r_2t$ to remove the exceptional divisor r_2. Thus in chart κ_2 the dynamics is given by

$$\begin{aligned}
\dot{x}_2 &= 1\\
\dot{y}_2 &= x_2^2 - \lambda - y_2^2 + \mathcal{O}(r_2^2x_2^4)\\
\dot{r}_2 &= 0
\end{aligned} \tag{5.31}$$

With the dot meaning derivative respect to the new, slower time t_2. Note that the dynamics on chart κ_2 is just a rescale of the original dynamics (5.14) to remove the ε-dependence.

There are no fixed points in this chart. For $r_2 = 0$, the solutions of the Riccati equation depending on the value of λ has already been found in section 5.4. Since the chart κ_2 is defined only locally, when the trajectory is going to the borders of the chart, it is necessary to make a coordinate transform from one chart to the other one, in order not to loose any information about the trajectory. The trajectory solutions for $\lambda = 1$ and $\lambda = 3$ are now analysed and it is observed where these trajectories will end up at the borders of chart κ_2 for the case of $r_2 = 0$.

CASE OF $\lambda = 1$
The trajectory $\gamma_2^{(\lambda=1)}$ is a solution of equation (5.31) for $\lambda = 1$ and $r_2 = 0$:

$$\gamma_2^{(\lambda=1)}(t): \quad \begin{aligned} x_2 &= t \\ y_2 &= -t \\ r_2 &= 0 \end{aligned}$$

the aim is to see what this orbit is approaching for $t \to \pm\infty$ in the other two charts. Since the $\gamma_2^{(\lambda=1)}$ solution is symmetric respect to the origin, it is enough to study what it is approaching for $t \to -\infty$.

For negative times, which means $y_2 > 0$, the trajectory can be described on both the κ_2 and κ_1 charts. A generic point of time $t < 0$ has position and tangency given by

$$\kappa_{21}(\gamma_2^{(\lambda=1)}(t))_{\text{s.t.}y_2>0}: \begin{cases} x_1 &= -1 \\ \varepsilon_1 &= (-t)^{-2}, \\ r_1 &= 0 \end{cases} \quad \frac{d}{dt}\left(\kappa_{21}(\gamma_2^{(\lambda=1)})\right) = \begin{cases} \dot{x}_1 &= 0 \\ \dot{\varepsilon}_1 &= -2t^{-3} \\ \dot{r}_1 &= 0 \end{cases}$$

Thus for $t \to -\infty$ it is obtained

$$\lim_{t\to-\infty} \kappa_{21}(\gamma_2^{(\lambda=1)}(t)) = p_a^- = \begin{bmatrix} -1 \\ 0 \\ 0 \end{bmatrix}, \quad \lim_{t\to-\infty} \frac{d}{dt}\left(\kappa_{21}(\gamma_2^{(\lambda=1)}(t))\right) = \begin{bmatrix} 0 \\ \infty \\ 0 \end{bmatrix}$$

which means that for $t \to -\infty$ the orbit $\gamma_2^{(\lambda=1)}(t)$ is approaching p_a^- being tangent to the $N_{a,1}^-$ manifold. On the other hand, for positive times, which means $y_2 < 0$, the trajectory can be described by both the charts κ_2 and κ_3. Thus, for $t \to +\infty$ the trajectory $\gamma_2^{(\lambda=1)}(t)$ is approaching p_r^+ being tangent to the manifold $N_{r,3}^+$.

It is possible to conclude that $\gamma_2^{(\lambda=1)}$ is an heteroclinic connection between p_a^- and p_r^+.
By the Poincarè Bendixon theorem it is possible to conclude that for $\lambda = 1$ and $r_2 = 0$ the dynamics is the one depicted in figure 5.12. There is one heteroclinic connection between p_a^- and p_r^+ tangent respectively to the manifolds $N_{a,1}^-$ and $N_{r,3}^+$. Orbits can be backwards asymptotic to q^{out} and forward asymptotic to p_a^+ otherwise they are backwards asymptotic to p_r^- and forward asymptotic to q^{in}.

CASE OF $\lambda = 3$
The trajectory $\gamma_2^{(\lambda=3)}$ is a solution of equation (5.31) for $\lambda = 3$ and $r_2 = 0$:

$$\gamma_2^{(\lambda=3)}(t): \quad \begin{aligned} x_2 &= t \\ y_2 &= -t + \frac{1}{t} \\ r_2 &= 0 \end{aligned}$$

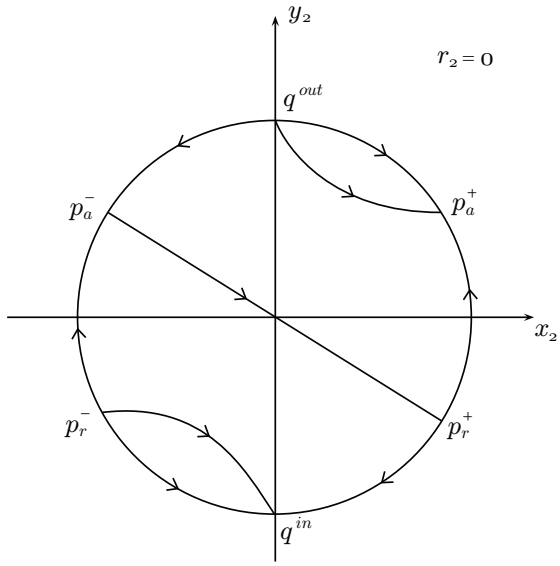

Figure 5.12: Dynamics on chart κ_2 for $\lambda = 1$ showing the limit points for the trajectories on the other charts κ_1 and κ_3.

For $t \to \pm\infty$ the orbit is approaching $p^+_{r,a}$ being tangent to $N^+_{r,a}$ in charts κ_1 and κ_3 as in the previous case. Figure 5.12 shows the trajectory of $\gamma_2^{(\lambda=3)}$ and the limit points in the other charts κ_1 and κ_3. The computation are very similar to the ones done for the case of $\lambda = 1$ and are only briefly stated here. Since also in this case the solution $\gamma_2^{(\lambda=3)}$ is symmetric respect to the origin, only the computation for negative times are shown.

$$\kappa_{21}(\gamma_2^{(\lambda=3)}(t))_{\text{s.t.}y_2>0} : \begin{cases} x_1 &= \frac{-t^2}{t^2-1} \\ \varepsilon_1 &= \frac{t^2}{(t^2-1)^2} \\ r_1 &= 0 \end{cases}$$

Thus

$$\lim_{t\to-\infty} \kappa_{21}(\gamma_2^{(\lambda=3)}(t))_{\text{s.t.}y_2>0} = p_a^- = \begin{bmatrix} -1 \\ 0 \\ 0 \end{bmatrix}$$

$$\kappa_{23}(\gamma_2^{(\lambda=3)}(t))_{\text{s.t.}y_2<0} : \begin{cases} x_3 &= \frac{t^2}{t^2-1} \\ \varepsilon_3 &= \frac{t^2}{(t^2-1)^2} \\ r_3 &= 0 \end{cases}$$

Thus

$$\lim_{t\to 0^-} \kappa_{23}(\gamma_2^{(\lambda=3)}(t))_{\text{s.t.}\, y_2<0} = q_{in} = \begin{bmatrix} 0^- \\ 0^+ \\ 0 \end{bmatrix}$$

Moreover

$$\lim_{t\to 0^+} \kappa_{21}(\gamma_2^{(\lambda=3)}(t))_{\text{s.t.}\, y_2>0} = q_{out}$$

$$\lim_{t\to +\infty} \kappa_{23}(\gamma_2^{(\lambda=3)}(t))_{\text{s.t.}\, y_2<0} = p_r^+$$

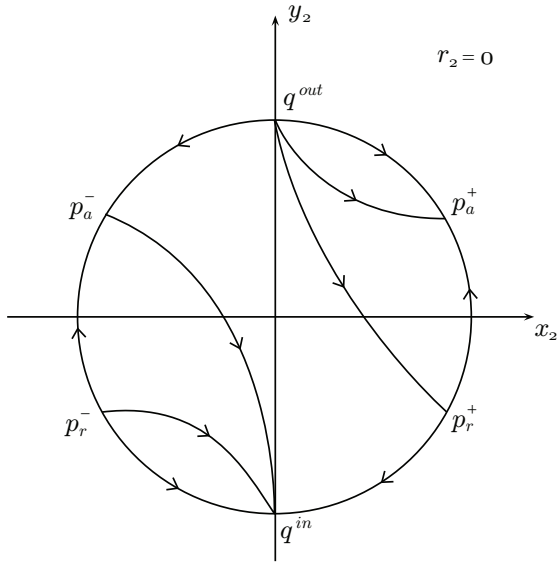

Figure 5.13: Dynamics on chart κ_2 for $\lambda = 3$ showing the limit points for the trajectories on the other charts κ_1 and κ_3.

5.9 Connecting all the building blocks

The aim now is to use all the information obtained in each different chart and glue them together to get a complete overview of the solution we want to find. This solution is the one connecting a slow manifold $S^-_{a,\varepsilon}$ to a slow manifold $S^+_{r,\varepsilon}$ for a value of $\varepsilon \neq 0$, as it is shown in figure 5.14 with a dotted line. In section 5.4 it has been found a connection between the critical manifolds S^-_a and S^+_r for $V(x) = x^2$. This case correspond to a connection of the critical manifolds through chart κ_2 for $\varepsilon = 0$. Remember that Fenichel's theorem describes the slow manifold only for a compact submanifold of the critical manifold. However the solution we aim

to find is the one that remains ε-close to the critical manifold on all the x-axis. Thus the conclusion we are going to state in this section are not complete, and an additional analysis is required to extend the results to all the x-axis.

Consider for the fixed value $y = \rho$ a suitable interval of values for x such that the critical manifold S_a^- is contained in the interval, see figure 5.14. Moreover consider $\varepsilon \in [0, \varepsilon_0], \varepsilon_0 > 0$.

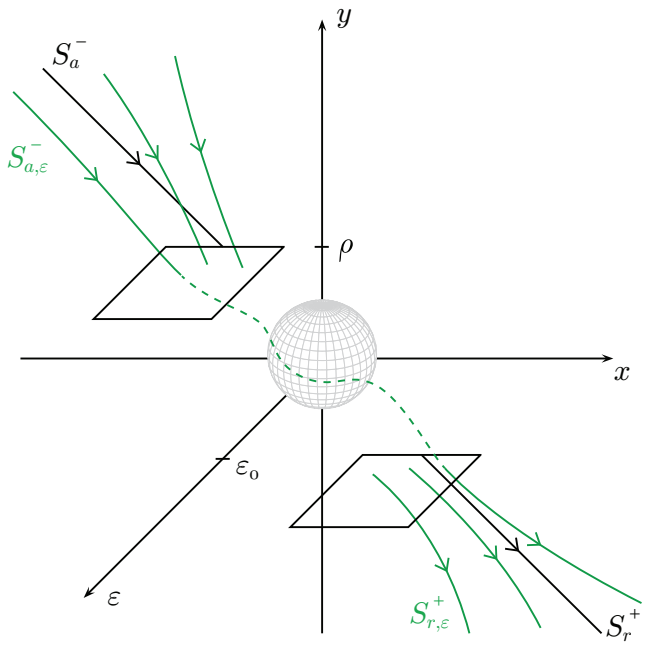

Figure 5.14: Critical branches S_a^- and S_r^+ in black for $\varepsilon = 0$. In green are plotted the slow manifolds $S_{a,\varepsilon}^-$ and $S_{r,\varepsilon}^+$. The dotted line is the solution we aim to find using the blow-up method: a connection between the two slow manifolds.

Since the local map μ_1 is defined as (5.24) then the set considered is translated in chart κ_1 in the rectangle

$$R_1 : \qquad x_1 \in I(-1), \quad r_1 = \rho, \quad \varepsilon_1 \in [0, \frac{\varepsilon_0}{\rho^2}]$$

with $I(-1)$ an interval containing the -1 value. The rectangle R_1 is shown in figure 5.15. Note that any trajectory in chart κ_1 with initial point in R_1 corresponds to a slow manifold $S_{a,\varepsilon}^-$ on the original chart (x, y, ε). The line $S_{a,1}^-$ lying on the invariant plane $\{\varepsilon_1 = 0\}$ crosses transversally R_1. Remember that this line is the translation in chart κ_1 of the critical branch S_a^-.

From Fenichel's theory, the slow manifold curves $S^-_{a,\varepsilon}$ depicted in figure 5.14 are ε-close to the critical manifold S^-_a and are exponentially close one from each other. Thus it is not possible to distinguish between the different slow manifold curves $S^-_{a,\varepsilon}$ and and it is enough to do the analysis for only one of them without loss of information.

As it is possible to see in figure 5.15 the centre manifold $M^-_{a,1}$ is transverse to the rectangle R_1. Moreover $M^-_{a,1}$ is foliated by a family of curves $\varepsilon = r_1^2\varepsilon_1 = \text{const}$. Thus we decide to select as initial condition in chart κ_1 the point lying in the bold line of figure 5.15 which is the intersection line between $M^-_{a,1}$ and R_1 with $\varepsilon_1 = \frac{\varepsilon}{\rho}$. From this point it departs in chart κ_1 a trajectory $\hat{\gamma}$, see figure 5.15. Note that all the other initial points in R_1 not lying in $M^-_{a,1}$ have the corresponding trajectory in chart κ_1 which are going to approach exponentially fast the centre manifold $M^-_{a,1}$, since we have a contraction along the x_1 direction.

The picked trajectory $\hat{\gamma}$ on the centre manifold has the initial condition

$$\hat{\gamma}_0 : \qquad x_1 = \frac{x}{\rho}, \quad r_1 = \rho, \quad \varepsilon_1 = \frac{\varepsilon}{\rho^2}$$

which is $\mathcal{O}(\varepsilon)$-close to the invariant plane $\{\varepsilon_1 = 0\}$. Since the trajectory $\hat{\gamma}$ is evolving along the foliation $\varepsilon = r_1^2\varepsilon_1 = \text{const}$, then it will approach the value of $\varepsilon_1 = \delta \quad \sqrt{\varepsilon}$-close to the invariant plane $\{r_1 = 0\}$.

The next step is to study the variation of the trajectories on the centre manifold $M^-_{a,q}$ respect to the parameter λ. Consider indeed the parameter λ as a variable, then the intersection of the line $N^-_{a,1}$ with the value $\varepsilon_1 = \delta$ can be seen as a straight curve C_0 on the extended space $(x_1, \varepsilon_1, r_1, \lambda)$. There is a second curve $C_{\sqrt{\varepsilon}}$ which is $\sqrt{\varepsilon}$-close to the curve C_0 and is determined by the variation of the picked trajectory $\hat{\gamma}$ upon λ for $\varepsilon_1 = \delta$.

In figure 5.16 are shown the curves C_0 and $C_{\sqrt{\varepsilon}}$ as a function of $(\lambda, \varepsilon_1, r_1)$. The evolution of the trajectories on the variable x_1 can be obtained by the centre manifold theorem since it is possible to write $x_1 = h_1(\varepsilon_1, r_1, \lambda)$.

It is possible to translate these curves on chart κ_2 and follow their evolution there. In chart κ_2 depending on the value of λ considered, we need to make different considerations. Thus we first consider the interval $I_1(\lambda) : \lambda = 1 \in I_1(\lambda)$ in section 5.9.1 and subsequently in section 5.9.2 the case of interval $I_3(\lambda) : \lambda = 3 \in I_3(\lambda)$.

5.9.1 First eigenfunction for $\lambda = 1$

In section 5.8.3 it has been shown that for $\lambda = 1$ and $\varepsilon = 0$ there exists a connection between $N^-_{a,1}$ and $N^+_{r,3}$ by a $\gamma_2^{(\lambda=1)}$ solution, see figure 5.12.

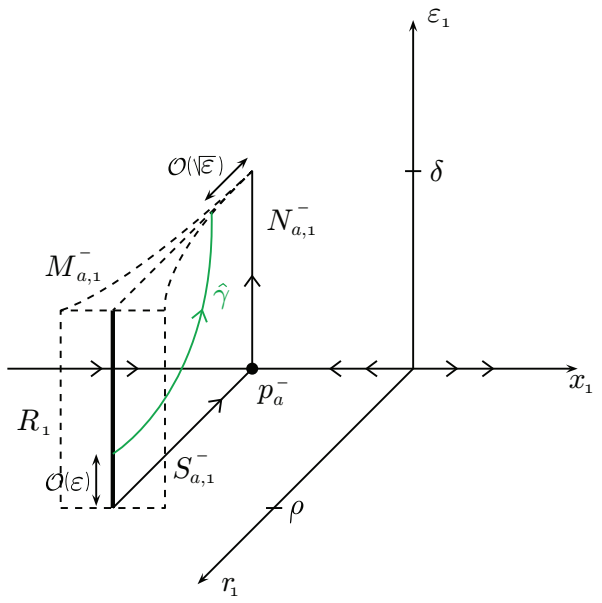

Figure 5.15: In black are plotted the building block for $\varepsilon = 0$ such as the lines $S^-_{a,1}$ and $N^-_{a,1}$. The trajectory $\hat{\gamma}$ determined for $\varepsilon \neq 0$ is lying on the centre manifold $M^-_{a,1}$. This centre manifold crosses transversally the rectangle of initial points R_1.

The transformation of curve C_0 in chart κ_2 is $\kappa_{12}(C_0)$. This curve is containing information about the $N^-_{a,1}$ line for $\lambda = 1$. Moreover the curve $\kappa_{12}(C_0)$ is lying in the extended space (x_2, y_2, λ) and it is defined for $r_2 = 0$. Consider the evolution of $\kappa_{12}(C_0)$ in chart κ_2. This curve of initial points, creates a manifold of trajectories under the flow (5.31) for $r_2 = 0$ in the extended space (x_2, y_2, λ). Consider the Poincarè section

$$P_0 : \{\kappa_{12}(C_0)\} \to \{y_2 = 0\}$$

Thus it is possible to identify a line L_0 determined by the evolution in chart κ_2 of the curve $\kappa_{12}(C_0)$ with the Poincarè section in $y_2 = 0$, see figure 5.17.

Consider the tangent space to the curve L_0. This tangent manifold $T(L_0)$ is crossing transversally the λ axis for the value of $\lambda = 1$ as it is shown in figure 5.18. Remember that the point on curve C_0 corresponding to $\lambda = 1$ is backwards asymptotic to $N^-_{a,1}$.

In the case of $\varepsilon \neq 0$ then the trajectories starting from $\kappa_{12}(C_{\sqrt{\varepsilon}})$ evolves following equation (5.31) with $r_2 \neq 0$. In equation (5.31) the r_2-term appears as a regular perturbation term, which is of order $\mathcal{O}(r_2^2) \sim \mathcal{O}(\varepsilon) < \mathcal{O}(\sqrt{\varepsilon})$. Thus considering

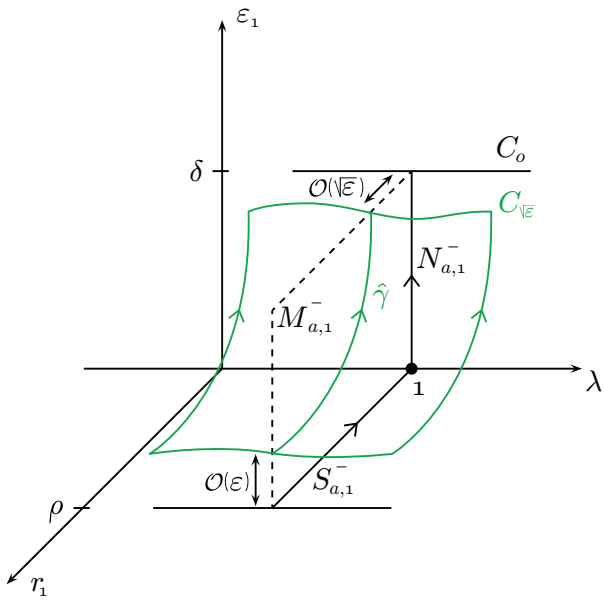

Figure 5.16: The variation of $N^-_{a,1}$ and of $\hat{\gamma}$ depending on the parameter $\lambda \in I_1(\lambda)$ determines the two curves C_0 and $C_{\sqrt{\varepsilon}}$respectively.

the new Poincarè section

$$P_{\sqrt{\varepsilon}} : \{\kappa_{12}(C_{\sqrt{\varepsilon}} :)\} \to \{y_2 = 0\}$$

it is possible to find the curve $L_{\sqrt{\varepsilon}}$ determined by the evolution in chart κ_2 of the curve $\kappa_{12}(C_{\sqrt{\varepsilon}})$. The curve $L_{\sqrt{\varepsilon}}$ is $\sqrt{\varepsilon}$-close to L_0 and their tangent manifolds are as well. Thus the tangent manifold of the curve $L_{\sqrt{\varepsilon}}$ is still crossing the λ axis transversally for small values of r_2 at a distance which is $\mathcal{O}(\sqrt{\varepsilon})$ from $\lambda = 1$.

All these considerations can be repeated by taking a slow manifold $S^+_{r,\varepsilon}$ which is ε-close to the critical branch S^+_r as in figure 5.14 and flowing the trajectory backwards along chart κ_3 and then κ_2. By the symmetry of the solution in chart κ_2 we expect to obtain the black and green dashed curves in figure 5.18.

The transversality of the $T(L_0)$ to the λ axis and subsequently of $T(L_{\sqrt{\varepsilon}})$ has been shown by Krupa and Szmolyan in [KS01b].
Consider a trajectory of initial point in $C_{\sqrt{\varepsilon}}$ determined for a value of $\lambda \in I_1(\lambda)$. Using the Poincarè section defined above it is possible to determine the point $x_2^- \in L_0$ where the trajectory intersects the x_2 axis. Note that $x_2^- = x_2^-(\lambda, r_2)$. Consider the symmetric problem of starting from a generic repelling slow manifold $S^+_{r,\varepsilon}$. Then it is possible to find the point x_2^+ of intersection of the trajectory with the x_2 axis, for the same value $\lambda \in I_1(\lambda)$.

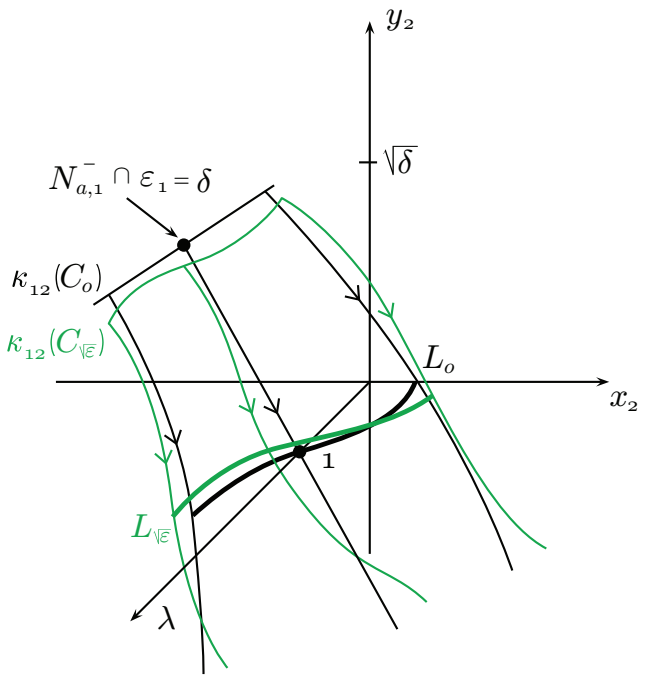

Figure 5.17: Evolution in chart κ_2 of the curves $\kappa_{12}(C_0)$ and $\kappa_{12}(C_{\sqrt{\varepsilon}})$. Their intersection with the plane $\{y_2 = 0\}$ determines the two curves L_0 and $L_{\sqrt{\varepsilon}}$.

Define the function $F_2(\lambda, r_2) = x_2^+ - x_2^- = -2x_2^-$ by the symmetry condition on the potential $V(x)$. The following conditions holds

$$F_2(1, 0) = 0$$

Moreover Krupa and Szmolyan have shown in [KS01b] that

$$\frac{\partial}{\partial \lambda} F_2(1, 0) \neq 0$$

which means that the tangent manifold to L_0 has to cross transversally the x_2 axis for $\lambda = 1$, see figure 5.18.

Thus by the implicit function theorem $\exists \lambda_c(r_2) : \lambda(0) = 1$ and an interval $I_{r_2} : 0 \in I_{r_2}$ such that $F_2(\lambda_c(r_2), r_2) = 0$. We can conclude that $\exists \lambda_c = 1 + \mathcal{O}(\sqrt{\varepsilon})$ such that the two slow manifolds $S^-_{a,\varepsilon}$ and $S^+_{r,\varepsilon}$ flowed in chart κ_2 are transverse and thus there exists a solution $\gamma_2^{(\lambda_c)}$ on chart κ_2 that connects the two slow manifolds and give rise to a canard type solution for $\varepsilon \neq 0$.

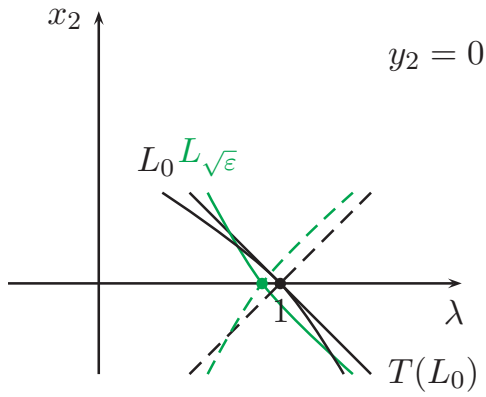

Figure 5.18: Curve L_0 in black and $L\sqrt{\varepsilon}$ in green. The dashed lines are the symmetric case starting from $S^+_{r,\varepsilon}$ and flowing backwards.

In terms of our original eigenvalue problem (5.8) in the case of a generic symmetric potential $V(x)$, this means that we can find an eigenvalue λ_c which is $\mathcal{O}(\sqrt{\varepsilon})$-close to -1 with related eigenfunction ψ given by equation (5.17):

$$\psi(x) = Ce^{\frac{-x^2}{2\varepsilon}}$$

5.9.2 Second eigenfunction for $\lambda = 3$

The arguments on chart κ_1 are the same ones as for the case of $\lambda = 1$ apart that now we consider the curve C_0 and $C_{\sqrt{\varepsilon}}$ defined around the value of $\lambda = 3$ in chart κ_1, see figure 5.16.

The transformation of curve C_0 in chart κ_2 is $\kappa_{12}(C_0)$. This curve is containing information about the $N^-_{a,1}$ line for $\lambda = 3$. Moreover the curve $\kappa_{12}(C_0)$ is lying in the extended space (x_2, y_2, λ) and it is defined for $r_2 = 0$. Consider the evolution of $\kappa_{12}(C_0)$ in chart κ_2 as shown in figure 5.19. This curve of initial points, creates a manifold of trajectories under the flow (5.31) for $r_2 = 0$ in the extended space (x_2, y_2, λ). It is possible to identify a Poincarè section determined by the evolution of the curve $\kappa_{12}(C_0)$ for $y_2 = -\beta^{-1}$, with β a small, positive value.

$$P_0 : \{\kappa_{12}(C_0)\} \to \{y_2 = -\beta^{-1}\}$$

In figure 5.20 on the left it is shown the Poincarè section P_0 for trajectory obtained for $\lambda = 3$.

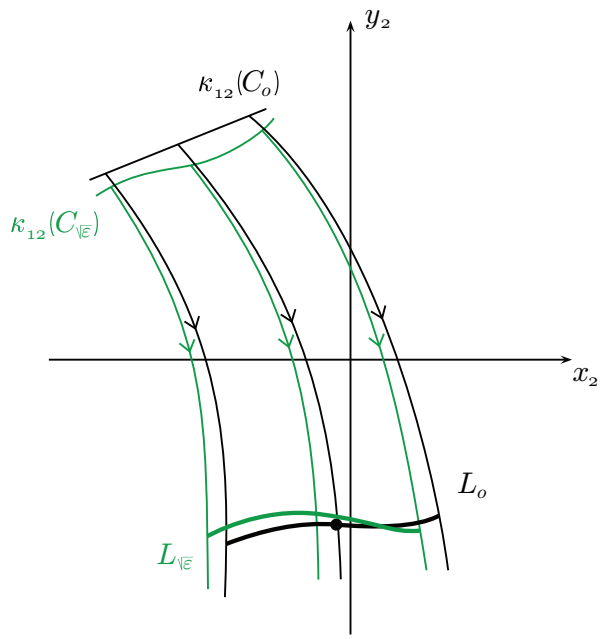

Figure 5.19: Evolution in chart κ_2 of the curves $\kappa_{12}(C_0)$ and $\kappa_{12}(C_{\sqrt{\varepsilon}})$. Their intersection with the plane $\{y_2 = 0\}$ determines the two curves L_0 and $L_{\sqrt{\varepsilon}}$.

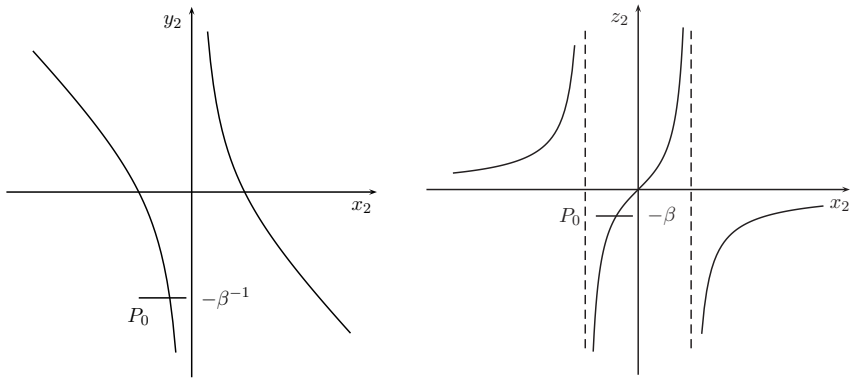

Figure 5.20: Solution for $\lambda = 3$ and $r_2 = 0$. Definition of the Poincarè section for $r_2 = 0$ in the two coordinates systems (x_2, y_2) and (x_2, z_2).

The intersection of the flowed curve $\kappa_{12}(C_0)$ with the Poincarè section determines

a line L_0, see figure 5.19. Consider now the change of coordinates

$$z_2 = \frac{1}{y_2}$$

which is well defined for $y_2 \neq 0$. For $\beta < \infty$ the Poincarè section is well defined for the new set of variables (x_2, z_2, r_2, λ) and lies in $z_2 = -\beta$ as shown in figure 5.20 on the right.

The curve L_0 can be transferred to the new extended coordinates (x_2, z_2, r_2, λ) and it is lying at the fixed value of $z_2 = -\beta$.

The dynamics on chart κ_2 can be rewritten in the new system of variables (x_2, z_2, r_2) as

$$\begin{aligned} \dot{x}_2 &= 1 \\ \dot{z}_2 &= 1 + \lambda z_2^2 - z_2^2 x_2^2 + z_2^2 \mathcal{O}(r_2^2 x_2^4) \\ \dot{r}_2 &= 0 \end{aligned} \tag{5.32}$$

and we can see that the set of equations (5.32) is well defined for $z_2 = 0$. Thus it is possible to flow the curve L_0 forward and we can define a new Poincarè section for $z_2 = 0$:

$$\tilde{P}_0 : \{L_0\} \to \{z_2 = 0\}$$

The flowed curved L_0 makes a new curve $\tilde{L}_0$ when intersected with the Poincarè section $\tilde{P}_0$. See figure 5.21.

Consider the tangent manifold $T(\tilde{L}_0)$. This manifold is crossing transversally the λ axis for the value of $\lambda = 3$ as it is shown in figure 5.22. Remember that the point for $\lambda = 3$ on curve C_0 is backwards asymptotic to $N^-_{a,1}$.

Repeat the same procedure starting from the slow manifold $S^-_{r,\varepsilon}$ and flow backwards along chart κ_3 and κ_2 to obtain the curve $\tilde{L}^r_0$ for $r_2 = 0$. Since the equations (5.31) have a symmetric solution in chart κ_2 for $r_2 = 0$ it is possible to conclude that also the curve $\tilde{L}^r_0$ obtained in this way crosses transversally the λ axis and the curve $\tilde{L}_0$.

By the use of the change of coordinates we have been able to glue together the attracting branch of the critical branch S^-_a to the repelling one $S^+_{r,}$ in chart κ_2 for the case of $r_2 = 0$. The aim now is to show that it is possible to do the same thing considering the corresponding slow manifolds $S^-_{a,\varepsilon}$ and $S^+_{r,\varepsilon}$ for $\varepsilon \neq 0$.

Consider for case $\varepsilon \neq 0$ the curve $C_{\sqrt{\varepsilon}}$ which is $\sqrt{\varepsilon}$-close to the curve C_0. Transform the curve into chart κ_2 obtaining in this way the new curve $\kappa_{12}(C_{\sqrt{\varepsilon}})$. The solution of (5.31) with starting points in $C_{\sqrt{\varepsilon}}$ creates a manifold which will intersect the Poincarè section

$$P_{\sqrt{\varepsilon}} : \{\kappa_{12}(C_{\sqrt{\varepsilon}})\} \to \{y_2 = -\beta^{-1}\}$$

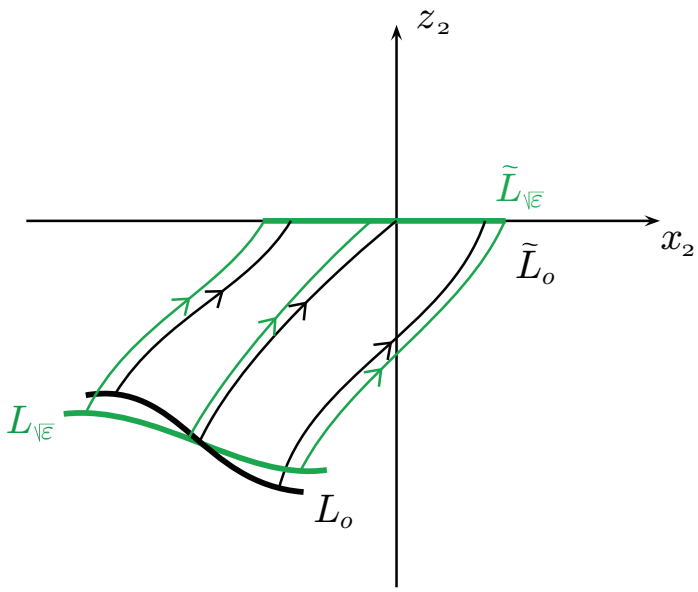

Figure 5.21: Evolution in chart (x_2, y_2, r_2, λ) of the curves L_0 and $_{\sqrt{\varepsilon}}$. Their intersection with the plane $\{z_2 = 0\}$ determines the two curves $\tilde{L}_0$ and $\tilde{L}_{\sqrt{\varepsilon}}$.

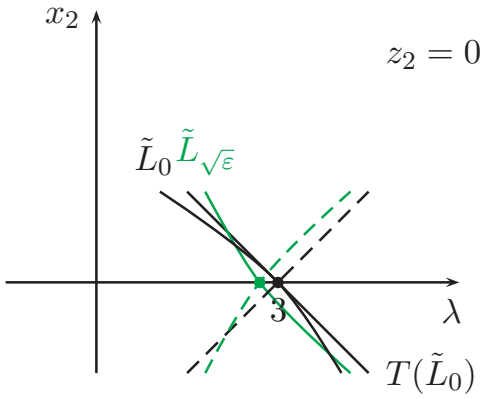

Figure 5.22: Curve $\tilde{L}_0$ in black and $\tilde{L}_{\sqrt{\varepsilon}}$ in green. The dashed lines are the symmetric case starting from $S^+_{r,\varepsilon}$ and flowing backwards.

determining a curve $L_{\sqrt{\varepsilon}}$ as it is shown in figure 5.19. Since in equations (5.31) the terms in r_2 are regular perturbation terms, the curve $L_{\sqrt{\varepsilon}}$ is $\mathcal{O}(\sqrt{\varepsilon})$-close to L_0. As previously done for the curve L_0, the curve $L_{\sqrt{\varepsilon}}$ can be transformed to the

extended system of coordinates (x_2, z_2, r_2, λ). Since in equation (5.32) the terms in r_2 are still a regular perturbation term, the curved can be flowed forward until the Poincarè section $\tilde{P}_{\sqrt{\varepsilon}}$ determined for $z_2 = 0$. This intersection creates a new curve $\tilde{L}_{\sqrt{\varepsilon}}$. This flowed curve is $\sqrt{\varepsilon}$-close to $\tilde{L}_0$ and thus it still keeps the transversal properties.

We have not shown that the transversality condition holds, but we assume it does: indeed it is a non-degeneracy condition, and in general these conditions holds. A way to show the condition holds would be writing the variational equations for the vector field (5.31). This would have been the next step if there was more time for the project.

5.9.3 Next eigenfunctions for $\lambda > 3$

As it is possible to see from equation (5.16) the solution of the Riccati equation for $\lambda = 2n + 1, n \in \mathbb{N}_0$ is crossing n times the x-axis on chart κ_2. For instance the case of $\lambda = 5$ depicted in figure 5.23 is crossing the x_2 axis three times. Using in a proper way the analysis made for the cases of $\lambda = 1$ and $\lambda = 3$ it is possible to conclude that the slow manifolds $S^-_{a,\varepsilon}$ and $S^+_{r,\varepsilon}$ are always crossing transversally for any $\lambda = 2n + 1, n \in \mathbb{N}_0$.

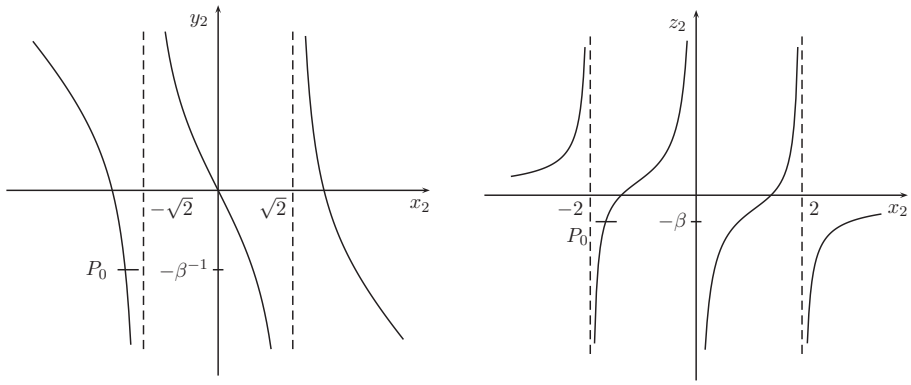

Figure 5.23: Solution for $\lambda = 5$ and $r_2 = 0$. Definition of the Poincarè section for $r_2 = 0$ in the two coordinates systems (x_2, y_2) and (x_2, z_2).

We outline now briefly how to understand the last statement. As done in the two previous cases of $\lambda = 1$ it is possible to determine in chart κ_2 the two curves $\kappa_{12}(C_0)$ and $\kappa_{12}(C_{\sqrt{\varepsilon}})$ obtained from chart κ_1 as in figure 5.16. Using the equations (5.31) it is possible to flow forward the two curves until either they reach the Poincarè section P_0 or $P_{\sqrt{\varepsilon}}$ defined for $y_2 = -\beta^{-1}, \beta > 0$ depending on the value of ε, see figure 5.23.

Next introduce the coordinate transformation $z_2 = \frac{1}{z_2}$ which is well defined for $y_2 \neq 0$. The two Poincarè sections are now defined for $z_2 = -\beta$ and it is possible to flow them forward using the equations (5.32) until they reach the new Poincarè sections $\hat{P}_0$ or $\hat{P}_{\sqrt{\varepsilon}}$ defined for $z_2 = \beta^{-1}$. It is possible to transform back the two sections to the old coordinate y_2 and keeping flowing forward using equation (5.31) until they reach the final Poincarè sections $\tilde{P}_0$ or $\tilde{P}_{\sqrt{\varepsilon}}$ defined for $y_2 = 0$. In this case it is then possible to use Krupa and Szmolyan lemma as done for $\lambda = 1$ to conclude that these sections cross transversally the λ axis for $y_2 = 0$ in $\lambda = 5$.

Repeating the same procedure backward starting from $S^+_{r,\varepsilon}$ it is possible to conclude that the two slow manifolds $S^-_{a,\varepsilon}$ and $S^+_{r,\varepsilon}$ cross transversally. Thus for $\varepsilon \neq 0$ it is possible to find an eigenvalue $\lambda_c = 5 + \sqrt{\varepsilon}$ such that a picked up slow manifold $S^-_{a,\varepsilon}$ will be connecting with a slow manifold $S^+_{r,\varepsilon}$.

It is possible to understand then that the procedure and the conclusions are independent on how many time the solution $\gamma_2^{(\lambda)}$ is crossing the x_2 axis in chart κ_2. For $\varepsilon = 0$ this trajectory will intersect the origin either in the (x_2, y_2) plane or in the (x_2, z_2). Thus using the transversality conditions determined for the cases of $\lambda = 1$ and $\lambda = 3$ it is possible to conclude that the slow manifolds $S^-_{a,\varepsilon}$ and $S^+_{r,\varepsilon}$ are always crossing transversally for any $\lambda = 2n + 1, n \in \mathbb{N}_0$.

Chapter 6

Conclusion

In this thesis we have seen two different applications of the blow-up method for slow-fast systems. This method have resulted to be a very powerful tool.

- In the case of the analysis on the behaviour of non-Newtonian fluids the method has been able to glue together the small and large scale dynamics. Moreover the blow-up method has been used by Krupa and Szmolyan as well to show the behaviour of the system close to the fold point for the case of $T_{12}^M < \tau < T^e$. With this analysis we have been able to validate the model presented by Renardy in [Ren10] and correct some imprecision in his paper. We can understand his minor errors as a lack of information since he has only studied the slow, the fast and the large scale dynamics without gluing them together as we have done with the blow-up method. Moreover the use of the blow-up method has made the analysis of the non-Newtonian fluid behaviour much neat and clear.
- The second problem analysed was the Schrödinger eigenvalue problem at the classical limit. The classical limit is non-trivial and its numeric resolution is very hard since the set of equations present stiffness issues. The blow-up method has been a powerful tool to find the solution for a generic symmetric potential $V(x)$ with ε small. In particular the particular behaviour of the solution in chart κ_2 is such that once it is proven that the transversality condition is satisfied for the first two cases of $\lambda = 1$ and $\lambda = 3$ then it is satisfied for any other case $\lambda > 3$ odd.

Appendix A

Main results of Dynamical Systems theory

A.1 Implicit function theorem

The implicit function theorem is one of the most powerful theorems of dynamical systems when considering a vector field which depends upon a parameter. There are different versions of this theorem[1], and hereby it is presented the theorem as stated in the book by Meiss [Mei07], which is the version used in general in bifurcation theory.

Theorem A.1 Implicit function theorem, [Mei07]

Let U be an open set in $\mathbb{R}^n \times \mathbb{R}^k$ and $F \in C^r(U, \mathbb{R}^n)$ with $r \geq 1$. Suppose there is a point $(x_0, \mu_0) \in U$ such that $F(x_0; \mu_0) = c$ and $D_x F(x_0; \mu_0)$ is a non-singular $n \times n$ matrix. Then there are open sets $V \subset \mathbb{R}^n$ and $W \subset \mathbb{R}^k$ and a unique C^r function $\xi(\mu) : W \to V$ for which $x_0 = \xi(\mu_0)$ and $F(\xi(\mu), \mu) = c$.

[1] The simpler version for vector fields $F : \mathbb{R} \times \mathbb{R} \to \mathbb{R}$ is called Dini's theorem by the italian mathematician who first found a sufficient condition to write an implicit function $F(x, \mu) = 0$ locally in its explicit form $x = F(\mu)$.

A.2 Center manifold theorem

Definition A.2 Local invariant manifold, [Car81]

Consider the system

$$\dot{x} = F(x), \qquad x \in \mathbb{R}^n \tag{A.1}$$

A set $S \subset \mathbb{R}^n$ is said to be a local invariant manifold for (A.1) if for $x_0 \in S$, the solution $x(t)$ of (A.1) with $x(0) = x_0$ is in S for $|t| < T$ where $T > 0$. If it is always possible to choose $T = \infty$, then S is said an invariant manifold.

Consider a system of equations

$$\begin{aligned} \dot{x} &= Ax + f(x, y) \\ \dot{y} &= By + g(x, y) \end{aligned}, \qquad x \in \mathbb{R}^n, y \in \mathbb{R}^m \tag{A.2}$$

and A a constant matrix with all the eigenvalues having zero real part, while B is a constant matrix with all the eigenvalues having negative real part. Suppose moreover that the functions f, g are at least quadratic in x, y and that they don't have any constant term, i.e.

$$f(0,0) = 0, \quad f'(0,0) = 0, \quad g(0,0) = 0, \quad g'(0,0) = 0$$

with f', g' the Jacobian matrices of f, g.

Theorem A.3 Center manifold theorem, [Car81]

There exists a centre manifold for (A.2)*,* $y = h(x), |x| < \delta$*, where* h *is* C^2*. The flow on the centre manifold is governed by the* n*-dimensional system*

$$\dot{u} = Au + f(u, h(u)) \tag{A.3}$$

which generalises the corresponding problem $\dot{x} = Ax$ *for the linear case.*

Theorem A.4 Asymptotic behaviour of small solutions of (A.2)**, [Car81]**

(a) Suppose that the zero solution of (A.3) *is stable (asymptotically stable) (unstable). Then the zero solution of* (A.1) *is stable (asymptotically stable) (unstable).*

(b) Suppose that the zero solution of (A.3) *is stable. Let* $(x(t), y(t))$ *be a solution* (A.1) *with* $(x(0), y(0))$ *sufficiently small. Then there exists a solution* $u(t)$ *of* (A.3) *such that as* $t \to \infty$*,*

$$\begin{aligned} x(t) &= u(t) + \mathcal{O}(e^{-\gamma t}) \\ x(t) &= h(u(t)) + \mathcal{O}(e^{-\gamma t}) \end{aligned}$$

where $\gamma > 0$ is a constant.
If we substitute $y(t) - h(x(t))$ into the second equation in (A.1) *we obtain*

$$h'(x)[Ax + f(x, h(x))] = Bx + g(x, h(x)). \tag{A.4}$$

Equation (A.4) *together with the condition $h(0) = 0$, $h'(0) = 0$ is the system to be solve for the centre manifold.*

A.3 Dulac's criterion

Theorem A.5 Dulac's criterion, [Koo09] *Let R be a simply connected region in $\mathbb{R}^2$ and consider a planar dynamical system in $\mathbb{R}$ given by*

$$\dot{x} = f(x, y) \quad and \dot{y} = g(x, y), \tag{A.5}$$

where f, g are C^1 functions in $\mathbb{R}$. Suppose that there exists a C^1 function $h(x, y)$ in $\mathbb{R}$ so that

$$\nabla \cdot h(fe_x + ge_y)$$

has a definite sign in $\mathbb{R}$. Then the dynamical system (A.5) *cannot have any periodic orbits in $\mathbb{R}$.*

The proof is in [Koo09].

Appendix B

Theory for Continuum Mechanics

The modelling on the deformation of non-Newtonian fluids can be done at a macroscopic or microscopic level. Depending on which of the two ways is selected, different models appears. For instance the modelling at the macroscopic level requires the use of a deformation tensor F, which describes how a piece of material is deformed along time. This model is presented in this chapter, following the notation of [Kel14]. On the other hand when considering the deformation at a microscopic level, it is not possible anymore to describe the deformation of a piece of material. Instead it is required to describe the deformation of the polymeric chain. In general it is represented as a Dumbbell model and references to this model can by found in [Can10], [BE94], [HO97].

Consider a material element in space. This element can be described in two different system of coordinates, see figure B.1:

- the reference configuration X which remains fixed during the material evolution along time. This configuration is noted with capital letter, and it is also called the undeformed configuration.
- the local element configuration x which is attached to the material element and moves with it along its evolution. This configuration is noted with lower case letters and it is also known as the deformed configuration.

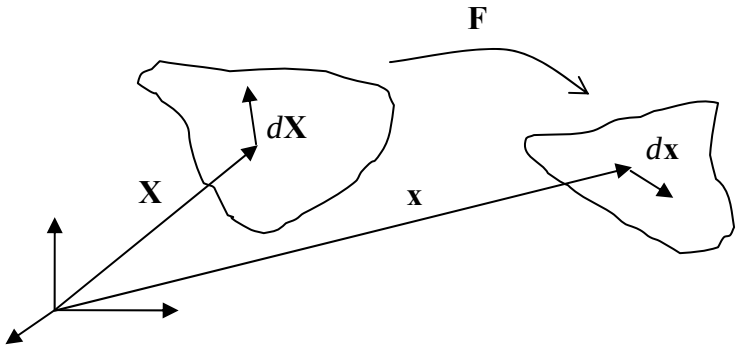

Figure B.1: Deformation of a material element, figure from [Kel14].

Consider a line dX in the material starting from position X in the reference configuration. This line corresponds to the line dx as a first order approximation in the deformed configuration. Call χ the map that translates points in the reference configuration to points in the local element configuration. Thus

$$\begin{aligned} dx &= \chi(X + dX) - \chi(X) \\ &= \nabla\chi(X)dX + \mathcal{O}(dX^2) \end{aligned}$$

Call $F = \nabla\chi(X)$ the deformation tensor. The first order approximation of the deformation of the material along space is then

$$dx = FdX$$

The deformation gradient F says how a line element in the reference configuration is mapped in a line of the local configuration. The aim is now to understand how two different lines of material $dX^{(1)}, dX^{(2)}$ starting from the same point X are mapped in the lines $dx^{(1)}, dx^{(2)}$. It is possible to show that in this case we have

$$dx^{(1)} \cdot dx^{(2)} = dX^{(1)}RdX^{(2)}$$

with $R = F^TF$ the right Cauchy-Green Strain tensor. This tensor is also called as the material tensor. On the other hand, the inverse mapping from the deformed configuration to undeformed one gives

$$dX^{(1)} \cdot dX^{(2)} = dx^{(1)}L^{-1}dx^{(2)}$$

with $L = FF^T$ the left Cauchy-Green Strain tensor. This second tensor is also known as the Finger tensor or the spatial tensor.

Bibliography

[AFJ11] M.J. Alvarez, A.M. Ferragut, and X. Jarque. A survey on the blow up technique. *INTERNATIONAL JOURNAL OF BIFURCATION AND CHAOS*, 21(11):3103–3118, 2011.

[Agg07] N. Aggarwal. *Computational Viscoelastic Drop Dynamics and Rheology*. University of Delaware, 2007.

[AS96] G. Avdelas and T.E. Simos. Embedded methods for the numerical solution of the schrodinger equation. *COMPUTERS and MATHEMATICS WITH APPLICATIONS*, 31(2):85–102, 1996.

[Bar99] H.A. Barnes. The yield stress-a review or '$\pi\alpha\nu\tau\alpha$ $\rho\varepsilon\iota$'-everything flows? *Journal of Non-Newtonian Fluid Mechanics*, 81(1-2):133–178, 1999.

[BE94] A.N. Beris and B.J. Edwards. *Thermodynamics of Flowing Systems : with Internal Microstructure: with Internal Microstructure*. Oxford engineering science series. Oxford University Press, USA, 1994.

[Boh85] N.H.D. Bohr. *Niels Bohr: collected works*. North-Holland, Amsterdam, 1985.

[BW85] H.A. Barnes and K. Walters. The yield stress myth? *RHEOLOGICA ACTA*, 24(4):323–326, 1985.

[Can10] B. Cankurt. Smoothed particle hydrodynamics simulations of viscoelastic flows around a periodic array of cylinders confined in a channel. Master Thesis, Technische Universität München, 2010.

[Car81] J. Carr. *Applications of centre manifold theory*. SPRINGER-VERLAG BERLIN, 1981.

[CB08] F. Caton and C. Baravian. Plastic behavior of some yield stress fluids: from creep to long-time yield. *RHEOLOGICA ACTA*, 47(5-6):601–607, 2008.

[Che86] D.C.H. Cheng. Yield stress - a time-dependent property and how to measure it. *RHEOLOGICA ACTA*, 25(5):542–554, 1986.

[Dir58] P.A.M. Dirac. *The principles of quantum mechanics*. Clarendon Press, 1958.

[DR96] F. Dumortier and R. Roussarie. Canard cycles and center manifolds. *MEMOIRS OF THE AMERICAN MATHEMATICAL SOCIETY*, 121(577), 1996.

[Fen71] N. Fenichel. Persistence and smoothness of invariant manifolds for flows. *INDIANA UNIVERSITY MATHEMATICS JOURNAL*, 21(3):193, 1971.

[FS05] E. Fried and S. Sellers. Orientational order and finite strain in nematic elastomers. *Journal of Chemical Physics*, 123(4):–, 2005.

[HK89] G.Q. Hassoun and D.H. Kobe. Synthesis of the planck and bohr formulations of the correspondence principle. *AMERICAN JOURNAL OF PHYSICS*, 57(7):658–662, 1989.

[HO97] M. Herrchen and H.C. Öttinger. A detailed comparison of various fene dumbbell models. *JOURNAL OF NON-NEWTONIAN FLUID MECHANICS*, 68(1):17–42, 1997.

[Hul14] M. Hulsen. Lecture notes on computational rheology. Eindhoven University of Technology, 2014.

[Jon95] C.K.R.T. Jones. Geometric singular perturbation theory. *DYNAMICAL SYSTEMS*, 1609:44–118, 1995.

[Kap98] T. J. Kaper. An introduction to geometric methods and dynamical systems theory for singular perturbation problems. *PROCEEDINGS OF SYMPOSIA IN APPLIED MATHEMATICS*, 56:85–132, 1998.

[Kel14] P. Kelly. Lecture notes in solid mechanics part iii: Foundations of continuum solid mechanics. Department of Engineering Science, University of Auckland, 2014.

[Kle12] U. Klein. What is the limit h -> 0 of quantum theory? *AMERICAN JOURNAL OF PHYSICS*, 80(11):1009–1016, 2012.

[Koo09] W.S. Koon. Lectures on periodic orbits. Caltech notes, 2009.

[KS01a] M. Krupa and P. Szmolyan. Extending geometric singular perturbation theory to nonhyperbolic points—fold and canard points in two dimensions. *SIAM Journal on Mathematical Analysis*, 33(2):286–314, 2001.

[KS01b] M. Krupa and P. Szmolyan. Extending slow manifolds near transcritical and pitchfork singularities. *Nonlinearity*, 14(6):1473–1491, 2001.

[Kue07] C. Kuehn. Multiple time scale dynamics, 2007.

[Lar84] R.G. Larson. A constitutive equation for polymer melts based on partially extending strand convection. *JOURNAL OF RHEOLOGY*, 28(5):545–571, 1984.

[Mei07] J.D. Meiss. *Differential dynamical systems*. Society for Industrial and Applied Mathematics, 2007.

[MS07] T. Monovasilis and T.E. Simos. Symplectic methods for the numerical integration of the schrodinger equation. *COMPUTATIONAL MATERIALS SCIENCE*, 38(3):526–532, 2007.

[NB92] Q. D. Nguyen and D.V Boger. Measuring the flow properties of yield stress fluids. *Annual Review of Fluid Mechanics*, 24:47–88, 1992.

[Pic00] L.E. Picasso. *Lezioni di meccanica quantistica*. ETS, 2000.

[Pla10] M. Planck. *Vorlesungen Über Die Theorie Der Wärmestrahlung*. BiblioBazaar, 2010.

[Rap81] A.D. Raptis. On the numerical solution of the schrödinger equation. *Computer Physics Communications*, 24(1):1 – 4, 1981.

[Ren10] M. Renardy. The mathematics of myth: Yield stress behavior as a limit of non-monotone constitutive theories. *JOURNAL OF NON-NEWTONIAN FLUID MECHANICS*, 165(9-10):519–526, 2010.

[San13] A.W. Sandvik. Numerical solutions of the schrödinger equation. Department of Physics, Boston University, 2013.

[Sha80] R. Shankar. *Principles of Quantum Mechanics*. Plenum Press, 1980.

[ST04] J.R. Stokes and J.H. Telford. Measuring the yield behaviour of structured fluids. *JOURNAL OF NON-NEWTONIAN FLUID MECHANICS*, 124(1-3):137–146, 2004.

[vGS05] M. van Gils, S. Krupa and P. Szmolyan. Asymptotic expansions using blow-up. *ZEITSCHRIFT FUR ANGEWANDTE MATHEMATIK UND PHYSIK*, 56(3):369–397, 2005.

[Wig90] S. Wiggins. *Introduction to applied nonlinear dynamical systems and chaos*. Springer, 1990.

[ZVCM08] Zhou, Vasquez, Cook, and McKinley. Modeling the inhomogeneous response and formation of shear bands in steady and transient flows of entangled liquids. *JOURNAL OF RHEOLOGY*, 52(2):591–623, 2008.